VOLTAGE TRANSDUCER FOR FAULT MONITORING ON HIGH VOLTAGE OVERHEAD LINES

Thesis submitted to Cardiff University in candidature for the degree

of Doctor of Philosophy.

By

Mohd Fahmi Hussin

M.Eng (Hons)

School of Engineering, Electrical Division, Cardiff University

2014

ACKNOWLEDGEMENT

I would like to express my gratitude to my supervisors Prof. A. Haddad and Dr. N. Harid for their encouragement, guidance and advice throughout my research.

I also would like to thanks to HIVES technical staffs; Dr. Dong Sheng Guo and Mr. Christopher Stone for their knowledge in helping me conducting the high voltage measurements in the laboratory and field. The knowledge and experience that they shared with me is valuable and useful in my research.

Many thanks to my research colleagues for their friendship and precious discussions; David Clark, Roshan Batharai, Muhammad Ahmeda, Stephen Robson, Alex Bogious and others. Their idea contribution is much appreciated.

Thanks to Malaysia government organization; Majlis Amanah Rakyat (MARA) and University Kuala Lumpur (UNIKL) for sponsoring my PhD.

Special thanks to my mother, Fatimah Ismail and my family for being supportive throughout my studies and never lost hope on me.

Last but not least very special thanks to my beloved wife, Siti Mazlan and my son, Umar Hakim for being inspirational and especially my wife for her selfless support, encouragement, motivation throughout the years thick or thin always believe in me, thank you.

ABSTRACT

Overhead lines are the backbone of electrical power transmission. In most cases, the overhead line provides the best economic and practical solution for energy transmission. Nevertheless, overhead lines suffer more faults due to the vulnerability of the overhead lines to adverse weather condition, transient overvoltage and falling trees. An extensive literature review of existing condition monitoring and impulse a voltage measurement technique of overhead lines are covered in this work, and ultimately leads to the development of the proposed voltage transducer. Although conventional transducers such as voltage transformers and voltage dividers are widely used for monitoring and voltage measurement, yet they have several drawbacks in terms of their size and cost. These are the key factors that limit their widespread deployment for monitoring and measuring voltage on overhead lines and, in particular, rural areas.

The proposed transducer is based on a non-contact capacitive voltage probe developed at Cardiff University. However, the proposed transducer uses a high voltage conductor rather than the ground as a measurement reference. The proposed transducer is based on a cylindrical-shaped in order to avoid sharp edges, which can initiate a partial discharge effect. Commercial numerical field computation software packages are used to assist in the development of the proposed transducer for simulation of the electric field distributions around the HV conductor and the transducer. The computed electric field magnitudes obtained on the sensing probe surface are then used for calibration of the proposed transducer. The proposed transducer is developed using low cost materials and tested in a laboratory environment with a low amplitude impulse supply using a surge generator and the corresponding output voltage amplitude obtained from the transducer was validated against a low ac voltage supply using variable output voltage source. The effects of variation in the input voltage, the integrating capacitor inserted between the HV conductor and the sensing probe and height of the transducer above ground on the output voltage amplitude are also investigated.

The developed transducer is subsequently tested in field experiments using test overhead lines with low and high voltage supplies. Only a single-phase measurement setup was used in this test as there is only one voltage transducer fabricated in this work. Therefore, each phase of the overhead line was tested individually. Results obtained from the laboratory and field experiments have demonstrated the suitability of the developed transducer for measuring both ac and impulse voltages, which would be useful for fault monitoring on the high voltage overhead lines. However, the computed results obtained from the simulation demonstrated the presence of end-effects at the transducer sensing probe edges. Therefore, an improved design was proposed in this work by introducing a floating electrode between the sensing probe and the guard electrode, with the aim to reduce the fringing effects by preventing the sensing probe from sensing unwanted electric field. The physical development of this improved transducer design is yet to be initiated, and is thus proposed for future work.

TABLE OF CONTENTS

CHAPTER 1

INTRODUCTION

In the UK, approximately 2.7 million customers are supplied from 11kV overhead line (OHL) distribution networks [1.1]. Each of these customers is disconnected from their electrical supply for up to an average of four hours each year due to power outages. By contrast, customers living in urban areas supplied by underground cables experience a statistically shorter average supply interruption of around 30 minutes per year [1.1]. This circumstance has prompted electricity suppliers and network operators to mitigate the effect of power outages experienced by customers (particularly those who live in rural areas) by reducing outage duration and minimising maintenance and repair costs.

Much effort has been undertaken by the electricity companies to reduce the incidence of outages, including, but not limited to, improvements in the design of overhead lines and tree-trimming in the immediate vicinity of said lines. However, there are still issues that cannot be mitigated effectively, such as overvoltages, susceptibility to adverse weather conditions and deterioration of the overhead line conductor strands.

A common practice adopted by electricity suppliers for fault location on overhead lines is isolation and trial re-closures of the suspected faulted lines [1.1]. This practice is time consuming, however, and results in an overstressing of the overhead lines, which could subsequently lead to other modes of failure. Another method known as condition monitoring (CM) could be adopted, either for continuous failure monitoring or to ascertain the performance or health of an overhead line. This method would be advantageous in providing reliable and accurate indication of fault location, minimising outage duration and leading to cost-effective operation.

1.1 DIRECTION AND CONTRIBUTION OF PRESENT RESEARCH

The main objective of the present research is to develop a simple, reliable and low cost transducer for fault monitoring on high voltage overhead lines that is capable of measuring different types of voltage including impulse voltages. The research background is based on the fundamental principles of a non-contact voltage probe developed at Cardiff University [1.2], which uses the capacitive probe principle to achieve voltage measurement at the HV busbar from the ground. However, this probe requires careful calibration when dealing with three phase overhead lines, as the measurement results obtained are affected by the presence of stray capacitances from neighbouring phase conductors because the probes are installed at ground level.

A voltage transducer for measuring impulse voltages on the conductors of overhead lines is proposed in this research. The key distinction in the measurement approach between the proposed transducer and the non-contact voltage probe is the configuration or placement of the transducer at the high voltage overhead line conductor. Hence, the high voltage conductor potential is used as the measurement reference instead of the ground.

Through this research, the following contributions have been achieved:

- Accurate simulation of electric field distribution around the voltage transducer and the HV conductor using finite element (FEM) and boundary element (BEM) method software packages (SLIM and Coulomb) based on two-dimensional and three-dimensional model environments respectively.
- Design and fabrication of the proposed voltage transducer using low cost available materials such as aluminium and polyvinyl chloride (PVC).
- Extensive testing and calibration of the transducer in the HV laboratory and analysis of the output voltage characteristics through variation of the size of the

integrating capacitor (C_i), the height of the transducer above ground and applied voltage supplied to the HV conductor.

- Trial tests and application of the voltage transducer under a realistic overhead line environment.
- Satisfactory correlation between the computational and experimental results.

1.2 THESIS CONTENTS

Chapter 2: Condition Monitoring and Impulse Voltage Measurement Techniques on Electrical Networks: A Review

Comprehensive past and present knowledge on the development of voltage transducers or devices used to monitor and measure impulse voltages on overhead lines and in particular 11kV lines has been gathered and studied. Existing condition monitoring techniques employed on overhead lines are reviewed and the monitoring methods and key parameters are highlighted, along with the advantages and disadvantages of each. Causes of overhead line failures leading to customer power outages are also reported, as well as measures taken by energy providers to reduce the likelihood of failure, improve performance and monitor the lines. The non-contact voltage probe developed in previous research is also reviewed in this chapter.

Chapter 3: Proposed Design and Modelling of a New High Voltage Impulse Transducer

A novel voltage transducer for measuring impulse voltages on overhead lines is proposed, designed, developed and tested. The transducer uses the same principle implemented on the non-contact capacitive voltage probe, but in contrast, it is designed to be mounted on the HV conductor instead of locating it at ground level. Commercial numerical field computation software packages are used for simulation of the electric field distribution around the HV conductor and the transducer in two- and three-

dimensional models. The computed electric field magnitudes obtained on the sensing probe surface are used to calibrate the transducer by determining the geometric capacitance (C_T) of the proposed transducer. In order to replicate insertion of the physical integrating capacitor (C_i) between the HV conductor and the sensing probe in the actual laboratory experiment, an equivalent permittivity is used. The simulation results were found to be 21% different from the analytical approach derived using simplified circuit equations. These simulated results were later compared with the results obtained from the laboratory experiments.

Chapter 4: Laboratory Setup and Calibration of the Developed New High Voltage Impulse Transducer

The proposed voltage transducer developed in Chapter 3 for impulse voltage measurement is calibrated by conducting laboratory experiments. A series of experiments were conducted with a low amplitude impulse voltage supply using a surge generator, and the corresponding output voltage amplitude obtained from the developed transducer was compared with a low ac voltage supply using a variable output voltage source. The effects of variation in the applied voltage, height of the transducer above ground and the integrating capacitor at the voltage output are then investigated. It has been observed that the output voltage is linearly proportional to the applied voltage, but is related to the height above ground and the value of the integrating capacitor in a nonlinear manner. At a fixed height, the capacitance to ground was maintained at a constant value despite changes in the value of the integrating capacitance and the input voltage. Experimental results indicate that the output voltage produced from the transducer can also be controlled by changing the transducer height above ground, the applied voltage and the integrating capacitance inserted between the HV conductor and the sensing probe. The experimental results are also compared with the computational

results obtained from the earlier modelling simulation, and a reasonably close agreement, approximately 15% has been achieved.

Chapter 5: Calibration and Trial Tests of the New High Voltage Impulse Transducer on a Test Overhead Line

Field experiments are conducted to evaluate the developed transducer when employed on test overhead lines. Low amplitude voltage experiments using impulse and ac supplies were undertaken as a preliminary work to quantify the basic parameters of the transducer under a realistic field environment, as well as the adaptation of the field experiment equipment, before progressing with the HV field experiment. For high voltage experiments, only an ac voltage source is used due to safety restrictions and concerns about possible damage to the HV impulse generator. Prior to commencement of the field experiments, a 2D model is developed to determine a suitable integrating capacitance according to the measurement specifications on site. Subsequent comparisons are made between results of the field experiment and simulation model.

Chapter 6: Further Design Refinement of the New High Voltage Impulse Transducer

Refinement analysis involves investigating alternative designs of the developed voltage transducer with smaller dimensions designed to produce a more compact and lightweight transducer. These refinement models are labelled Model B and Model C. Numerical field computation software as used in Chapter 3 is utilised, and the results obtained from simulation of the smaller compact models are evaluated against the simulation results of the developed or original model (Model A). Moreover, the effect of reducing the sensing probe surface area on the transducer geometric capacitance is also investigated. In addition, an improved design is proposed by introducing a floating electrode between the sensing probe and the guard electrode, with the aim of reducing

fringing effects at the edges of the sensing probe. The original dimensions of Model A are nevertheless retained for evaluation of the improved design, enabling direct comparison of cases with and without the addition of the floating electrode.

CHAPTER 2

CONDITION MONITORING AND IMPULSE VOLTAGE MEASUREMENT TECHNIQUES ON ELECTRICAL NETWORKS

2.1 INTRODUCTION

Electrical networks are part of high voltage systems and are composed of power stations and power grids. Electricity is generated from high voltage (HV) generators in the power station and subsequently transmitted and distributed via the respective transmission and distribution power grids that are interconnected with each other. The transmission grid transmits the electrical power by stepping up the voltage of the power generated at the power station to other higher voltage levels at the substation, and then through HV overhead transmission lines. In contrast, the distribution grid is used to step down voltage from high voltage levels at the substation and distribute the power to end users and customers via lower voltage power lines [2.1]. The transmission grid transfers electrical power from one substation to another located tens or hundreds of kilometres apart. Due to the long distance, towers are placed along the route between the two substations in order to support the transmission line conductors [2.1, 2.2].

Overhead lines and underground cables are the common media used in the transmission and distribution of electrical energy, as they are practical and economical – particularly the overhead line, which has low installation and maintenance costs. The two media are considered to be the backbone of the electrical power distribution and transmission industry. Underground cables are buried and concealed in the ground or in tunnels, and thus are less susceptible to weather-related issues. Unfortunately, their maintenance cost is rather expensive when breakdown occurs, as well as time consuming in respect to

detection of cable failure. On the other hand, overhead lines have a relatively low repairs cost (in comparison with underground cables), as detection and repair of failure is relatively more straightforward. The drawbacks of overhead lines, however, are their vulnerability and higher exposure to faults – particularly at distribution networks of up to 11kV – due to adverse weather that can include heavy wind, snow, ice and growing or falling trees.

Surge voltages also contribute to faults occurring on HV overhead lines, where the onerous voltage is commonly caused by transient overvoltage originating either from lightning strikes to the line or switching operations on the power transmission network [2.3]. Therefore, it is paramount that measurement and condition monitoring of voltage on HV conductors and terminals are assessed as accurately as possible so that precautions can be taken to maintain safe and effective operation of HV substations and overhead line equipment.

Furthermore, as demand for electricity grows due to developments in sophisticated and greener technology (such as electric cars), electricity companies are compelled to ensure that the electrical power delivered to end users is as reliable and economical as possible. In this chapter, a review of condition monitoring of high voltage equipment, in particular, the overhead line, along with impulse voltage measurement techniques is presented. The non-contact capacitive voltage probe is also explained and this probe is later used and tested for comparison of this measurement technique with the newly developed voltage transducer (as discussed in Chapter 3 and Chapter 4).

2.2 CONDITION MONITORING

Condition monitoring (CM) can be defined as a process of seeking signs or parameters of HV electrical networks' conditions in order to obtain an indication of health and early diagnosis of symptoms that can lead to the failure or performance deterioration of the

HV equipment [2.4]. “Online” and “offline” are common terms used to describe two condition monitoring techniques. The online CM technique is employed when the monitoring process is conducted in real time without interrupting operation through the aid of a transducer or sensor. The equipment is monitored and data is stored in a computer database in a control room, allowing access for future analysis through commercial software. The main advantage of online CM is that HV equipment can be examined without taking it out of operation. Thus, there is no interruption to the normal service. Also, this method is economical in terms of time and financial costs [2.5].

In comparison, offline CM requires power to be disconnected from the HV equipment prior to conducting the monitoring process. Inspection can be carried out on site or at a warehouse or workshop where faulty equipment is sent for detailed examination. This inspection requires the expertise of a technician, as most of the procedures are conducted manually. The major drawback of this type of monitoring is a lower level of accuracy in the measurement data obtained, as the equipment is not subjected to actual operating conditions when it is being monitored. Thus, external factors such as the electrical or thermal conditions of the high voltage equipment are omitted, and this does not truly represent the actual site conditions [2.6]. Furthermore, offline monitoring inspection typically consumes a large period of time (up to several months or even years) when compared with online monitoring, which offers constant observation and provides more accurate data [2.7].

The main purpose of online and offline condition monitoring, in general, is the preparation of a maintenance schedule and arrangement for any necessary precautionary procedures to reduce or avoid system breakdown, leading to a more cost-effective approach (as opposed to replacing an entire failed unit when breakdown occurs). Despite the differences between these two methods, there are still many advantages to

both approaches, including:

- Minimisation of unscheduled plant and system downtime,
- Optimisation and proper planning for maintenance and service activities,
- Utilisation of equipment up to its wear limit,
- Reduction in running costs and enhancement in reliability of the equipment used.

Techniques of condition monitoring applied to HV electrical networks and equipment are explained in the subsection below.

2.2.1 Overhead Lines

Overhead lines (OHL) are a reliable means and a standard technique used to transfer electric energy from HV substations close to end users, as installation and their maintenance costs are relatively low and life spans relatively long. However, exposure to environmental factors such as ice formation and accumulation on the OHL surface can cause line disconnection, tower failure or flashover, which is detrimental to the safe operation of the power transmission system. This happened in 1998, when 150 transmission towers collapsed in a Canadian power system (as shown in Figure 2.1) [2.8, 2.9]. The common technique used to deal with ice accumulation on the OHL is a de-icing method, such as conductor heating or mechanical de-icing using a roller.

The initial damage that occurs is commonly considered minor and insignificant. However, over time, failure to detect and repair this problem effectively can cause serious damage that can lead to power outages and consequently incur significant costs (for compensation, maintenance and replacement work). In the UK, icing is less of problem compared with adverse weather, pollution and tree initiated faults. In fact, some of the OHL networks in the UK are now reaching “old age” (between 41 and 65

years old) [2.10]. Thus, their components (such as insulators, joints and others) have degraded and require replacement as part of standard maintenance procedure.

Figure 2.1: Damage to overhead line by ice accumulation in 1998, reproduced from [2.8].

There are various techniques used to monitor and inspect the health and faults occurring on the OHL to ensure the reliability of the transmission line and reduce high maintenance costs. The oldest and most basic technique is visual inspection, which involves patrol on foot or vehicle at the ground level. This technique is also associated with the sectional method, which involves the installation of sectionalising switches along the OHL [2.11]. Faults are located by re-energising the line in sections, enabling an operator (specialist) to patrol (walk or drive) along the line with the aid of a portable device that can detect indications of fault signal either from the line, poles or power circuits. This subsequently narrows the search area and prevents interruption of other OHL networks currently in operation. However, this method has limitations. It is especially time consuming, and is often not thorough due to a high dependence on the experience of the operator to identify fault locations [2.11, 2.12, 2.13].

Aerial inspection using a helicopter is also a standard method adopted by some utilities. This technique is used to compensate for the disadvantages of ground-level inspection

and allows for a close inspection of all components along the OHL route. Photography and videography techniques are common methods associated with aerial checks, which lead to better results than simply depending on the human eye. Subsequently, the photograph taken will allow better inspection of the faults. Nevertheless, this method is costly due to expensive hiring and fuel costs, and is limited by the availability of helicopters, which are typically not available at night and during adverse weather conditions [2.11, 2.12].

There is an advanced method for monitoring OHL condition that can be achieved by observing certain parameters as indicators. An example is thermography, which is used to detect hot defect sites where the points to be measured must be hotter than the system temperature and the surrounding weather should be dry and clear [2.11]. This method is performed in special cases for OHL monitoring, and is rarely used for regular inspection tasks due to the fact that it involves installing devices on the OHL. The key factors that contribute to changes in OHL conductor temperature are listed below [2.14]:

- Heat input by ohmic losses (I^2R) – varies according to circuit loading,
- Solar heat input – affected by solar duration and emissivity of the conductor surface,
- Heat loss by radiation – affected by conductor temperature, diameter and emissivity,
- Heat loss by convection – affected by conductor temperature rise, diameter, wind speed and direction.

Furthermore, conductor temperature can be a significant indicator for use by the energy operator in optimising electricity transmission capability, as it is bound by the highest operating temperature of the OHL conductor [2.15]. In order to optimise delivery of

power during peak demand and avoid unnecessary load shedding, the transmission line is operated at higher ratings [2.16, 2.17]. However, this can cause the conductor temperature to rise, consequently leading to a significant increase in sag due to an almost linear relationship between sag and conductor operating temperature [2.18]. Therefore, the OHL conductor sag is also a parameter that can be observed and used as an indicator in order to ensure the safe operation and performance of the OHL. Nevertheless, increases in sag can lead to the breach of safety clearance, particularly at mid-span. It is, therefore, vital to monitor the temperature (thermal rating) or sag of the OHL in order to utilise the full transmission capability of the OHL while providing safeguards to the ground clearance.

2.2.2 Underground Cables

Maintenance is easier for OHL when compared with underground (UG) cables [2.15]. However, due to aesthetics, environmental considerations and concern for public safety, underground cables are preferable, especially in urban areas in most developing countries. High demand for electricity leads to the expansion of underground cable systems, and to existing networks being loaded extensively by utility providers. Knowledge from the condition monitoring of underground cables ensures safe and reliable power transmission to end users.

Underground (UG) cables generally rely on the insulation system of the cable, which comprises a primary insulation, a secondary insulation and jacket material. These materials are fabricated from organic compounds such as polymers (polyethylene, polyvinyl chloride, ethylene propylene and many more) [2.19]. These materials of the UG cables are subjected to various stresses during operation, especially insulation of an in-service cable. The stresses on the cable can be categorised as listed below [2.20]:

- Electrical – including operating and transient voltages,

- Thermal – temperature under different load conditions,
- Mechanical – bending, stretching and vibration,
- Chemical – moisture and contamination caused by chemical reactions to the insulation materials.

Since thermal factors are some of the more dominant stressors, they can lead to irreversible changes to the structural and chemical properties of the cable, particularly for paper and cross-linked polyethylene (XLPE) insulated power cables. They will also accelerate the aging of the cable insulation and diminish the cable lifespan. It is estimated that cable insulation lifespan reduces by 50% for every 10°C increase in the cable normal operating temperature. The normal operating temperature for XLPE is approximately 115°C [2.20].

The hotspot method is an example that uses thermal (temperature) as an indication to inspect aging of the UG cable. The method uses an infrared camera and is usually performed offline, where the defective component (such as a cable joint) is removed from normal operation and examined (either three or four at a time). The camera is pointed at the cable joint and a video of the infrared images is recorded (approximately one or two minutes in length), and sample images are captured regularly during the thermal cycle. Results acquired from the hotspot test are mainly based on data where experimental evidence (image) is used to support the test finding by indicating the location of the hotspot.

However, time and other stress factors such as humidity, radiation and voltage also need to be included in order to determine the actual prediction of the cable reliability. Table 2.1 indicates temperature limits for respective cable materials, but the temperature values also depend on various factors like environment temperature, soil resistivity, humidity and depth of cable installation [2.21]. Transient overvoltages also can affect

the health of UG by accelerating the aging and weakening the cable insulator material [2.22].

Table 2.1: Conductor temperature limits for standard cable types [2.21].

Power cable type	Conductor temperature (°C)
Paper insulated cables	80–90
Rubber insulated cables	80–110
PE/PVC insulated cables	90–95
XLPE insulated cables	110–115
Oil pressure paper insulated cables	105–110

2.2.3 Voltage Transformer

Voltage transformers (VT) are also known as potential transformers (PT), and have been used for decades to step down high voltage magnitudes to a safe measurable level. They also ensure the stability and reliability of electrical network operation. Transformers are categorised as conventional transducers, and they are typically composed of bushings, magnetic cores and copper winding. There are three main types of voltage transformers used in the HV system, namely oil-immersed, gas-insulated and dry-type transformers.

Although transformers are able to provide accuracy and reliability of voltage measurement data, their cores are heavy, bulky and expensive. These cores can cause saturation effects in their irons when dealing with transient voltages or faults, and are susceptible to electromagnetic interference (EMI), which can lead to magnitude and phase errors [2.23]. Moreover, increases in power distribution system voltages (up to

several hundred kV) and load growth have led to increase operating stresses on the voltage transformers and transformer insulation, which are becoming increasingly complex and costly.

There are many well-known preventive maintenance techniques commonly used to monitor voltage transformers, such as dissolved gas analysis (DGA) and partial discharge (PD) measurement. Dissolved gases in transformers' insulating oil are produced through chemical reactions, and these gases have been utilised for many years as an indicator of the condition of a transformer's insulation. Although DGA is employed to detect internal electrical discharge in voltage transformers, it is unable to provide enough information about the present condition of the transformer. Since gas information is a cumulative process, sufficient data and a longer period are required prior to proper examination of the transformer's condition [2.24].

An online partial discharge (PD) detection technique was also adopted in [2.25], alongside the DGA, to verify the integrity of the voltage transformer's insulation. This technique also provides information about the PD location. PD detection is performed to monitor the condition of the insulation, as it is a vital parameter. Occurrence of PD within transformers is caused by excesses in the electric field beyond the dielectric strength of the insulation within a localised volume, typically due to overvoltages or insulation deterioration from the effects of aging.

As stated by a CIGRE working group and quoted by S. Meijer et al. [2.26], the following PD magnitudes can be used as indicators of insulation condition:

- Defect free 10–50 pC
- Normal deterioration <500 pC
- Questionable 500–1000 pC
- Defective condition 1000–2500 pC

- Faulty (Irreversible) > 2500 pC
- Critical >100,000–1,000,000 pC

Partial discharge in the range of 500 to 1000 pC is classified as questionable due to voids in the insulation, cracking in brittle insulation, manufacturing defects of the PD source and many other factors.

There are various methods for detecting PD, such as electromagnetic waves, acoustic waves, local heating and chemical reactions produced during the occurrence of partial discharge. Since the early 1960s, acoustic waves have been used to detect PD sources in voltage transformers [2.24]. This technique is based on the detection of mechanical waves propagated from the discharge site to the surrounding medium. The wave signal is created when a streamer is formed within the void and the material around the hot streamer is vaporised. This vaporization causes an explosion of mechanical energy, which then propagates through the transformer tank in the form of a pressure field [2.27]. Acoustic detection can provide the PD or fault location, although there are limitations to this technique, as waves do not propagate equally in all directions. Therefore, there are multiple on-site acoustic sensors installed at different positions inside the transformer tank [2.24]. Piezoelectric transducers are mostly used to detect PD in transformers, and are a favourable approach widely used in the diagnosis of transformers [2.27].

It is crucial to monitor the performance of the transformers (VT or PT) and ensure that they are in good working condition. Online and offline condition monitoring are both common diagnostic methods applied to detect the occurrence of faults at an early stage, thus preventing catastrophic errors such as transformer explosions due to excessive overloading or interior faults. In addition, both online and offline condition monitoring can also be used to monitor the life span of transformer insulation systems.

2.2.4 Switchgear

Switchgear equipment is used as a safety mechanism, as it can control and protect equipment in high voltage systems [2.28]. On the EDF energy networks system there was an average of 32 switchgear faults per year over a three year period (2009 - 2012), which affected 1150 primary (33kV and 11kV) substations [2.29]. The faults caused interruption of power supply to end users and cost the electricity provider compensation payout, as well as vast repair expenses.

Most switchgear assembly failures originate from insulation failure, but various other factors, such as mechanics and temperature, also contribute to the failure of switchgear operations [2.28, 2.30]. The standard technique for examining the insulation condition of switchgear is through monitoring PD activity. This can be carried out through routine testing, whereby voltage is applied and increased gradually to above service levels. The voltage is subsequently reduced steadily, and PD magnitudes are measured and recorded when PD occurs within the insulation. In general, PD measurement provides information regarding localised insulation defects, which may ultimately lead to the defect's source, such as chemical degradation [2.31]. Figure 2.2 shows an example of substation destruction caused by a switchgear failure.

Figure 2.2: Damage to HV substation caused by switchgear failure reproduced from [2.30].

Clearly, it is of the utmost importance to monitor the health of the switchgear in order to ensure the safety and reliable operation of the HV system.

2.3 FACTORS CAUSING DETERIORATION OF OVERHEAD LINES

Overhead lines (OHL) are cost effective media used for electric energy transfer but exposure to environment causes OHL health deterioration. Many of OHL health deterioration factors are inter-related, and it is important to identify these factors in order to maintain safe operation of the OHL.

2.3.1 Conductor Corrosion

Many of overhead lines in the UK are reaching an age where the mechanical safety is inadequate due to corrosion of the conductor aluminium strands. This corrosion is formed by an aqueous solution containing chloride ions, and this solution infiltrates between the aluminium strands of the conductor and then attacks the galvanising layer on the steel core [2.10], which exposes the steel substrate. If the corrosion continues with time, it may lead to the loss of a section of the aluminium strands, hence reducing the current-carrying capability as well as loss of mechanical strength of the conductor. Moreover, corrosion of the inner aluminium strands can results in strand breakage and line failure.

Overhead lines located in areas close to the coast or exposed to sea salt aerosol and industrial areas where the conductive dust can impinge on the line surface. Also, this exposed the conductors to corrosion due to the reaction with surface of the conductor galvanisation. However, this conductor corrosion problem can be resolved by applying grease within the conductor strands. The grease is able to limit penetration of the aqueous pollutant. In late 1960s, the amount of grease applied in conductors was increased resulting the onset of corrosion in lines built beyond about 1965 is delayed by

about 10 years compared with earlier lines [2.10].

2.3.2 Overvoltages

Overvoltages also contribute to faults occurring on high voltage lines and in particular transmission line. This is due to the main operation that can produce switching overvoltages originating from line energization and re-energization, also capacitor and reactor switching [2.32]. If energization takes place in an HV system at an instant when the difference between supply and the line voltage is high, hence a large travelling wave would be injected on the transmission line and there is a possibility to initiate a high transient overvoltage if this wave gets reflected when it reaches the open far end of the line [2.33]. Such switching overvoltages are a main concern for high voltage transmission networks, particularly for long transmission lines [2.34].

2.4 IMPULSE VOLTAGE STANDARDS

Impulse voltages are also known as overvoltages, and include external and internal overvoltages. External overvoltages originate from lightning strikes as a result of atmospheric discharges, and strokes hitting overhead lines or bus bars of substations have extremely high voltage amplitudes, usually exceeding 1000kV or more. Each stroke may inject lightning currents of up to 100kA into the lines [2.3]. In contrast, internal overvoltages result from changes in operating conditions, such as switching, faults or load variations. Amplitudes of switching overvoltages are always correlated to the operating voltage, and their shapes are influenced by the impedances of the system, including the switching condition. Common factors that influence switching overvoltages include circuit configuration, circuit conditions between circuit breaker contacts and stray capacitances between the circuit breaker and shunt reactor [2.35]. Overvoltages are common sources of stress affecting HV systems, and particularly the

insulation, which can lead to catastrophic failure due to an excessive voltage amplitude above the peak value of normal operational levels [2.36]. It is, therefore, vital to protect the system against these impulse voltages.

High voltage testing is conducted to determine the safe operation of the HV system. Typical test standards are based on the ANSI/IEEE Standard 100-1984 and IEC 60060-1, and these standards are used when applying a voltage higher than the rated voltage for a specified time in order to investigate the capability of the HV equipment, particularly in regards to breakdown of insulation materials and spacing under normal conditions. The test is conducted as a proof test of new apparatus, a maintenance procedure or one of the methods of evaluation for insulation system development [2.38]. Impulse voltage tests (i.e., lightning and switching tests) in an HV laboratory are conducted using impulse or surge generators. The impulse waveforms are based on the relevant standard (i.e., IEC 60060-1), and these waveforms must be generated to estimate the expected impulse voltages that are likely to stress high voltage equipment. The standard defines an impulse as "an intentionally applied periodic transient voltage or current which usually rises rapidly to a peak value and then falls more slowly to zero" [2.38].

Waveforms for a lightning impulse test should have a front time (T_1) of 1.2μs and a tail time or time to half-value (T_2) of 50μs, which is normally referred to as T_1/T_2 or 1.2/50 impulse. The standard switching impulse, on the other hand, has a shape that is distinctly different from that of a lightning impulse. The standard front time to peak (T_p) is 250μs, and the time to half-value (T_2) is 2500μs. Thus, the standard switching impulse is described as a 250/2500 impulse [2.37, 2.38]. Figure 2.3 illustrates the general waveforms for standard lightning and switching impulse voltages.

Although impulse standards correspond to a particular period, an amount of tolerance is

acceptable for laboratory experiments, since smooth impulse shapes are difficult to obtain in practical situations due to stray capacitances and inductances that may cause oscillations in the measurement system. The tolerances for lightning impulse are ±30% for T_1 and ±20% for T_2, while for the switching impulses, the tolerance for T_p is ±20%, and, for T_2, is 60% [2.37, 2.38].

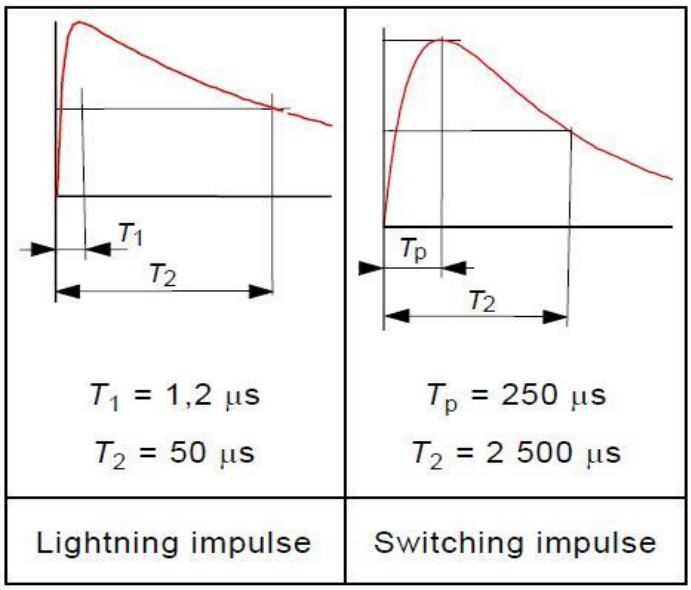

Figure 2.3: Standard waveforms of lightning and switching impulse voltages (reproduced from [2.38]).

2.5 EXISTING IMPULSE VOLTAGE MEASUREMENT TECHNIQUES

There are various methods used at present to study overvoltages, including computer simulations, laboratory experiments and online monitoring. Computer simulations are modelled on the actual environment with the aid of computers, yet is still not fully consistent or representative of the real situation. Laboratory experiments also cannot completely simulate the overvoltages due to the complexity of the actual situation (for instance, the requirement for connection between high voltage and ground, and the subsequent safety requirement of a good protection scheme). In addition, some laboratory equipment, such as high voltage surge generators, are large and expensive. Therefore, relocation or transportation of this equipment is difficult, as is recalibration.

Online monitoring is another technique introduced to study overvoltages, and this method is explained in Section 2.2. Due to the measurement and monitoring of actual overvoltage signals conducted in real time, this method is able to overcome the limitations of laboratory experiments and computer simulations. Nevertheless, both laboratory experiments and online condition monitoring require additional devices – categorised as conventional and non-conventional transducers – to measure or sense overvoltage signals. Voltage transformers (VT) are the most commonly used devices for measuring high voltage in power system environments, but because the transformers contain electromagnetic components, they can cause saturation when dealing with high frequencies and are, therefore, not suitable for overvoltage measurement. High voltage dividers and optical voltage transducers (based on fibre optic technology) are the main devices typically used to measure impulses in HV systems. Optical transducers are free from electromagnetic components, and inherit additional abilities such as immunity to interference, high bandwidth and others. Details regarding these devices and their measuring techniques are elaborated in the next-subsection.

2.5.1 High Voltage Divider

Voltage dividers are also known as potential dividers, and their construction is based on a simple linear circuit. The fundamental working principle is one of dividing measurement voltage by producing an output voltage as a fraction of its input voltage. This allows high voltage measurements to be taken safely, as high voltage values of hundreds of kilovolts can be reduced to a few volts. The scale of reduction in voltage is identified by a constant factor known as a ratio. Thus, the measured value displayed on the oscilloscope or voltmeter can simply be multiplied by this divider ratio in order to obtain the actual measured value [2.39].

There are various types of voltage dividers, including resistive and capacitive voltage

dividers. Design of these dividers requires special care and consideration depending upon the measurement application. Resistive dividers are typically used for direct current (DC) measurements, and can be less accurate due to current flow in the divider, which leads to temperature changes. In contrast, the capacitive divider is used for alternating current (AC) measurement, and it is designed to eliminate the effects of stray capacitance. Capacitive dividers are preferred over resistive dividers because of the difficulty in eliminating inductance from resistors due to their expensive and complicated design implementation [2.37]. In addition, usage of capacitive voltage dividers can eliminate the heating problems faced by resistive dividers, making them suitable for switching impulse voltage measurement.

The impulse voltage measurement technique utilising HV dividers is conducted by electrically connecting the divider using woven wires. It is important to ground the divider by connecting it to a ground network in the substation and at the surge generator. However, outside the substation, for example along the transmission line the tower legs were used for grounding (which can provide an adequate grounding due to the low tower-footing resistance ranging from 1 to 20 Ω) [2.40]. A coaxial cable is used to transmit the voltage from the low voltage arm of the HV divider to the oscilloscope for monitoring and recording of the measurement data. Furthermore, the ground sheath of the coaxial cable also provides a single ground for the oscilloscope.

2.5.2 Optical Voltage Transducer

Fibre optics technology is normally utilised in communication environments, but usage of this technology as sensors in industrial environments has notably increased in recent years. Optical voltage transducers are gaining popularity and have reached a high degree of maturity. This enables the transducers to compete with conventional types such as transformers [2.41]. Optical voltage transducers provide significant advantages

over conventional voltage transformers, such as high accuracy due to no saturation, wide bandwidth and dynamic range, as well as immunity to electromagnetic interference and near-perfect insulation (which prevents a galvanic connection between the HV side with the low voltage measurement side). All these advantages protect the HV system and substation equipment from the dangers of catastrophic failure. Furthermore, optical transducers exhibit compact construction, which allows integration with existing substation equipment (such as circuit breakers and bushings) and results in space saving [2.42]. Nevertheless, optical fibres are susceptible to mechanical vibration and ionising radiation, as even gradual bending over an extended period of time can cause attenuation. This issue is currently being addressed [2.43].

The basic elements in a fibre optic sensing system are a light source, optical fibre, sensing element or transducer and detector, as shown in Figure 2.4. The fibre optic system working principle is a modulation of parameters of the optic system, such as intensity, wavelength, polarization and phase by the transducer, which gives rise to changes in the characteristics of the optical signals received at the detector [2.44, 2.45].

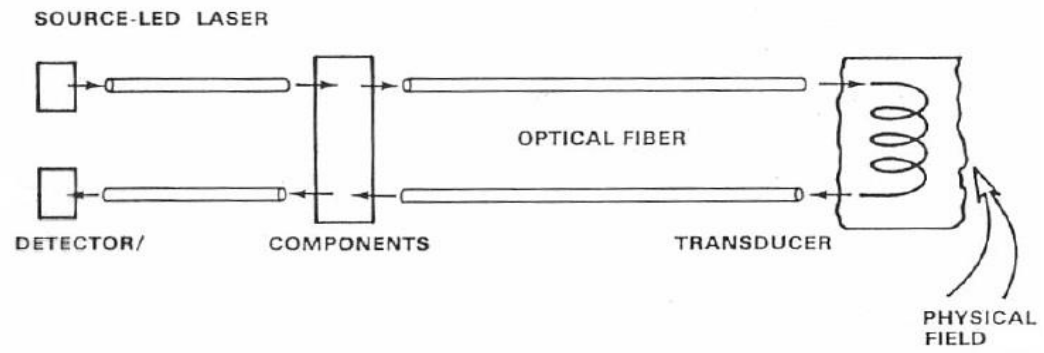

Figure 2.4: Basic elements of an optical fibre sensing system reproduced from [2.44].

Companies such as ABB Switzerland Ltd. report [2.41] that they have managed to develop voltage transducers based on optical fibre technology. The optical voltage transducer developed by ABB is called an electro-optic voltage transducer (EOVT), and is used for high voltage substation measurement. Figure 2.5 shows the physical

assembly of a transducer known as an optical metering unit (OMU) that combines EOVT and a magneto-optic current transducer (MOCT). The transducer operates in a sulphur hexafluoride (SF6) gas contained in a composite insulator with silicone rubber sheds. It is tested at lines with voltage ranging from 115kV to 550kV based on IEEE Standard 4 [2.41]. As an example, Figure 2.6 shows the optical sensor output against time generated when a constant ac voltage of 14.4 kV_{rms} is applied to a 420kV air-insulated ac electric power system. The authors in [2.41] reported that the measured signal is stable within ± 0.2%.

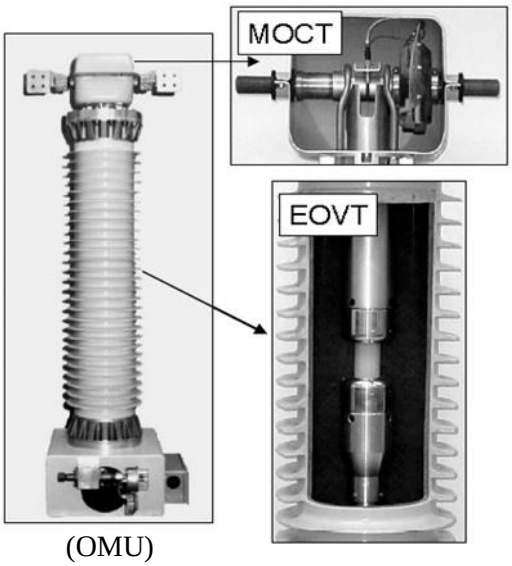

Figure 2.5: Optical metering unit (OMU) combining current (MOCT) and voltage transducer (EOVT) (reproduced from [2.41]).

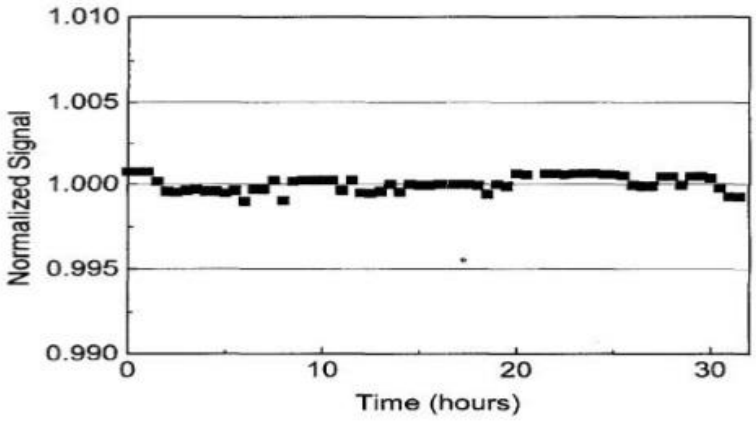

Figure 2.6: Normalised sensor signal as function of time for a constant applied ac voltage of 14.4kVrms (reproduced from [2.41]).

2.6 NON-CONTACT CAPACITIVE VOLTAGE PROBE

A non-contact capacitive voltage probe (NCCP) developed and constructed at Cardiff University is also studied and tested for comparative studies in this research programme, and the results of this work are given in Chapter 4. The objective of the NCCP test is to acquire an in-depth understanding of the capacitive divider measurement techniques. The design of the probe is of circular shape in order to eliminate sharp edges and minimize end-effects, and it consists of two main components: a sensing probe and an earthed guard plate. The sensing probe is surrounded by the earthed guard plate to reduce end-effects. Figure 2.7 shows the design and dimensions, while Figure 2.8 depicts the physical diagram of the non-contact capacitive voltage probe. It is made from aluminium, and four perspex insulation blocks are used to separate the sensing probe from the earthed guard plate, with a distance of 1mm between them. The thickness of the sensing probe and the earthed guard plate is approximately 5mm.

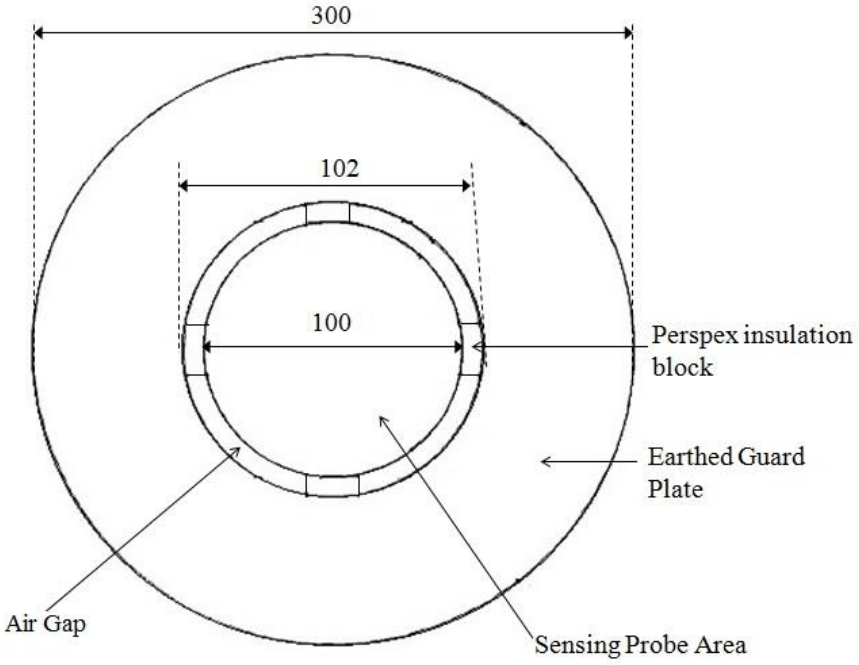

Figure 2.7: Non-contact **c**apacitive voltage probe design and dimension shown are in mm (not to scale).

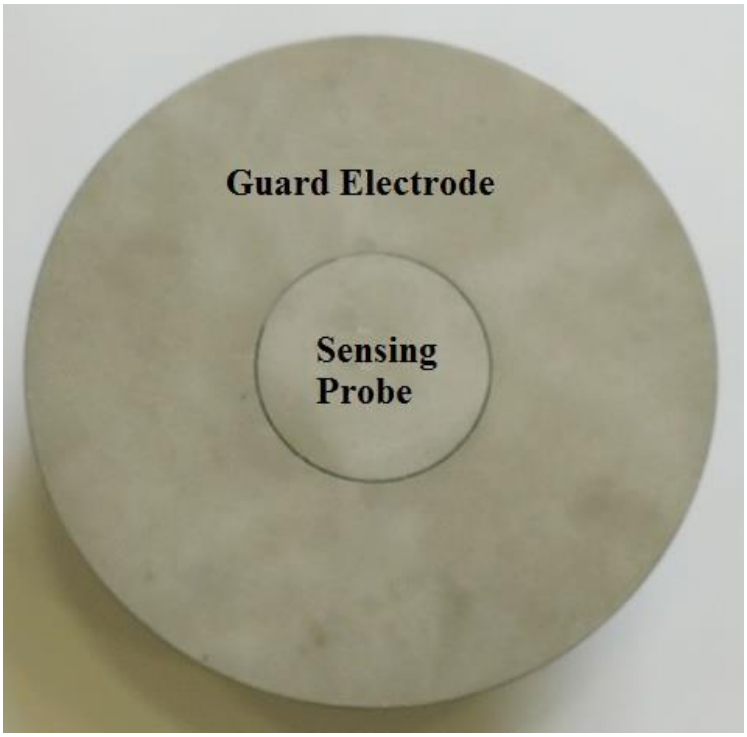

Figure 2.8: The actual non-contact capacitive voltage probe.

A shield enclosure is installed underneath the probe for housing the probe low voltage arm capacitor (C_p), and a buffer/amplifier circuit. This circuit is built to prevent phase shift from occurring when integrating the induced charge. Figure 2.9 shows a schematic diagram of the circuit that includes two stages, namely the buffer and the amplifier stage. The buffer stage uses a buffer amplifier (RS-3140) that has a high input resistance and a low input offset current. The high input resistance ensures that a long-term time constant can be obtained, and the small input current prevents the probe integrating capacitor from overcharging. The amplifier circuit (RS-351) is used to amplify the output voltage measured by the probe by adjusting the amplifier gain through a potentiometer (10kΩ) that is inserted into the amplifier feedback path and also additional potentiometer (10kΩ) connected between the amplifier output path and ground. Researchers [1.2] achieved a gain of 20dB increased the probe's sensitivity and improved the signal-to-noise ratio, which is vital when performing on-site measurement in an environment that is prone to noise interference from other HV equipment.

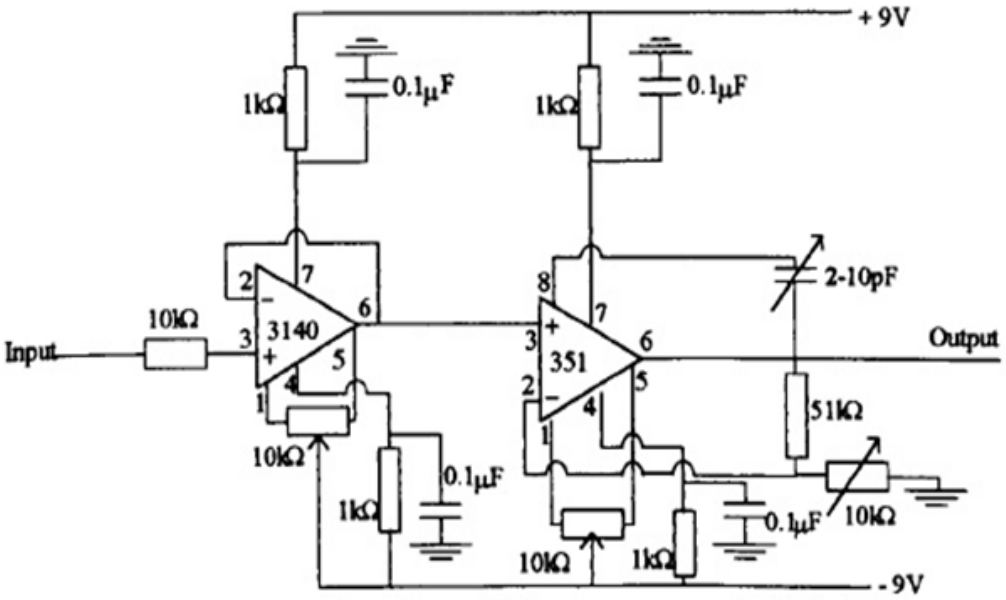

Figure 2.9: Schematic diagram of the buffer / amplifier circuit reproduced from [1.2].

This probe is placed underneath high voltage conductors or bus bars with an exposed conducting sensing surface, and operates based on the capacitive divider concept. A single-phase measurement configuration is used to describe the basic principle of this non-contact capacitive voltage probe, as portrayed in Figure 2.10.

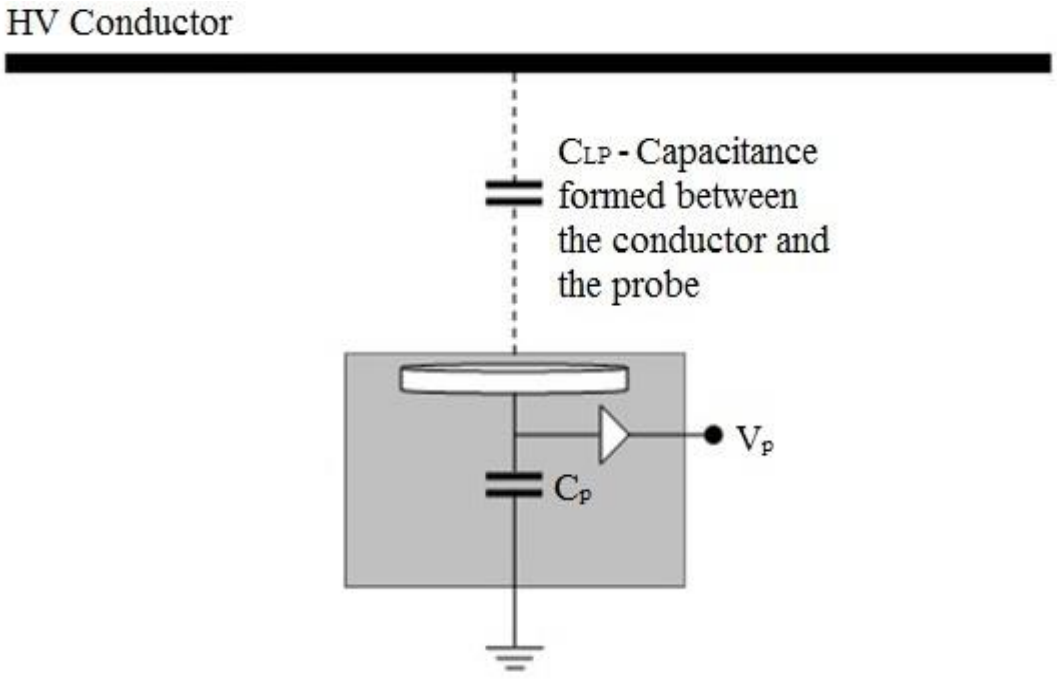

Figure 2.10: Single-phase measurement of the non-contact capacitive voltage probe reproduced from [2.46].

When an HV conductor induces a charge on the sensing probe surface, a capacitance, C_{LP}, is formed between the line and the probe through air distribution. A voltage divider is created when a low voltage arm capacitor, C_p, is inserted into the probe. The capacitive probe output, V_p, can, therefore, be stated as Equation (2.1).

$$V_p = \frac{C_{LP}}{C_P + C_{LP}} V_{in} \tag{2.1}$$

Where, V_{in} is the applied voltage supplied to the HV conductor. Some of the advantages of the non-contact capacitive voltage probe are a straightforward construction process, low cost, portability and, most importantly, no requirement for disconnection of the HV line supply prior to probe installation. This probe is suitable for both time varying field measurements and also high voltage measurements.

However, for three-phase voltage measurement, the use of the probe placed directly under the HV conductor, would result in a voltage induced by the neighbouring phase conductors as shown in Figure 2.11.

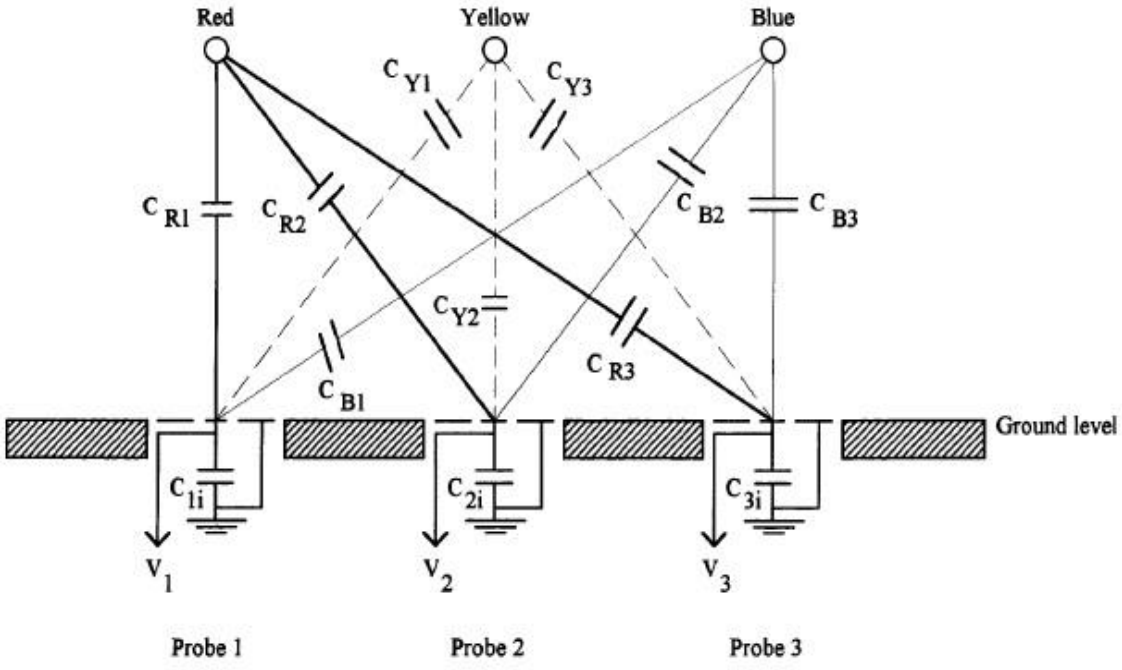

Figure 2.11: Configuration of the non-contact capacitive voltage probe for three-phase overhead lines (reproduced from [1.2]).

This resulting phase and magnitude (output voltage) measured by the probe are affected by the presence of adjacent phase stray capacitances from neighbouring phase conductors since the probes are installed at ground level. Therefore, the probe requires careful calibration for deployment in a long-term continuous voltage monitoring system and also the need to consider the optimum position during installation. On the other hand, the newly developed transducer is able to eliminate this stray capacitance problem (as shown in Figure 2.11) by installing the transducer at the HV conductor instead of ground, as described in Chapter 3, Section 3.4.

2.7 DISCUSSION AND CONCLUSION

A literature review ranging from condition monitoring of HV substation equipment to impulse voltage measurement techniques is covered in this chapter. Condition monitoring is crucial to observing and examining the health of HV substation equipment, as well as providing an indication as to what preventive or maintenance work needs to be carried out in order to prevent failures. Online and offline monitoring are two common methods of condition monitoring, but online monitoring provides a better approach, as the assessment can be carried out continuously and in real time without interrupting the normal service operation of HV equipment.

Overvoltages normally weaken the dielectric strength of HV equipment insulation. Partial discharge (PD) can be considered a universal indicator of the health of HV equipment insulation, and is widely used as such by electricity utility companies. There are various methods that can be used to detect defective insulation. For example, acoustic waves can be used to locate PD inside voltage transformers when acoustic sensors are installed at different points inside the transformer tank, as the wave does not propagate equally in all directions. Other than PD detection, other parameters such as sag and conductor temperature are also appropriate for use in monitoring overhead line

condition and operation. Increase in OHL sag can lead to safety clearance being breached, and the relationship between sag and conductor operating temperature is almost linear. The thermal monitoring technique is contactless and can monitor OHL operating temperature by using an imaging system such as thermal cameras, as well as the hot spot measurement method.

There are various techniques used to study overvoltages (or lightning and switching impulse voltages) in HV networks systems, including laboratory experiments and online monitoring. It is important to conduct overvoltage tests on HV equipment, as overvoltages normally cause stress to HV equipment insulation. Both laboratory experiments and online monitoring, however, require the installation of additional instruments in their measurement system, such as high voltage dividers and optical voltage sensors. These two types of devices are more favourable than conventional voltage transducers due to their construction, which is free from electromagnetic components (which causes saturation when dealing with high frequencies).

High voltage dividers are used to scale voltage down from high voltage to a smaller level, which enables voltage measurements to be taken safely using an oscilloscope. Divider types include capacitive, resistive and a combination of the two. For most ac voltages, measurement is typically conducted using a capacitive divider. Capacitive dividers can prevent heating problems, which may be encountered with resistive dividers. Measurement results obtained from the dividers are ideally a mirror of the actual high voltage measurement values, and this measurement is influenced by the divider ratio. The divider measurement technique involves connecting the high voltage arm capacitance to the HV line and the low voltage arm capacitance to the ground. A coaxial cable is used to transmit the measurement data from the divider to the oscilloscope.

Optical voltage transducers based on optical fibre technology are also used to measure impulses in the HV substation environment. Characteristics of the optical fibre include wide bandwidth, a wide dynamic range and, most importantly, immunity to electromagnetic field interference, which allows the optical transducer to be placed in harsh environments. Optical fibre technology also allows for a combination involving the transducer and other measurement devices due to the transducers' ability to fit into compact devices. A previously developed non-contact capacitive voltage probe is also discussed in this chapter in order to provide knowledge on different types of approaches towards capacitive dividers. This probe is also modelled and tested, as mentioned in the next few chapters.

CHAPTER 3

PROPOSED DESIGN AND MODELLING OF A NEW HIGH VOLTAGE IMPULSE TRANSDUCER

3.1 INTRODUCTION

In the course of this research, the non-contact capacitive voltage probe (NCCP), previously described in Chapter 2, Section 2.6, is also modelled and evaluated using commercial numerical field computation software packages as part of the preliminary work with the aim of understanding the non-contact voltage probe characteristic and performance. The software packages were used to assist in the development of a new voltage transducer – namely for the simulation of the electric field distribution around the HV conductor and the transducer – while the validation of the computed results gathered from the modelling simulation were done using Matlab computation and analytical calculation. The results obtained from the model are compared with the measurement results from the laboratory experiments in Chapter 4.

A new voltage transducer is designed based on a cylindrical-shaped model and utilises the capacitive voltage divider measurement principle, but it uses the HV conductor as the measurement reference rather than ground, as commonly found in the literature [1.2]. The relative merits of the transducer lie in its simple construction and low cost. Moreover, the transducer does not require proper housing in order to protect it from vandalism or theft, since the transducer is installed on the HV conductor and away from ground. This transducer was designed and constructed for fault monitoring on high voltage overhead lines and is capable of measuring different types of voltages (including impulse voltages).

3.2 MODELLING OF NON-CONTACT CAPACITIVE VOLTAGE PROBE

The non-contact capacitive voltage probe is modelled in this work using finite element method software. Figure 3.1 shows the 2D model based on single-phase overhead line configuration with the boundary area spanning 1m by 3m. The probe is located underneath the HV conductor and uses the ground as a measurement reference. This model is based on the low voltage experiments carried out in the HV laboratory, with the conductor placed at 0.1m (measured from the centre of the conductor) above the sensing probe surface.

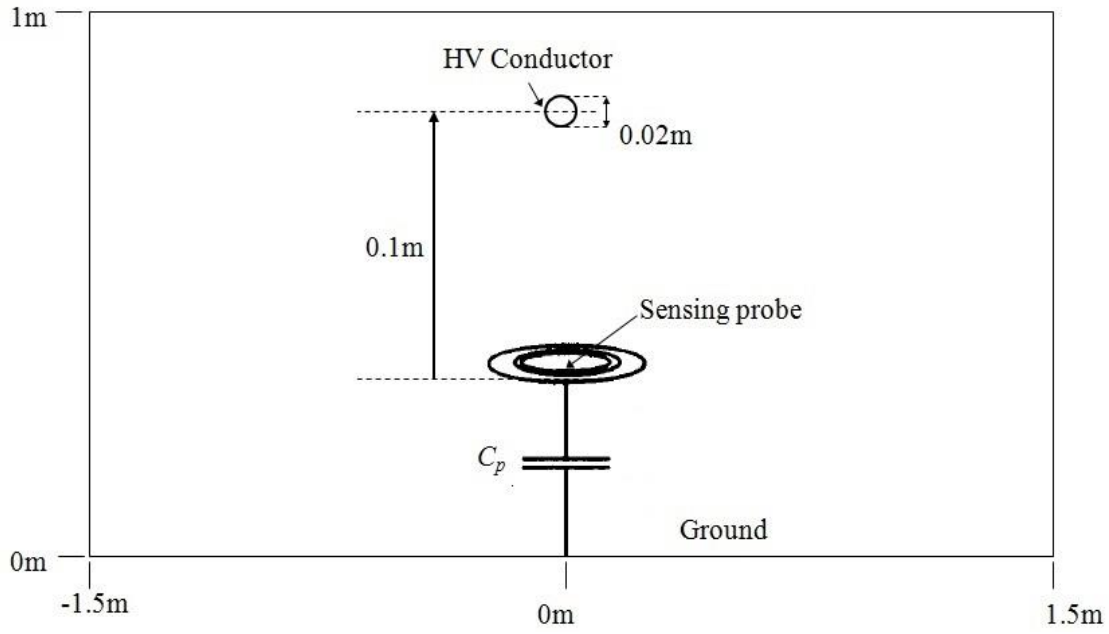

Figure 3.1: Non-contact capacitive voltage probe modelling configuration (not to scale).

Figure 3.2 shows the equipotential distribution computed when the voltage is applied to the HV conductor. As can be observed, the electric field distribution is highly concentrated between the sensing probe and the ground. The electric field profile on the ground plane, as plotted in Figure 3.3, indicates that the maximum electric field peaked at approximately 910 V/m when an applied voltage of 200V was supplied.

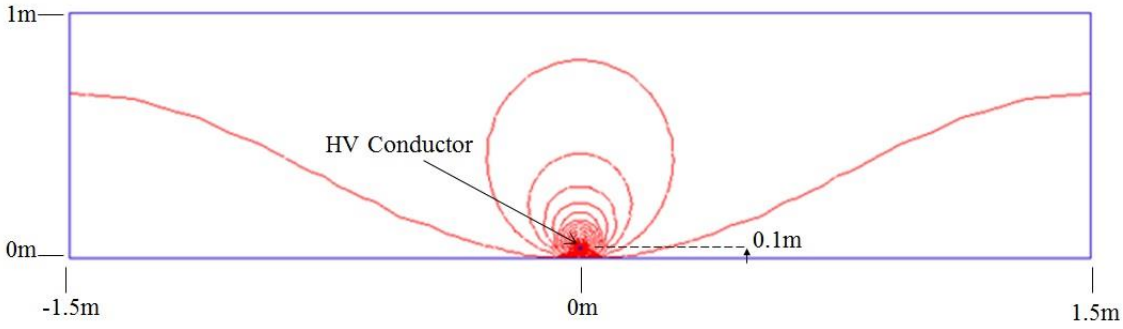

Figure 3.2: Computed equipotential lines for the NCCP modelling as shown in Figure 3.1 (not to scale).

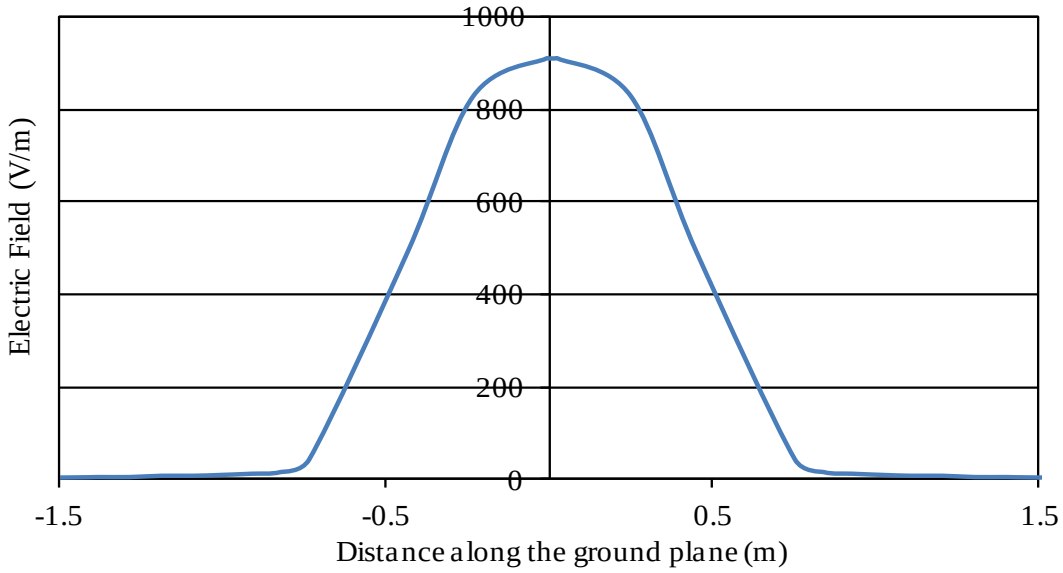

Figure 3.3: Computed electric field magnitude profile along the ground plane.

The output voltage (V_p) produced by the probe can be calculated using Equation (3.1) [1.2],

$$V_p = \frac{E\varepsilon_0 A}{C_p} \tag{3.1}$$

Where:

E is the maximum electric field magnitude,

ε_0 is free space permittivity (8.854 x 10^{-12} F/m),

A is the sensing probe surface area,

C_P is the low voltage arm capacitor located underneath the probe.

The sensing probe has a circular shape with a radius of 0.05m. Thus, the surface area is simply calculated as πr^2 to give the value of 78.6cm^2, whilst the low voltage arm (C_p) used in the actual experiment is 10nF. Substitution of all these values and the maximum electric field magnitude of 910 V/m into Equation (3.1) gives an output voltage (V_P) of 6.3mV$_p$. This voltage value will be compared with results obtained from the corresponding laboratory experiment in the next chapter.

3.3 WORKING PRINCIPLE OF THE PROPOSED VOLTAGE PROBE

The simplest way to illustrate the working principle of this new HV impulse transducer is by using a single-phase (1Ø) measurement configuration. Insertion of an integrating capacitor (C_i) between the HV conductor and the sensing probe creates a capacitance to ground (C_G) when there is a voltage present in the conductor, as shown in Figure 3.4.

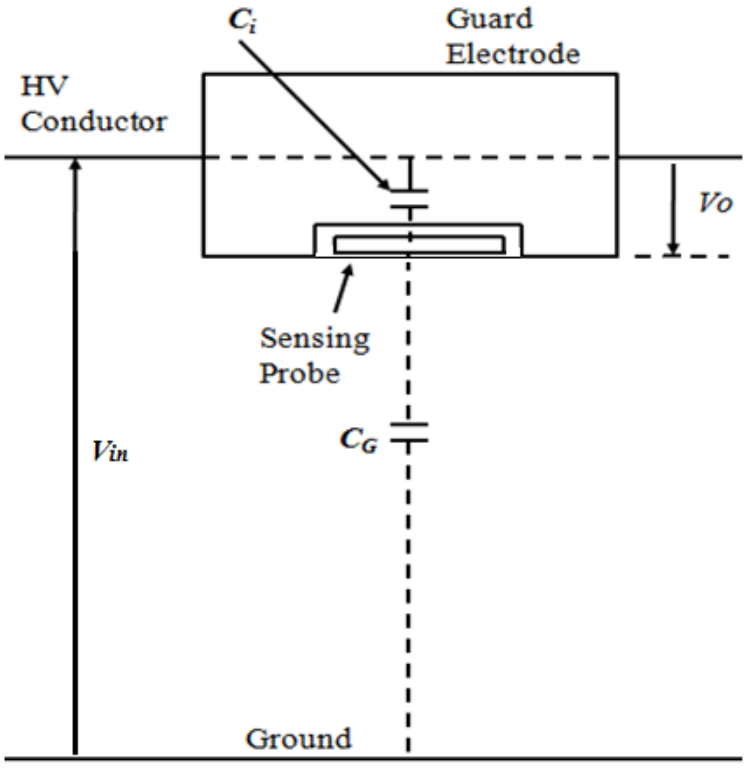

Figure 3.4: Transducer working principle based on single-phase measurement configuration.

Therefore, the transducer output voltage (V_T) can be derived as in Equation (3.2).

$$V_T = \frac{C_G}{C_G + C_i} V_{in} \tag{3.2}$$

Where:

C_i is the integrating capacitor,

C_G is the capacitance to ground (from the transducer sensing probe to ground),

V_{in} is the applied voltage to the HV conductor,

V_T is the transducer output voltage (wrt the conductor line voltage).

The derivation of the equation is similar to the conventional capacitive divider, although in this case, the HV conductor is taken as the measurement reference instead of the ground. Rearrangement Equation (3.2) gives the equation of capacitance to ground, C_G, as shown in Equation (3.3).

$$C_G = \frac{V_T C_i}{V_{in} - V_T} \tag{3.3}$$

The ratio of the capacitive divider (R) is expressed as a fraction of the output voltage from the applied voltage, which can also be derived from Equation (3.2), expressed as Equation (3.4).

$$R = \frac{V_T}{V_{in}} = \frac{C_G}{C_G + C_i} \tag{3.4}$$

From the single-phase measurement configuration, the electric charge (Q) induced on the sensing probe surface can be determined using the electric field measurement, and is given by Equation (3.5) [1.2].

$$Q = \int_0^{\ell} \int_0^{w} \varepsilon_0 \varepsilon_r E(x, y).dx.dy \tag{3.5}$$

Where:

ε_0 is the permittivity of free space (8.854 x 10^{-12} F/m),

ε_r is the equivalent permittivity,

E (x,y) is the electric field at coordinates x, y on the sensing probe surface,

ℓ is length of the sensing probe (0.3m),

w is width of the sensing probe (0.2mm).

Assuming E is constant all over the sensing probe surface, Equation (3.5) can then be simplified to denote Q as Equation (3.6).

$$Q = E\varepsilon_0 A \tag{3.6}$$

Where A is the total area of the sensing probe surface, and using the computed electric charge value on the sensing probe surface obtained from two- and three-dimensional modelling, the geometric capacitance of the transducer (between the HV conductor and the sensing probe surface) can be determined using Equation (3.7). The computed geometric capacitance of the voltage transducer (C_T) can be estimated, as given in Equation (3.7).

$$C_T = \frac{Q}{V} \tag{3.7}$$

Where, V is the computed output voltage obtained from the transducer.

3.4 COMPUTER MODELLING OF VOLTAGE TRANSDUCER

Two- and three-dimensional models of the transducer are simulated using commercial finite (FEM) and boundary element (BEM) method software packages – Single Layer Iterative Method (SLIM) and Coulomb respectively. This modelling computation is essential for determining the electric field distribution around the HV conductor and the transducer, facilitating the transducer development and enabling prediction of transducer characteristics and performance. Furthermore, the computation of the electric field distribution was used to calibrate the transducer and determine the geometric capacitance (C_T) of the voltage transducer.

Software of this type is one of multiple essential means used to study electromagnetic

problems analytically due to its ability to model complex geometry. For instance, C.A. Gerrard et al. [3.1] reported that Feldman et al. [3.2] used finite element models (FEM) to select optimum placement positioning for an electric field sensor in order to estimate the potential of an overhead line. The computation models are based on the actual single-phase laboratory experimental configuration for ease of comparison with experimental results.

The SLIM software used in the present research work has been licensed for educational purposes, so it only allows for a maximum of 1500 nodes, as shown in Appendix 3.1. Due to this limitation, up front and careful planning was required during model development to optimise the accuracy of the simulation results. The accuracy of the simulation results can be controlled by manually increasing mesh density on the model. On the other hand, Coulomb (3D) modelling requires more time and higher computer performance and capacity for simulation when compared with two-dimensional (2D) modelling due to the complexity of the model and the simulation process. Nonetheless, both software packages are commonly used in the HV engineering sector (such as power transmission and distribution) for electric field analysis in order to improve product design and reduce development time and cost.

3.4.1 Two-Dimensional Model of Voltage Transducer

The finite element software (SLIM) was used to model the transducer in an X-Y geometry modelling representation. The model was used to simulate a vertical section of the HV conductor, with the voltage transducer placed around it in close proximity. Geometries of single- and three-phase overhead line configurations were modelled based on the actual experimental measurement setup arrangement, as elaborated in the following subsections.

3.4.1.1 Single-Phase Model

Figure 3.5 shows the 2D model as simulated in SLIM, with the boundary area spanning 10m by 10m and the transducer placed at 2.5m above the ground level, which is measured from the centre of the HV conductor. Within the simulation software, the entire space is meshed into a set of triangular elements, set as free space and labelled as "Air" – except for the HV conductor, the sensing probe and the guard electrode. The HV conductor and the guard electrode are connected together and assigned a high potential (H_i), whilst the ground surface is assigned a low potential (L_o). The sensing probe (S_p) is represented by a foil, which acts as a floating electrode. An initial simulation was carried out using the generated model in free space in order to evaluate the computed geometric capacitance (C_T) of the transducer (between the HV conductor and the sensing probe surface) with respect to the ground surface.

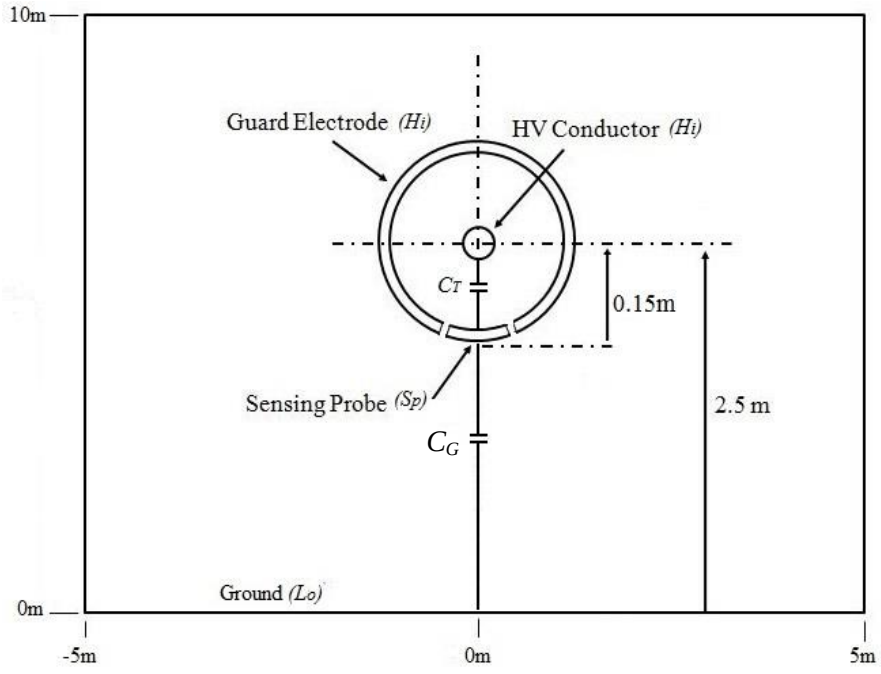

Figure 3.5: Single-phase modelling based on laboratory experiment configuration (not to scale).

3.4.1.2 Three-Phase Model

Figure 3.6 shows the 2D model for three-phase overhead line representation based on an 11kV three-phase wood pole configuration, as shown in Figure 3.7. The HV conductors have a diameter of 16.75mm and are labelled as *a*, *b* and *c* respectively, with a distance of 1.2m between them. The sag consideration should be set to the minimum level permitted so that a minimum height of 7.5m above ground is guaranteed. Thus, taking the 0.15m radius of the voltage transducer into account, a minimum of 7.65m is measured from the centre of the conductor. Similar to the single-phase model within the simulation software, the entire space is divided into a set of triangular mesh elements and assigned as free space except for the HV conductor, the sensing probe and the guard electrode.

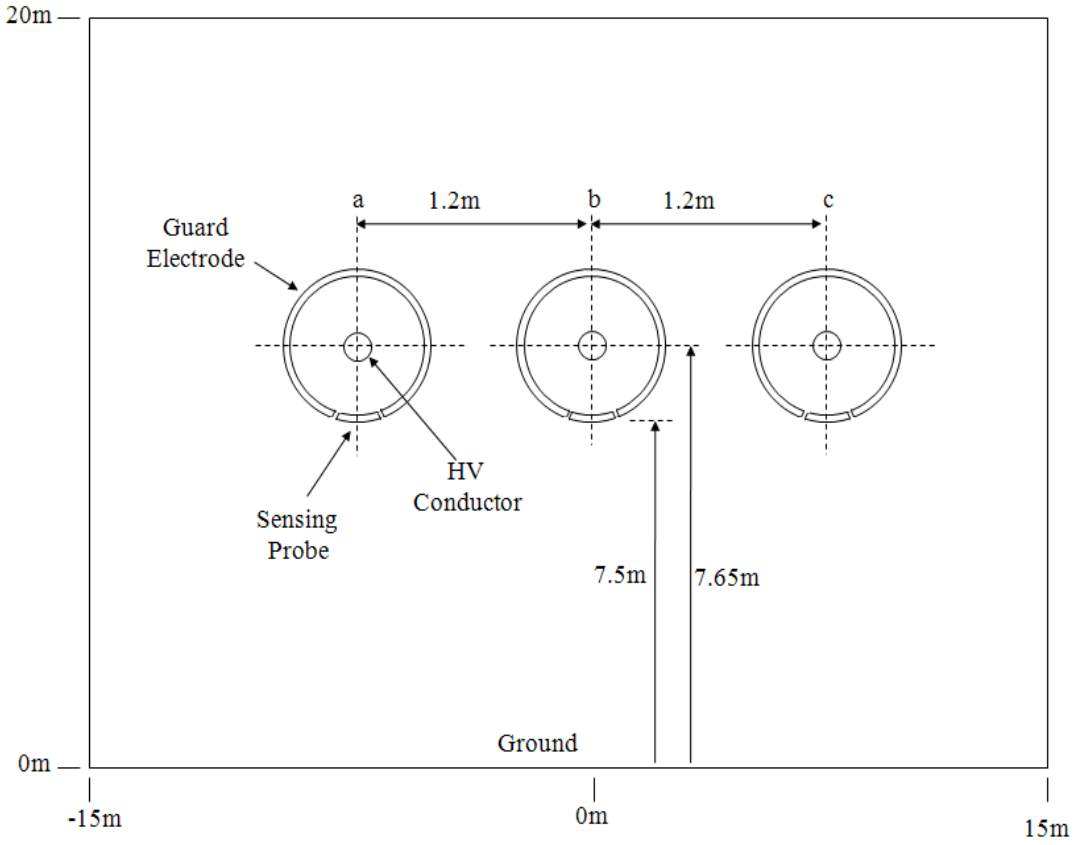

Figure 3.6: Three-phase 2D modelling representation (not to scale).

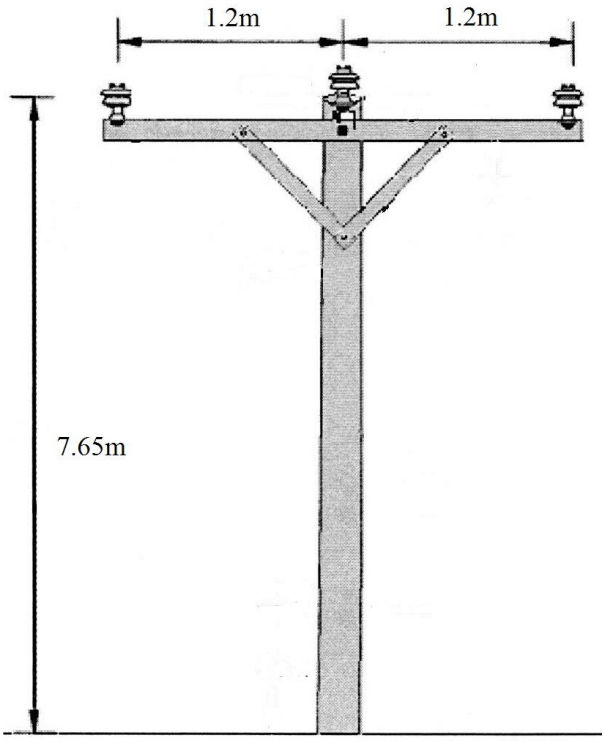

Figure 3.7: Three-phase wood pole overhead lines configuration (not to scale).

3.4.2 Three-Dimensional Model

The boundary element method (Coulomb) is used to model the voltage transducer in 3D configurations as shown in Figure 3.8 with a defined measurement for the length of the transducer, the HV conductor and the sensing probe. Figure 3.9 shows the enlarged view of the voltage transducer and the HV conductor (as identified within the dashed circle line in Figure 3.8).

The initial stage of the 3D modelling process involved specifying the coordinates of various key nodes of the geometry. The physical boundaries with their assigned potentials were then defined, and the surfaces were meshed into triangular elements. This enabled simulation to be carried out, in addition to computation of the electric field profile on the sensing probe surface. Similar to the 2D modelling, the initial simulation was used to evaluate the geometric capacitance (C_T) of the transducer, and this

capacitance was subsequently compared with the results from the 2D modelling, as well as the analytical results.

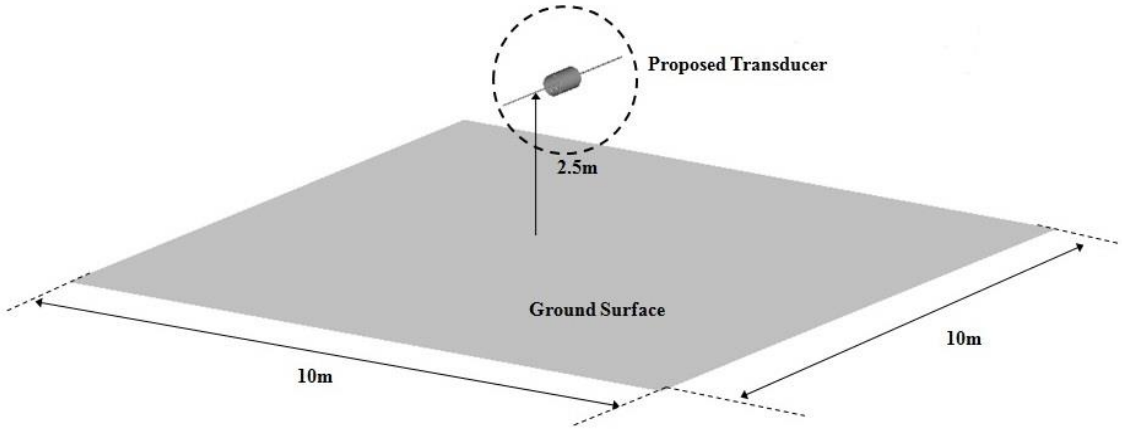

Figure 3.8: 3D model configuration computed in Coulomb.

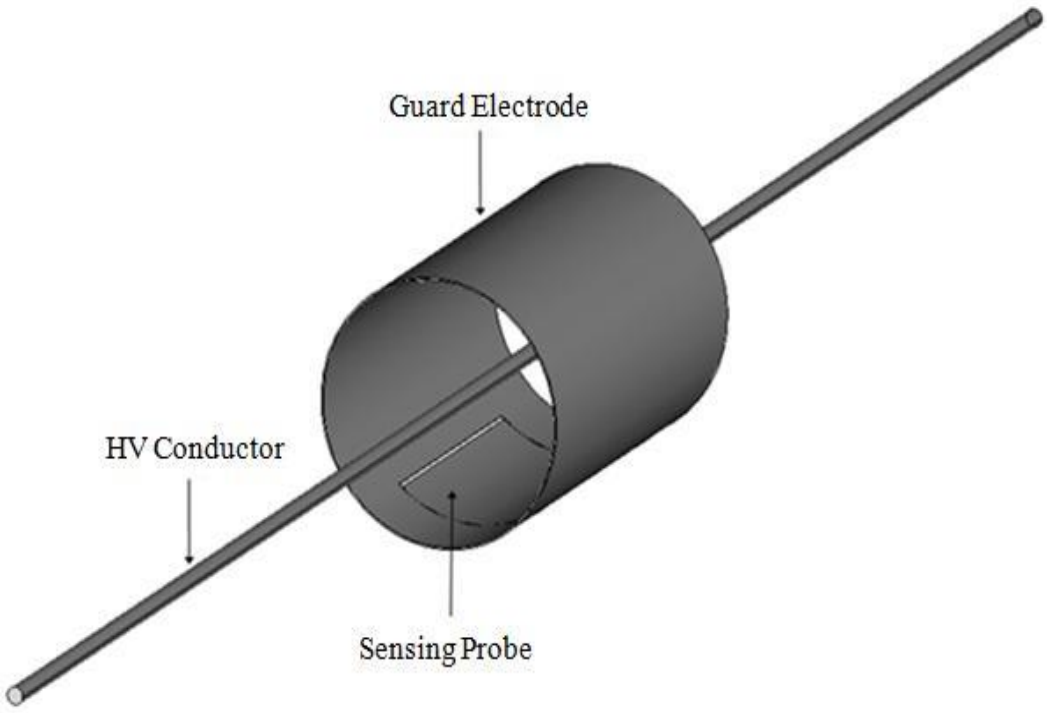

Figure 3.9: Zoom-in detail of the voltage transducer and the HV conductor.

3.5 SIMULATION RESULTS

3.5.1 Two-Dimensional Simulation Results

3.5.1.1 Single-Phase Simulation Results

The simulated equipotential distribution around the transducer and the HV conductor using SLIM is displayed in Figure 3.10. As can be observed, the equipotential contour lines indicate that the electric field around the HV conductor is expected to be high.

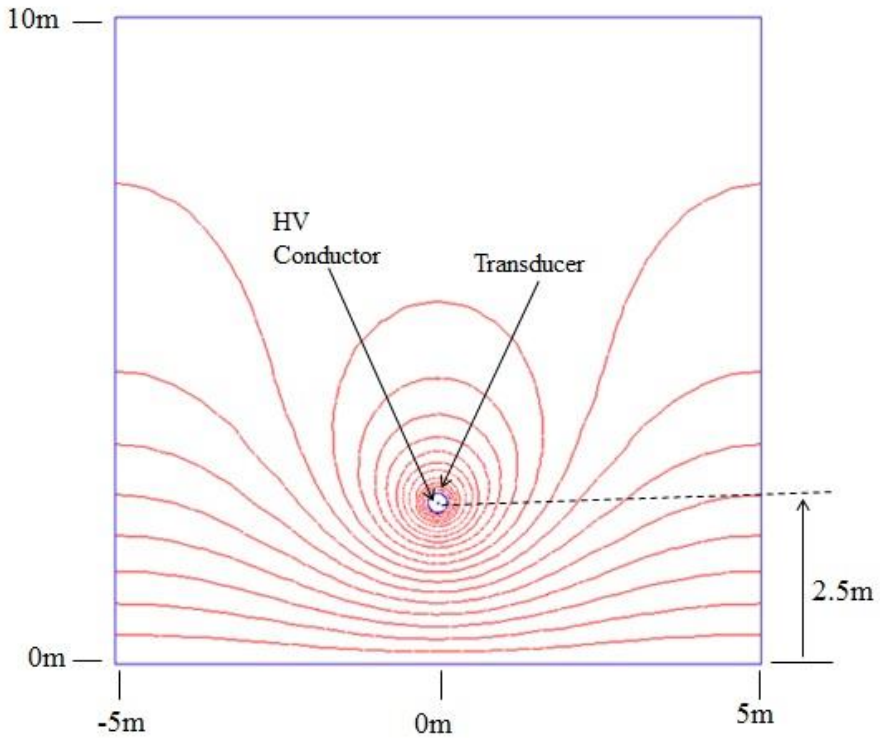

Figure 3.10: The equipotential distribution generated around the HV conductor and the transducer (not to scale).

Figure 3.11 plots the electric field magnitudes along the width of the sensing probe surface (as shown in Figure 3.12) when the applied voltage is set to 1kV alternating voltage on the HV conductor. These magnitudes are then used to calibrate the transducer and calculate the geometric capacitance of the voltage transducer. End-effects could be seen in the form of increasing field magnitudes appearing towards the edges of the sensing probe, with the peak value reaching approximately 8kV/m. This is mainly caused by the proximity of the sensing probe edges to the guard electrode.

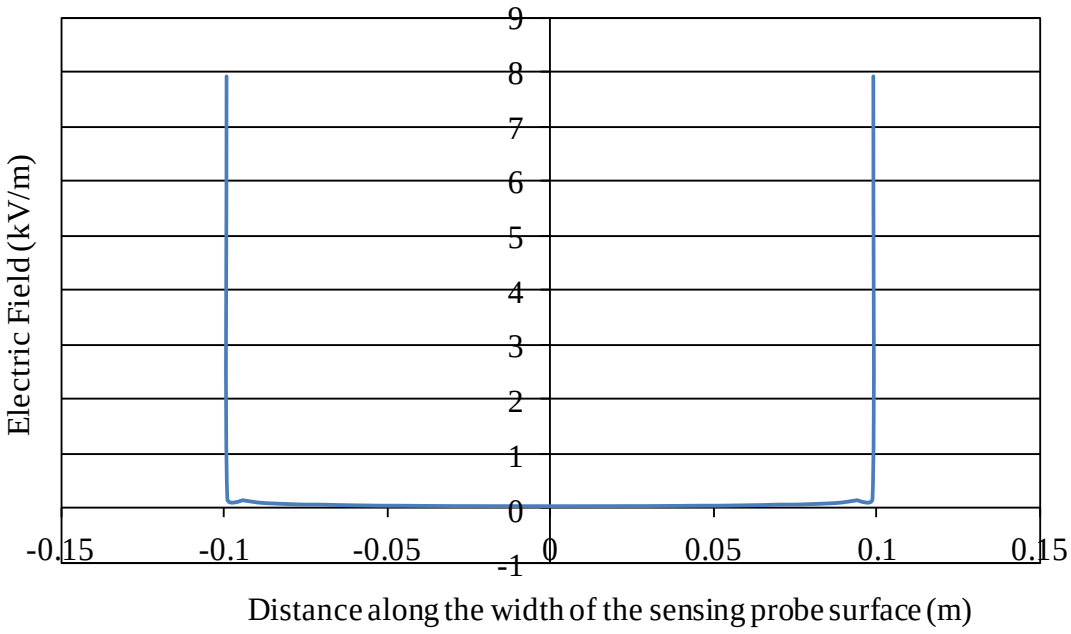

Figure 3.11: Electric field profiles along the surface of the sensing probe.

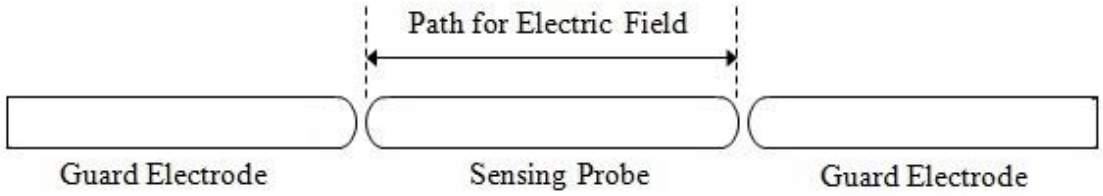

Figure 3.12: Path for electric field magnitude along the surface of the sensing probe.

The simulation incorporates the assumption that the lengths of the guard electrode, the HV conductor and the sensing probe are infinite since the model is constructed in 2D geometry. In order to generate the corresponding results for the whole probe surface, and assuming that the same profile of the field exists on the surface, a Matlab routine is developed to generate the field values, as depicted in Figure 3.13. Using the field values of Figure 3.13, the induced charge (Q) on the probe surface is computed through the integration of the electric field magnitudes over the entire probe surface area, and the computed charge determined in this way is approximately 0.13nC.

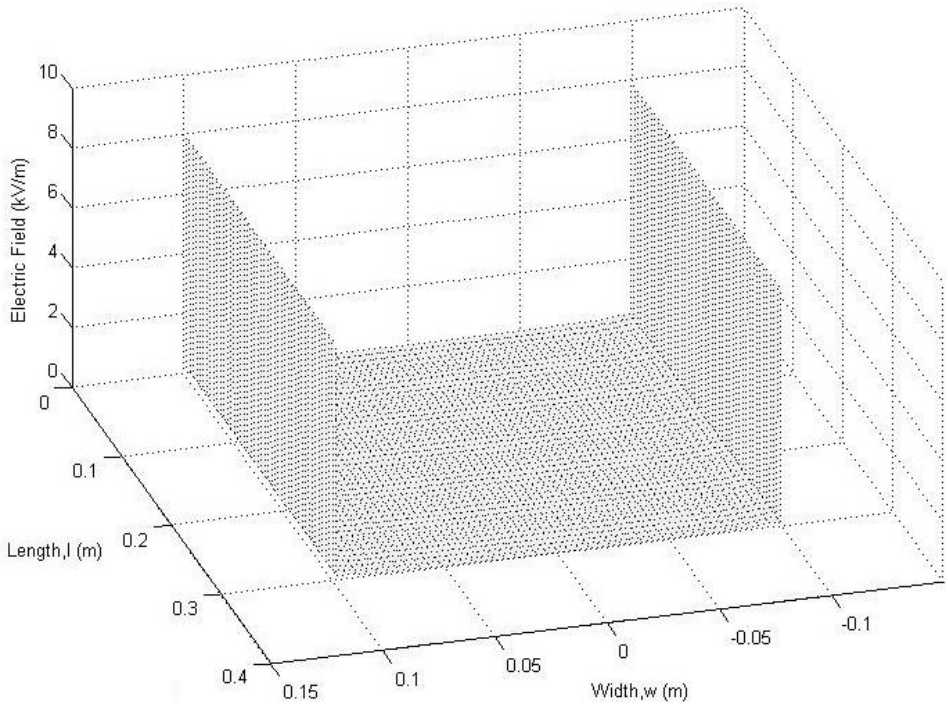

Figure 3.13: Matlab generated electric field distribution on the sensing probe surface.

The developed algorithm of the Matlab routine is listed in Appendix 3.2.

3.5.1.2 Three-Phase Simulation Results

For the three-phase overhead line modelling configuration, the three voltage transducers are in the same vicinity. Therefore, the effect of stray capacitances between the transducers needs to be determined and evaluated. The value of the capacitance between the HV line and sensing probe must be high enough to reduce the effects of the stray capacitances. Figure 3.14 shows that the relationship between the network of capacitances of the transducer and the output voltages (V_1, V_2 and V_3) from the transducers and the phase voltages as given by Equation (3.8),

$$\begin{bmatrix} V_1 \\ V_2 \\ V_3 \end{bmatrix} = \begin{bmatrix} C_{1a} C_{1b} C_{1c} \\ C_{2a} C_{2b} C_{2c} \\ C_{3a} C_{3b} C_{3c} \end{bmatrix} \begin{bmatrix} V_a \\ V_b \\ V_c \end{bmatrix} \tag{3.8}$$

Where:

V_1, V_2 and V_3 are the output voltage of the each transducer respectively,

C_{1a}, C_{2b} and C_{3c} are the integrating capacitance of transducers,

C_{1b}, C_{1c}, C_{2c} and others are the stray capacitances between the transducers,

V_a, V_b and V_c are the HV conductor phase voltages.

However, in this case the HV conductors are used as reference, hence the capacitances to ground (C_{1G}, C_{2G} and C_{3G}) can be omitted.

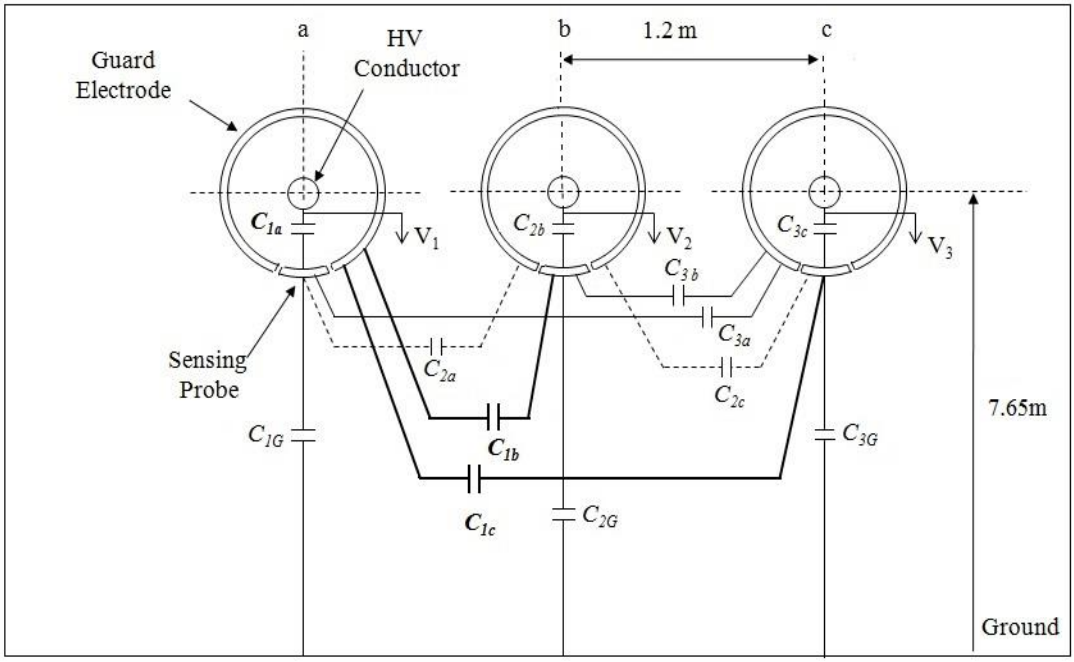

Figure 3.14: Stray capacitances network for three-phase modelling configuration.

The effect of stray capacitances (as stated in Equation (3.8)) is simulated by assigning a high potential (H_i) to one of the HV conductor phases and the guard electrode, while the others are assigned a low potential (L_o) as shown in Figure 3.15. This process is repeated for each of the phases and the transducer in turn, in order to generate a matrix capacitance as stated in Equation (3.9) and using the model as shown in Figure 3.14.

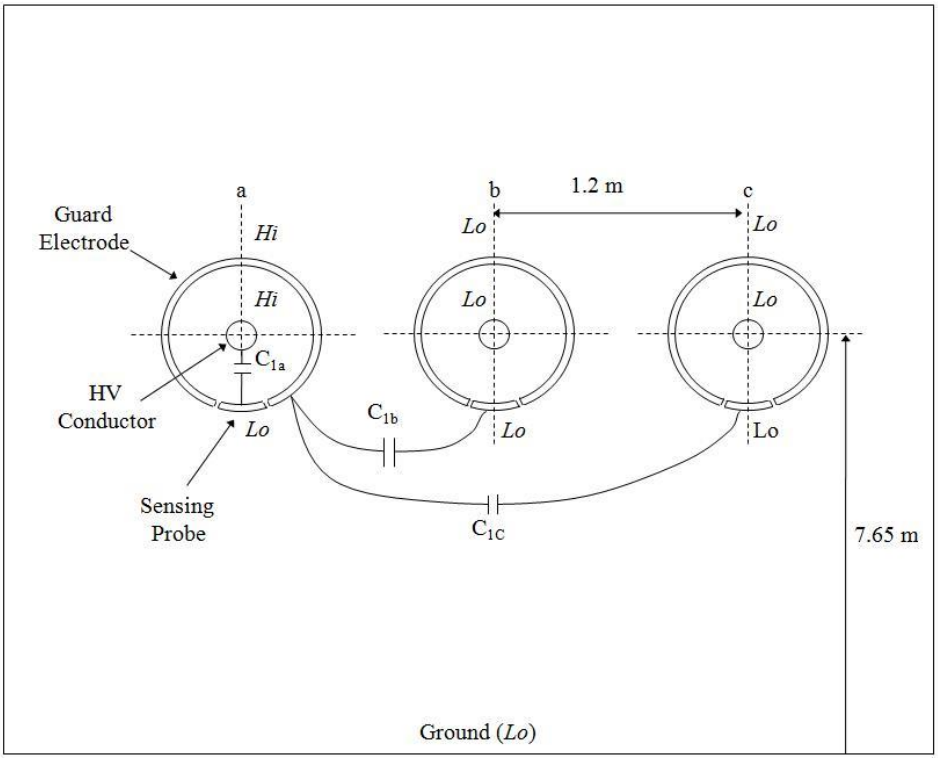

Figure 3.15: Computational of stray capacitances network for three-phase modelling.

$$C = \begin{bmatrix} C_{1a} & C_{1b} & C_{1c} \\ C_{2a} & C_{2b} & C_{2c} \\ C_{3a} & C_{3b} & C_{3c} \end{bmatrix} \tag{3.9}$$

The above matrix in Equation (3.9) is calculated to determine the geometric capacitance for the transducer at the energised conductor phase C_{1a}, and also the stray capacitances from un-energised conductors (phase b and phase c; C_{1b} and C_{1c} respectively). The capacitance C_{1a} value is calculated using the computed electric field value on the sensing probe surface, but C_{1b} and C_{1c} utilise the computed electric field obtained from the outer surface of the sensing probe of the transducers that are modelled at phase b and c respectively. These capacitance values are calculated based on Equation (3.5) and Equation (3.7) respectively. A similar process is repeated to calculate the remaining capacitance values for phase b and phase c.

The computed matrices for stray capacitances (based on Equation (3.9)) of the 11kV

three-phase overhead line (as shown in Figure 3.14) are given as:

$$C = \begin{bmatrix} 10 & 0.24 & 0.08 \\ 0.24 & 10 & 0.24 \\ 0.08 & 0.24 & 10 \end{bmatrix} \quad [pF] \tag{3.10}$$

This matrix is obtained when the model is injected with 1V input voltage, and the 10 pF matrix diagonal value corresponds to the geometric capacitance of the energised high voltage conductor and transducer. The effect of the stray capacitance [i.e., C_{1b}, C_{1c} ,C_{2c} and others] of the neighbouring transducer is relatively low compared to the geometric capacitance of the voltage transducer, and can be treated as negligible. It was verified that the further away the un-energised transducer is from the voltage source, the lower the stray capacitances are. Hence, a symmetrical capacitance matrix is produced. Figure 3.16 shows the computed equipotential distribution when the middle conductor (b) and transducer are set to high (H_i) potential. Most of the electric equipotential are concentrated around the middle conductor.

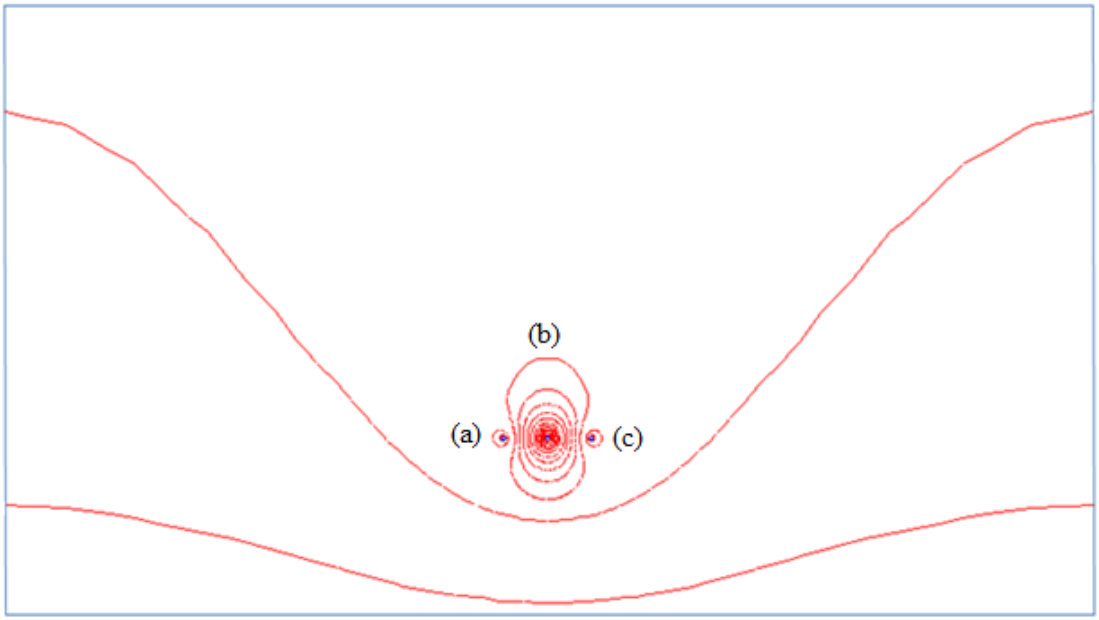

Figure 3.16: Equipotential contours on a three-phase overhead line configuration when the centre conductor and the transducer are energised while the other conductors are set to zero volts.

It should be highlighted that the above finding contrasts with the formerly developed non-contact capacitive voltage probe for the three-phase system, as described in Chapter 2, Section 2.6 (Figure 2.11). The developed voltage transducer measurement will not be affected by adjacent phase stray capacitances when dealing with three-phase overhead lines, because the transducers are directly connected to the HV conductor instead of the ground. Furthermore, the need to consider the optimum position during the installation of the transducer can also be omitted.

3.5.2 Three-Dimensional Simulation Results

Using the 3D BEM software, the magnitudes of the electric field on the sensing probe surface were computed. As expected, a high magnitude electric field was found towards the edges of the sensing probe, which is attributed to the end-effects discussed in the case of the 2D simulation, subsection 3.5.1.1. The electric field magnitude profile computed along the centre line of the sensing probe surface is shown in Figure 3.17.

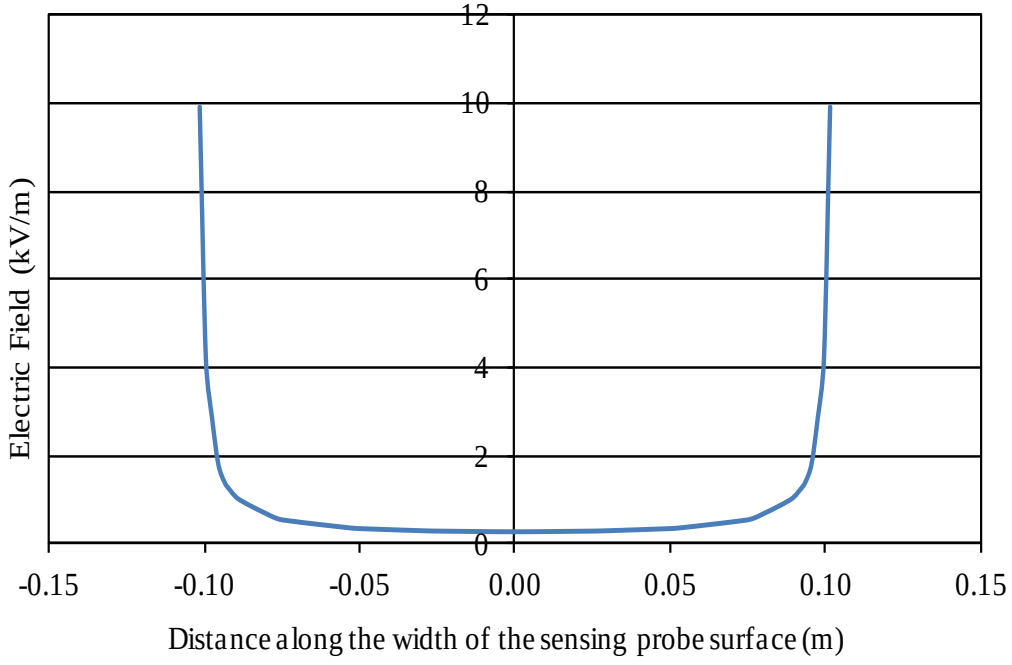

Figure 3.17: Electric field magnitude obtained along the centre of the sensing probe, computed using 3D model.

As can be observed in the figure, the end-effect at the edges of the probe is present, and is approximately 10kV/m when an input of 1kV alternating voltage is applied. Using the field values of Figure 3.17, the total induced charge (Q) on the sensing probe surface using these results is calculated as 0.86nC. The higher value obtained with the 3D model is attributed to the accuracy of the simulation model, which included the actual length of the sensing probe and the HV conductor.

3.6 EVALUATIONS OF VOLTAGE TRANSDUCER USING ANALYTICAL AND COMPUTATIONAL APPROACH

Using the computed electric charge value obtained on the sensing probe surface as presented for two- and three-dimensional modelling (Section 3.5), the computed geometric capacitance (C_T) of the transducers is calculated using Equation (3.5) and Equation (3.7) to be 19.9pF for the 2D model, and 21.7pF from the results of the 3D model.

These computed geometric capacitance values are then compared against the simplified analytical calculation. The simplified analytical approach is based on the coaxial cable configuration, with the assumption that end-effects can be neglected. In this case, the per unit length capacitance can be determined using Equation (3.11) [3.3].

$$C = \frac{2\pi\varepsilon_0}{\ln\frac{b}{a}} \quad \text{[F/m]} \qquad (3.11)$$

Where:

ε_0 is the permittivity of free space (8.854×10^{-12} F/m),
a is representing the radius of the HV conductor,
b is representing the radius of the transducer (0.15m).

In order to obtain the equivalent capacitance between the sensing probe and the HV conductor, the per unit length capacitance needs to be scaled to the dimension (length

and width) of the sensing probe, as shown in Equation (3.12).

$$C_{equ} = \frac{C\ell w}{2\pi b} \tag{3.12}$$

Where:

ℓ is representing the length of the sensing probe,

w is representing the width of the sensing probe.

However, due to end-effects at the edges of the sensing probe, the extra capacitance within the gap between the sensing probe and the guard electrode needs to be taken into consideration, and is approximated by Equation (3.13).

$$C_{gap} = \frac{\varepsilon_0 A}{d} \tag{3.13}$$

Where:

C_{gap} is the capacitance between the sensing probe and the guard electrode,

d is the air gap between the sensing probe and the guard electrode (1mm),

ε_0 is the free space permittivity,

$A = 2t(\ell + w)$ is the total surface area at the sides of the sensing probe, with t being the plate thickness.

The thickness of the sensing probe is 2mm, and the gap distance between the sensing probe and the guard electrode is 1mm. The total geometric capacitance (C_T) of the transducer is the combination of the surface capacitance as in Equation (3.12) and the air gap capacitance given by Equation (3.12), as shown in Equation (3.14).

$$C_T = C_{equ} + C_{gap} \tag{3.14}$$

Using the transducer's geometry equations as mentioned above, C_{equ} was calculated to be 1.3pF and C_{gap} was 17.7pF, which gives the total geometric capacitance of the transducer as 19pF. These capacitance values compare reasonably well with the computed capacitances using the computational approach, as tabulated in Table 3.1. As can be seen from the table, the geometric capacitance values computed from the models are much higher due to the fact that the analytical approach is based on the simplified coaxial cable approach, with the assumption that the end-effects of electric field fringing at the sensing probe edges are neglected.

Table 3.1: Comparison of the C_T between the analytical and modelling simulation results.

Method	Geometric capacitance, (capacitance between sensing probe and HV conductor, C_T (pF))
Analytical	19
2D model	19.9
3D model	21.7

In order to simulate the added effect of the integrating capacitance (C_i) inserted between the HV conductor and the sensing probe, and in parallel with C_T based on the actual laboratory measurement environment, an equivalent permittivity (ε_r) is used in the simulation model. This value of ε_r is derived by dividing C_i by C_T, as shown in Equation (3.15).

$$\varepsilon_r = \frac{C_i}{C_T} \tag{3.15}$$

Using this approach, the simulation with the new permittivity is used to predict the transducer output voltage generated based on the simulation model configuration. The

equivalent permittivity value is calculated using the measured value of the integrating capacitor (C_i) rather than those indicated by the standard manufacturer value in order to generate computation data as accurately as possible.

Table 3.2 shows computed output voltage values generated from the model simulation corresponding to respective C_i (measured) values. These computed results corresponds to the laboratory experimental configuration when the transducer is placed at 0.1m above the ground and the applied voltage is set to $100V_p$, while changing the value of C_i within the range of 2.03nF to 10.85nF. The computed data (output voltage) is later compared with the laboratory measurement results reported in Chapter 4.

Table 3.2: The computed transducer output voltage.

$C_{i\ \text{manufactured}}$ (nF)	$C_{i\ \text{measured}}$ (nF)	Computed output voltage, V_T (V_p)
2.2	2.03	0.33
3.3	2.98	0.23
4.7	4.22	0.17
6.8	6.24	0.11
10.0	10.85	0.07

3.7 PROPOSED AND CONSTRUCTED CONFIGURATION OF VOLTAGE TRANSDUCER

Figure 3.18 illustrates the configuration of the cylindrical-shaped voltage transducer, which comprises the transducer frame, the guard electrode, the sensing probe and the transducer's shielding cylinder. The diameter and length of the entire transducer are 300mm and 500mm respectively. The sensing probe is 200mm in width and 300mm in length, and this sensing probe is attached to the guard electrode using Polyvinyl Chloride (PVC) material. These two components are separated by an air gap of 1mm. An aluminum sheet was used to fabricate the voltage transducer components (the guard

electrode, the sensing probe and the shielding cylinder as the transducer cover). The thickness of the aluminum sheet is 2mm.

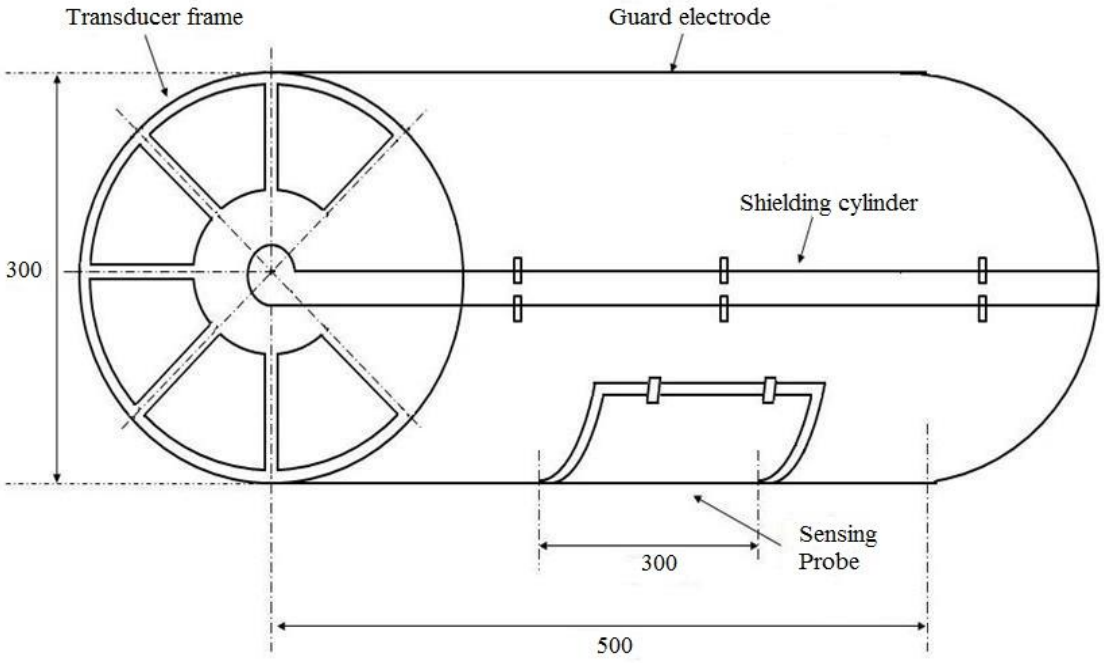

Figure 3.18: Configuration of the cylindrical-shaped voltage transducer (dimension in mm and not to scale).

Figure 3.19 shows the transducer frame configuration, which was constructed using PVC sheeting. This frame is used to support the entire structure of the voltage transducer. However, a portion of the plastic has been removed from the frame (this corresponds to the grey shaded areas) in order to allow for access to the electrical components and further reduce the transducer weight to approximately 4.5kg.

Figure 3.20 shows the actual frame structure of the voltage transducer before it was covered with the guard electrode and the sensing probe. A detailed drawing of the voltage transducer layout (guard electrode and sensing probe) and the relevant dimensions are shown in Figure 3.21. In order to facilitate the installation of the transducer during experimentation, the design also incorporates an opening at the side of the transducer to allow the HV conductor to be easily slotted in and held by the frame. This opening is covered with a cover plate (transducer shielding cylinder) 20mm

in width and 500mm in length, as shown in Figure 3.22. Figure 3.23 shows the top, bottom, side and front views of the actual voltage transducer developed and constructed in this work.

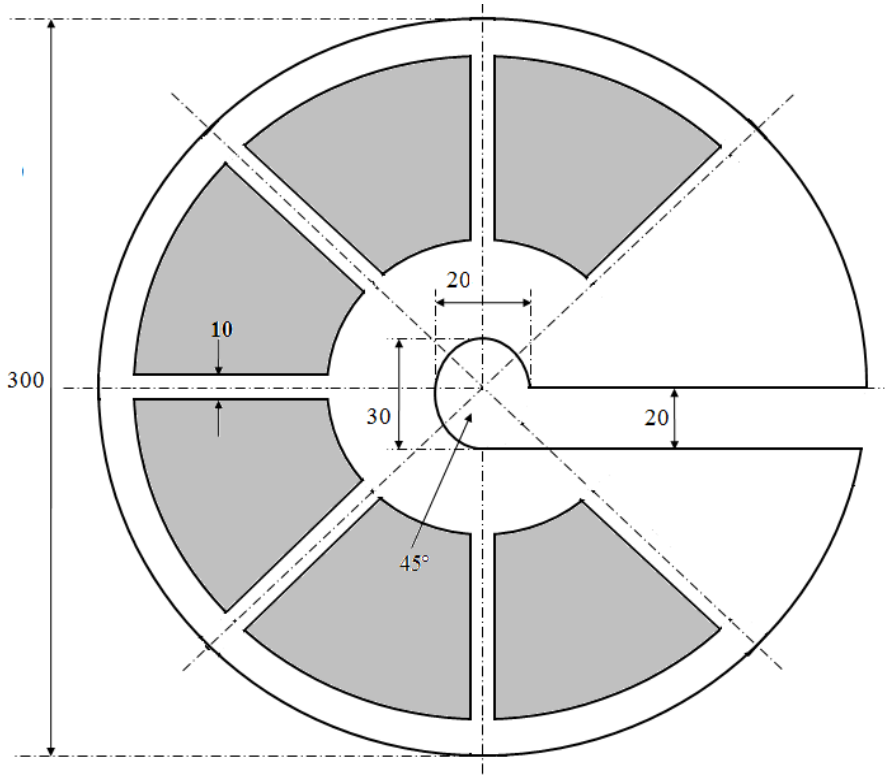

Figure 3.19: Voltage transducer frame (dimension in mm and not to scale).

Figure 3.20: The actual frame of the voltage transducer.

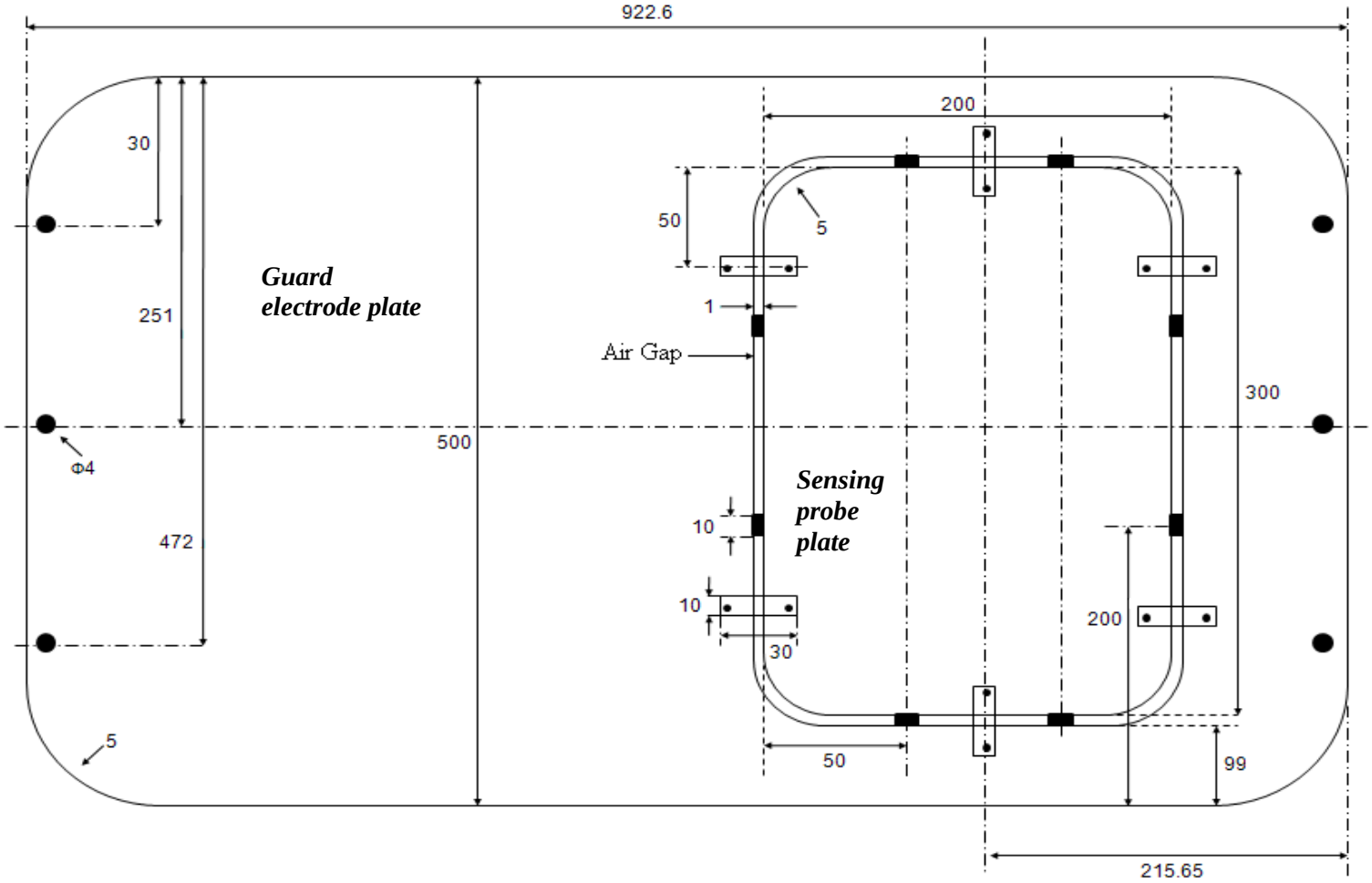

Figure 3.21: Layout of the guard electrode and the sensing probe (dimension in mm and not to scale).

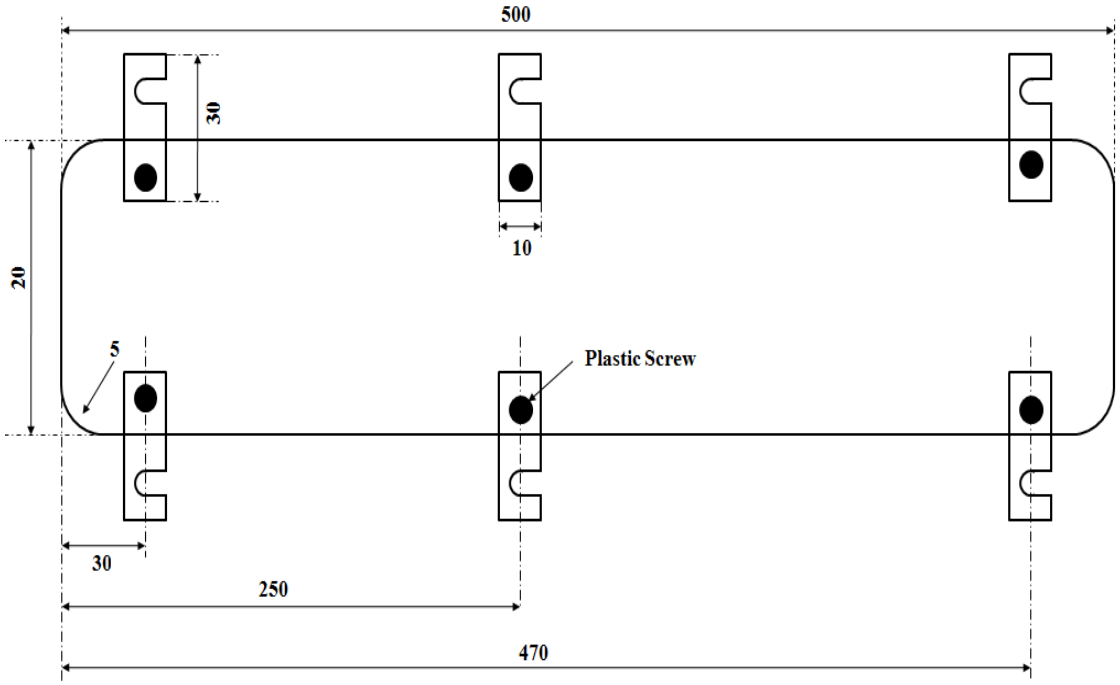

Figure 3.22: Configuration of the transducer shielding cylinder (dimension in mm and not to scale).

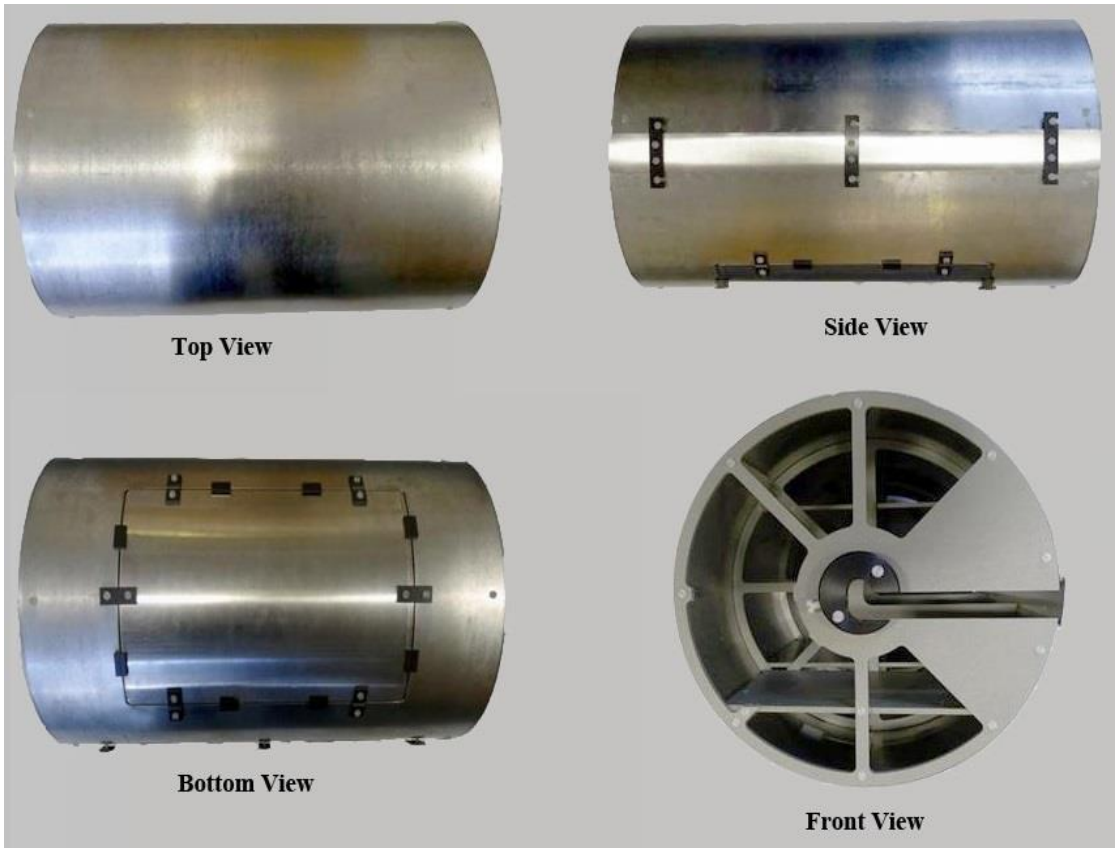

Figure 3.23: Physical figures of the constructed voltage transducer.

3.8 CONCLUSION

This chapter describes the design principles, construction and development of a new voltage transducer. The overall shape is cylindrical in design in order to match the HV conductor shape, thus eliminating any sharp edges that could lead to partial discharge effect. Unlike any previous transducer, it is proposed to locate the transducer near the HV conductor and use the capacitive network created between the probe and the HV and ground to obtain a capacitive divider-type transducer. The transducer utilises a working principle similar to that of the capacitive divider used in the previous non-contact capacitive voltage probe research, but improves on the design by using the HV conductor instead of the ground as the measurement reference. This improves the voltage measurement technique, as the effect of stray capacitances is reduced when evaluating the application of the transducer on three-phase overhead lines.

The modelling of the transducer is carried out in SLIM and Coulomb software packages based on finite and boundary element methods respectively, in which 2D and 3D models are constructed to simulate and evaluate the electric field distribution around the HV conductor and the transducer. The magnitude of the electric field obtained on the sensing probe surface in the simulation model is used to calibrate the transducer by determining the geometric capacitance of the developed transducer model. In addition to the built-in algorithms in both SLIM and Coulomb programs, simplified mathematical equations and a Matlab algorithm are also used to justify the simulation results. The modelling simulation from both the 2D and 3D models produce results that give the geometric capacitance values within an acceptable limit. The 3D model is relatively more accurate when used with a finite-length model, and thus practically closer to the real design of the transducer.

The simulations and analysis for the 2D model involve both the single- and the three-

phase overhead line configuration, but only the single-phase is simulated in the 3D model environment, given that it is shown that stray capacitances from adjacent phases and transducers are negligible (as described in Section 3.5.1.2). These simulation results are later used for comparison with the actual measurement results in Chapter 4.

CHAPTER 4

LABORATORY SET UP AND CALIBRATION OF THE DEVELOPED NEW HIGH VOLTAGE IMPULSE TRANSDUCER

4.1 INTRODUCTION

The developed voltage transducer is tested under a series of laboratory experiments in order to validate the simulation results. In addition, these experiments are also used to study the transducer's characteristics, as well as for calibration purposes, ensuring the practicality of the transducer prior to installing it in the real overhead line environment. Low magnitude impulse voltages are used to evaluate the transducer under lightning and switching impulse shape conditions. Low magnitude ac voltages are also used to corroborate the results obtained from the impulse tests, and to observe the transducer's characteristics under a steady state voltage condition for the calibration process. The effects of variations in the independent variables, namely the applied voltage (V_{in}), the transducer height above ground (*h)* and the use of different values of integrating capacitor (C_i) on the value of output voltage are also investigated. The non-contact capacitive voltage probe is also tested to contrast its approach and compare its output to the developed transducer.

4.2 LABORATORY SETUP

The laboratory experimental setup was based on a single-phase overhead line configuration for ease of testing and calibration. This experimental is conducted with a low magnitude impulse voltages applied to the measurement setup. The impulse voltages were according to the impulse voltage standard (described in Section 2.4). The low ac input voltage is then applied to validate the impulse test by comparing the

voltage magnitudes.

4.2.1 Physical and Circuit Arrangements for the Developed Transducer

Figure 4.1 shows the schematic diagram of the measurement setup used for the laboratory experiments. The setup is composed of the developed transducer, the surge generator (Haefely Surge Generator type 481), the HV divider and the optical fibre system. The surge generator is the source for the low-magnitude impulse voltage supplied to the test circuit. The optical fibre system is used to transfer the measurement data from the transducer to the digital storage oscilloscope (DSO). Voltage measurements are carried out using the transducer, and the measurement data are compared with the standard HV divider measured values.

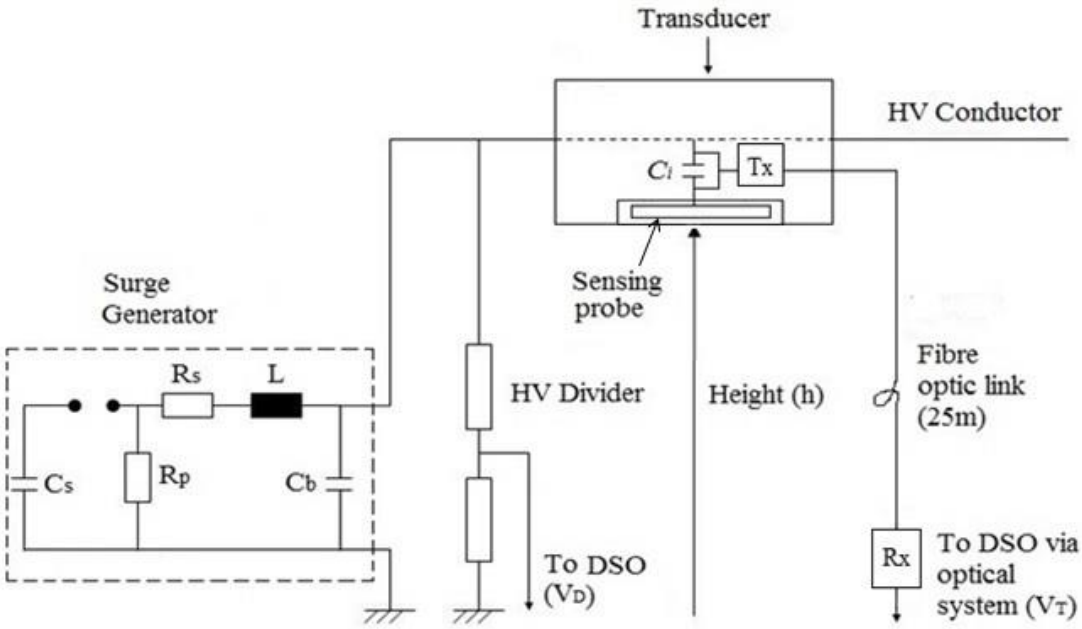

Figure 4.1: Schematic diagram of laboratory measurement setup for developed transducer.

Figure 4.2 shows the assembled transducer deployed in the experiment. As can be seen in the figure, the developed transducer is placed around a galvanised pipe, which acts as the HV conductor. Both ends of the transducer are shielded with aluminium foil that is attached to the guard electrode. The guard electrode and shield are connected to the HV line, hence, the electric field distribution within the inner space of the transducer is

controlled in order to limit fringing effects.

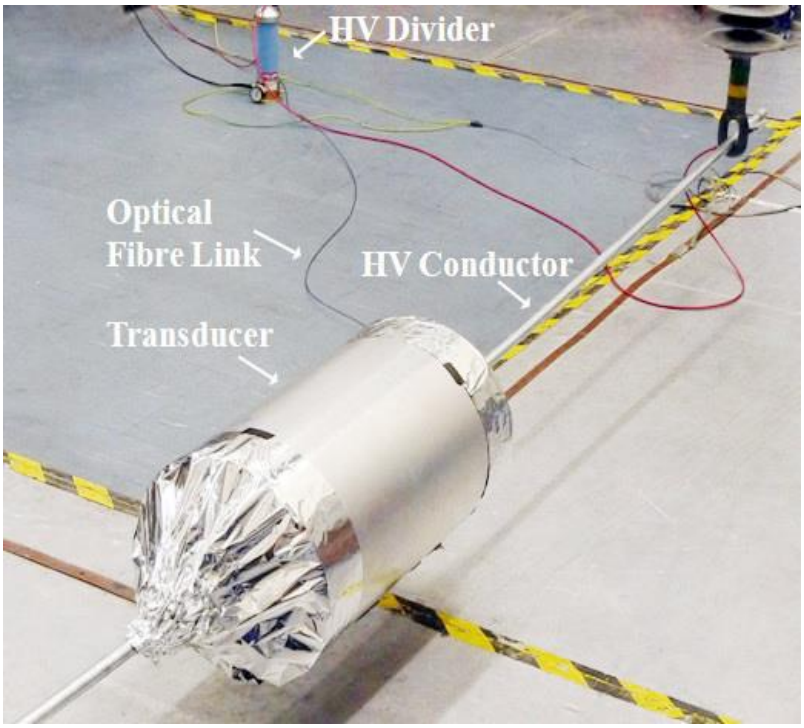

Figure 4.2: The developed transducer mounted on the HV conductor.

The experiments were carried out by inserting the integrating capacitor (C_i) between the HV conductor and the sensing probe, while the input to the optical fibre system (described in Section 4.3.1) was connected across the integrating capacitor (C_i) and used to transmit the measurement data. Furthermore, the optical fibre system also acted as an additional measure of protection by electrically isolating the measurement system from the HV area.

The low magnitude impulse voltages were injected and controlled using the surge generator. The amplitude calibration obtained from the impulse experiment was further verified with experiments using low ac voltage applied through a variac. To quantify the range of operation of the developed transducer, measurements were carried out for a value of C_i and varied within the range of 2.03nF to 10.85nF, along with an increase in the transducer's height above ground 0.1m to 0.5m, with 0.1m step increments measured from the sensing probe to the ground surface.

4.2.2 Physical and Circuit Arrangements of the Non-Contact Capacitive Voltage Probe

The non-contact capacitive voltage probe (NCCP) described in Section 2.6 was also tested in the laboratory experiment in order to contrast and distinguish the measurement technique of this probe and the developed new impulse voltage transducer, as well as to verify the computation results (described in Chapter 3, Section 3.2).

Figure 4.3 shows a diagram of the measurement setup, which is similar to the developed transducer mentioned in the previous section, except that the probe is placed underneath the HV conductor and the ground potential is used as the measurement reference. Figure 4.4 shows the actual probe tested in the laboratory experiment.

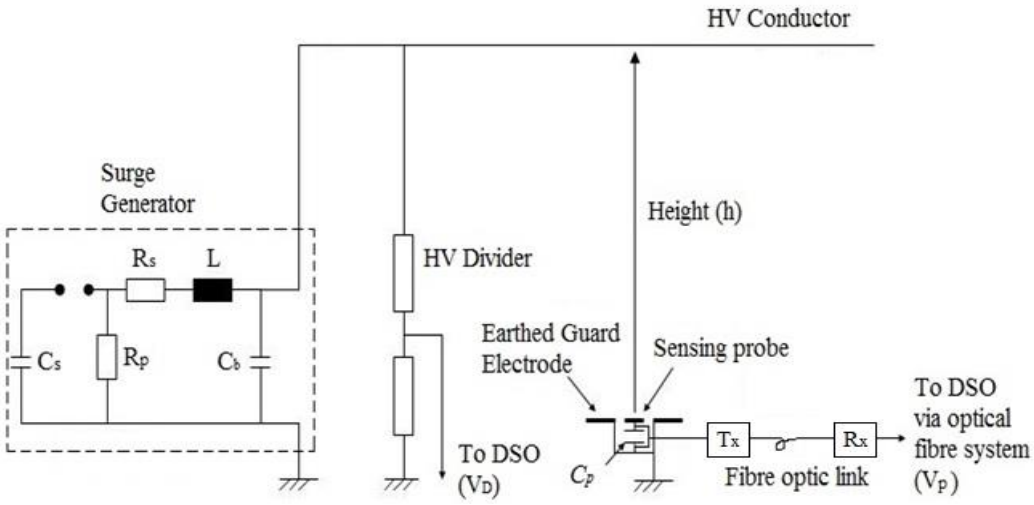

Figure 4.3: Schematic diagram of the non-contact capacitive voltage probe measurement setup.

Test procedures similar to those used for the developed transducer were repeated for this experiment. The measurement system was injected with a low magnitude impulse voltage using the surge generator, and the amplitude was verified with a low ac voltage test using the variac. However, only the height of the HV conductor above the probe surface was evaluated due to the fact that the low voltage arm capacitor, C_p (indicated with dashed circle lines) is permanently soldered to the printed circuit board (PCB), as shown in Figure 4.5. The height was varied from 0.1m to 0.5m in increments of 0.1m.

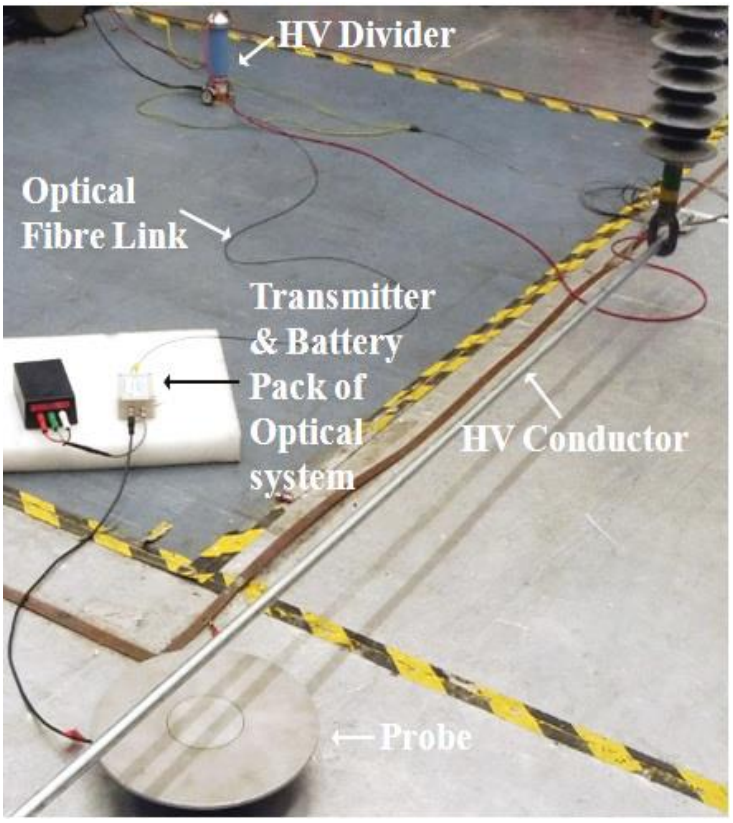

Figure 4.4: The actual measurement setup of the non-contact capacitive voltage probe.

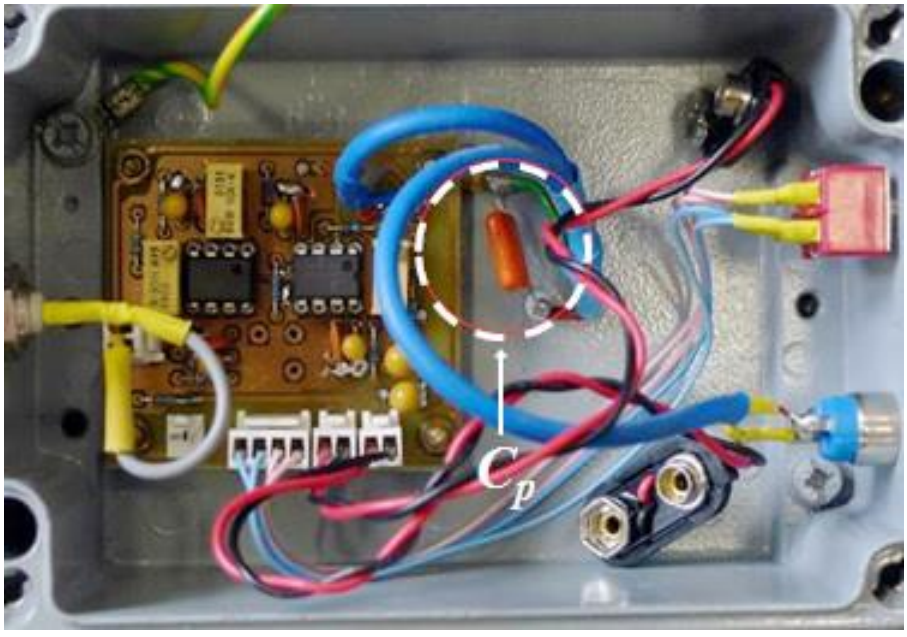

Figure 4.5: The low voltage arm capacitor (C_p) indicated with the dashed circle lines.

4.3 LABORATORY TEST EQUIPMENT

Various types of equipment were used in the laboratory experiment, such as an optical fibre system, a LeCroy digital storage oscilloscope (DSO), a standard HV divider, a variac and the surge generator. Some of this equipment needed to be calibrated prior to installation in the measurement setup in order to improve the accuracy of the measurement results. Details regarding the various laboratory equipment used, their working principles and the calibration process are discussed in the following subsections.

4.3.1 Optical Fibre System

An optical fibre system is used to transfer measurement data from the voltage transducer to the DSO. It also serves as a protection scheme, as fibre optics have the ability to isolate electrically the measurement setup and decouple the high voltage and low voltage sides, further eliminating ground loop problems [4.1]. A non-commercial optical fibre system [4.2], developed at Cardiff University and built at Korea Maritime University is used in this present work, and the actual components are shown in Figure 4.6.

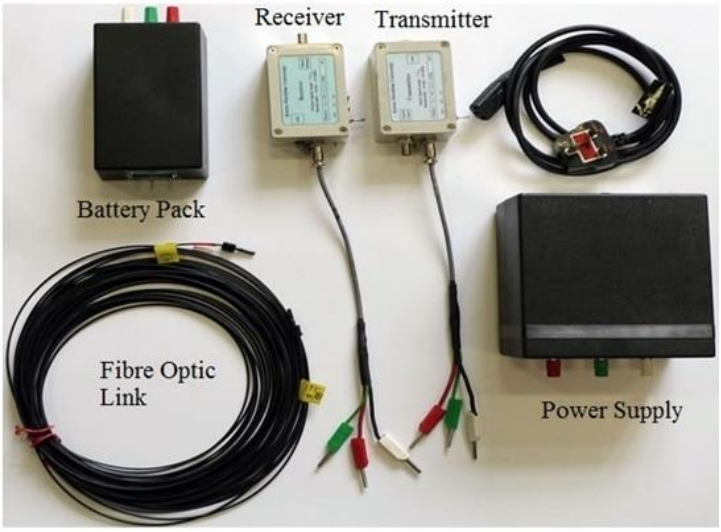

Figure 4.6: An optical fibre system developed at Cardiff University and constructed at Korea Maritime University.

The system consists of a transmitter (T_x), a receiver (R_x), a fibre optic link (25m), a power supply and a $\pm 9V_{DC}$ rechargeable battery pack made from a combination of six $1.5V_{DC}$ batteries. The transmitter is a stand-alone unit battery powered with an input signal range of $1V_{p\text{-}p}$, while the receiver has an output signal range of $5V_{p\text{-}p}$, although both devices have the same frequency bandwidths of 10Hz to 10MHz.

This optical fibre system required a calibration before incorporating it with the developed transducer in order to determine the system gain, denoted as the voltage peak to peak output to input ratio (V_o/V_{in}) and also to monitor the performance of the DC batteries. A simple calibration test setup was developed and setup using a Farnell function signal generator (FG3) and a DSO. These devices (FG3 and DSO) were connected to the transmitter and receiver respectively, while a Fluke digital multimeter was directly connected to the battery pack to measure the voltage level. The output voltage, (V_o) obtained from the receiver of the optical fibre system was approximately 0.26 $V_{p\text{-}p}$ when an applied voltage, (V_{in}) of $1V_{p\text{-}p}$ was supplied from the generator, as shown in Figure 4.7.

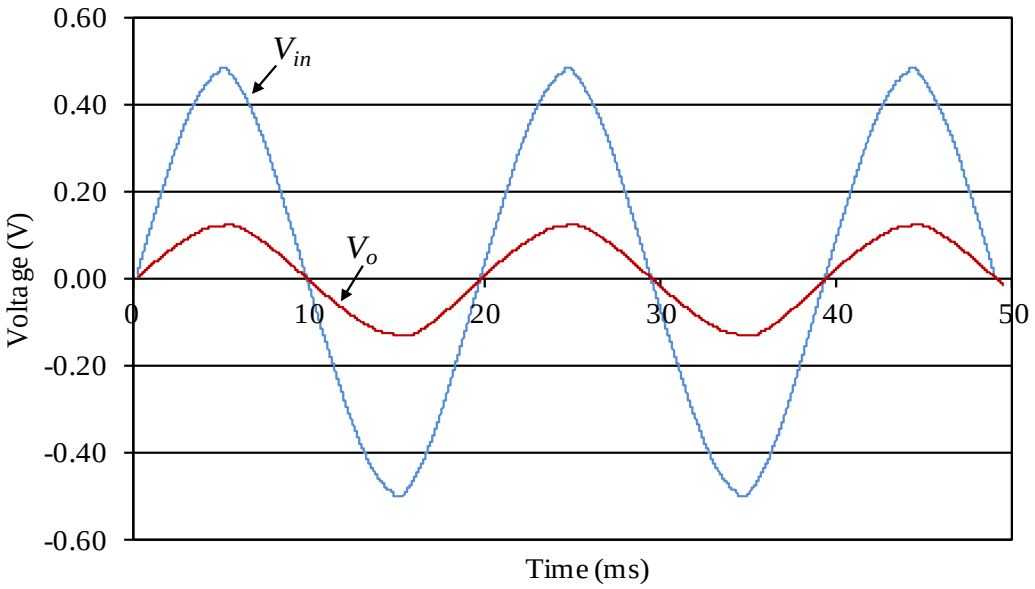

Figure 4.7: An optical fibre system calibration result.

The measurement tolerance between the input and output voltage is approximately 74%. The average system gain of the fibre optic system was approximately 0.26, as accumulated from a 15-hour continuous test with readings taken at one-hour intervals. Simultaneously, the battery performance was also monitored via the multimeter from its fully charged state, with a reading of $10.5V_{DC}$ until the batteries drained out. Figure 4.8 displays the plots of the battery performance and gain of the optical fibre system against time. The system gain dropped slightly within the first two hours, but remained constant at just above 0.25 thereafter until hour 12 of the test, when the gain suddenly rose a little before falling dramatically to zero. This is clearly linked to the battery status. The battery voltage, on the other hand, gradually decreased within the first 12 hours, but declined asymptotically afterwards. Based on the calibration results, the sensible duration to carry out an experiment with a considerably stable battery performance is 12 hours from the battery's fully charged state.

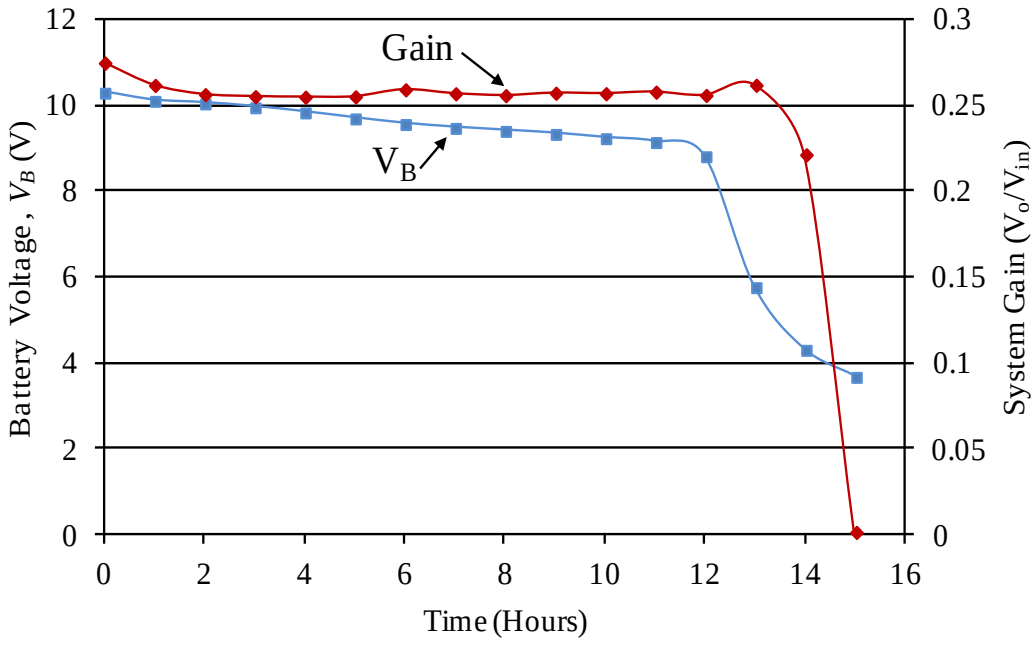

Figure 4.8: Battery performance and system gain obtained from a 15-hour continuous test.

For the actual experiments, the measured output voltage from the DSO needed to be divided by a ratio of 0.26 in order to reflect the actual measurement value, as the maximum input range permitted by the transmitter is around $1V_{p-p}$, and there is concern of malfunction or damage if the system specifications are exceeded.

4.3.2 Digital Storage Oscilloscope

A LeCroy Wavejet 314 digital storage oscilloscope (DSO) was used to monitor and record the measurement data obtained from the experiments. It consists of four input channels with specifications of 100MHz bandwidth and 1.0Gsa/sec of acquisition for a single shot sample rate per channel. The DSO can save the measurement data into a memory stick through a universal serial bus (USB) connector, thus enabling the data to be accessed later for further analysis.

4.3.3 Variac

A Regavolt variable transformer (or variac) with manual control to vary the output voltage from 0V to 240V was used to regulate the supply of AC voltage.

4.3.4 High Voltage Divider

A standard HV divider (model VD45-8) manufactured by Ross Engineering Corporation was used to compare the measurement data of both the input and output voltages obtained from the voltage transducer. The divider is a combination of resistive and capacitive types with a manufactured ratio of 1000:1. A simple calibration test consisting of the divider, a variac and an oscilloscope (DSO) was carried out beforehand to verify the given manufactured ratio.

4.3.5 Surge Generator

A Haefely recurrent surge generator (RSG 481) was used to generate low impulse voltages in the measurement system. The surge generator consists of an impulse

capacitance (C_s), a series resistor (R_s), a parallel resistor (R_p) and inductance (L) and load capacitance (C_b) components. Different amplitudes and impulse shapes can be produced by manually tuning the value of these circuit components within their respective limits. The generator can produce an output voltage in the range of $0V_p$ to $400V_p$.

4.4 LABORATORY EXPERIMENTAL RESULTS

Laboratory experiments for the developed impulse transducer and the non-contact probe (NCCP) were carried out by applying low-magnitude impulse and ac voltages to the HV conductor. Comparison of the measurement output voltage with a standard divider was performed in each case. The impulse transducer experiment is conducted by varying the value of the measured integrating capacitor (C_i) and the height of the HV conductor above ground from 2.03nF to 10.85nF and from 0.1m to 0.5m respectively. However, for the non-contact probe test the low voltage arm capacitor (C_p) was fixed due to the fact that the capacitor is permanently soldered onto the printed circuit board (PCB) as mentioned in Section 4.2.2.

4.4.1 Measurement under Different Voltage Types

4.4.1.1 New High Voltage Impulse Transducer

Figure 4.9 and Figure 4.10 show the measured output voltages obtained from the developed transducer for lightning and switching impulse voltage tests respectively. The measured transducer output voltages (V_T) shown in the figures are obtained for an integrating capacitor (C_i) of 10nF when inserted between the HV conductor and the sensing probe, and for a height above ground of 0.1m, measured from the outer sensing probe surface to the ground. As can be seen, when a peak applied voltage of $200V_p$ is supplied to the HV conductor, a maximum output voltage of approximately $0.15V_p$ is measured from the transducer for both cases. Similarities in shape and magnitude are

also measured for a range of impulse shapes, from slow to fast fronts.

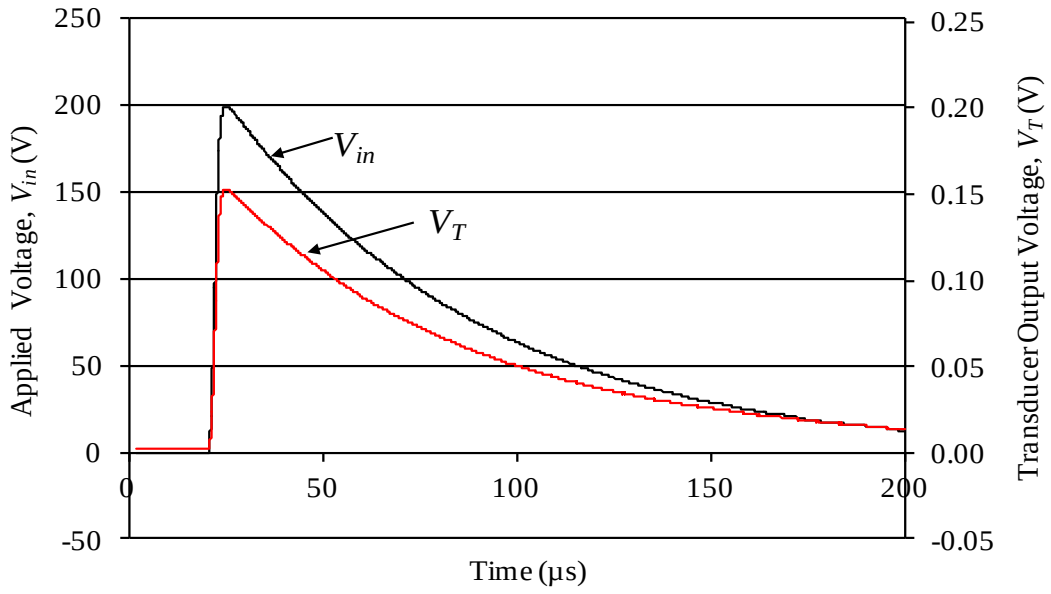

Figure 4.9: Measured transducer output voltage obtained from the lightning impulse test.

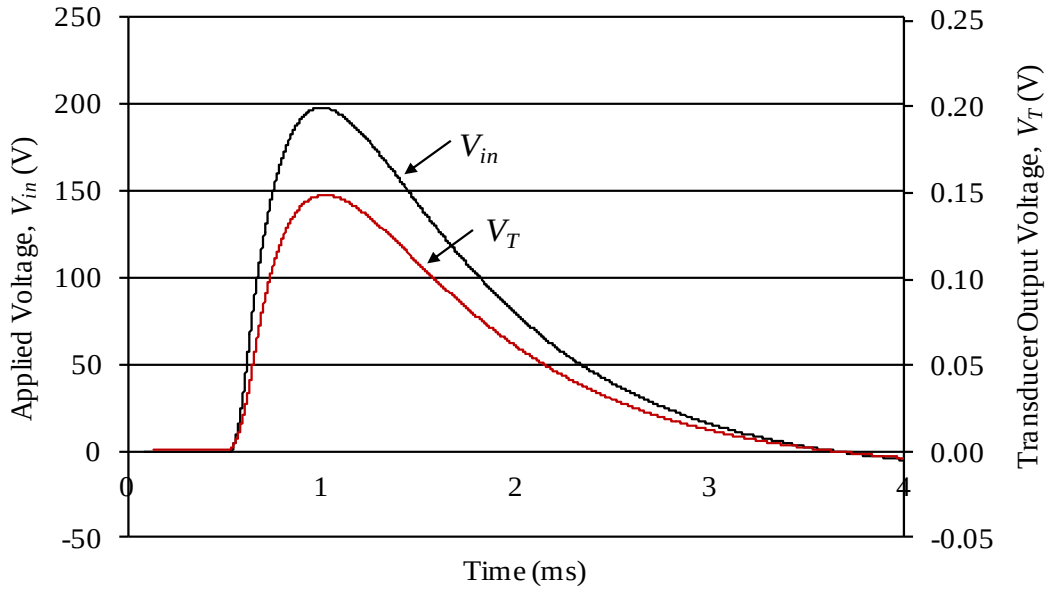

Figure 4.10: Measured transducer output voltage obtained from the switching impulse test.

Figure 4.11 portrays the measured output voltage acquired from the low magnitude ac voltage test. The result is used to verify the impulse test measurement results based on the output voltage amplitude. A good correspondence of voltage shapes can be observed for both impulse and ac voltage measurement.

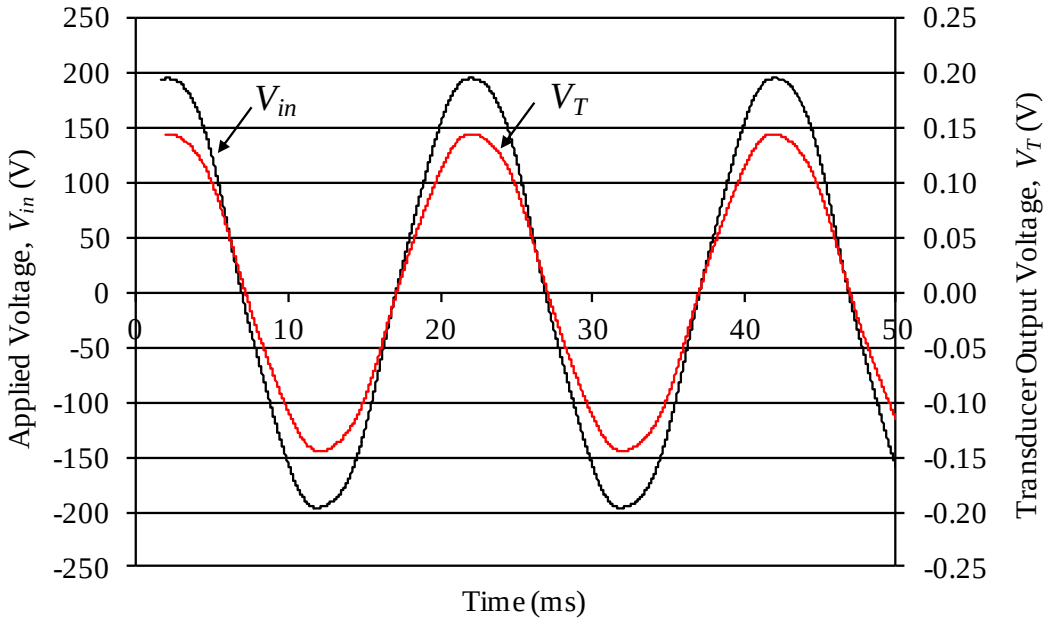

Figure 4.11: Measured transducer output voltage obtained from the ac voltage test.

Therefore, this demonstrates the suitability of the transducer for measurements of different types of voltages (ac and impulse voltages).

4.4.1.2 Non-Contact Capacitive Voltage Probe

Figure 4.12 and Figure 4.13 display the measurement results obtained when lightning and switching impulse voltages are applied to the measurement system respectively. The measurement results in these figures are obtained when the HV conductor is positioned 0.1m above the sensing probe surface and a fixed value of 10nF is used for the low voltage arm capacitor (C_p). A peak output value of 11.5mV_p is measured when an applied voltage of 200V_p is supplied to the HV conductor.

A low amplitude ac voltage supply is applied to the measurement setup in order to corroborate the results obtained from the impulse voltage test based on the voltage amplitude. Figure 4.14 shows the measurement result for the ac voltage test. Similar to the observation with the developed voltage transducer, the amplitudes of the output voltages shown in all three figures (Figure 4.12, Figure 4.13 and Figure 4.14) are

approximately 11.5mV$_p$, despite changing the input voltage source type from impulse to AC voltage.

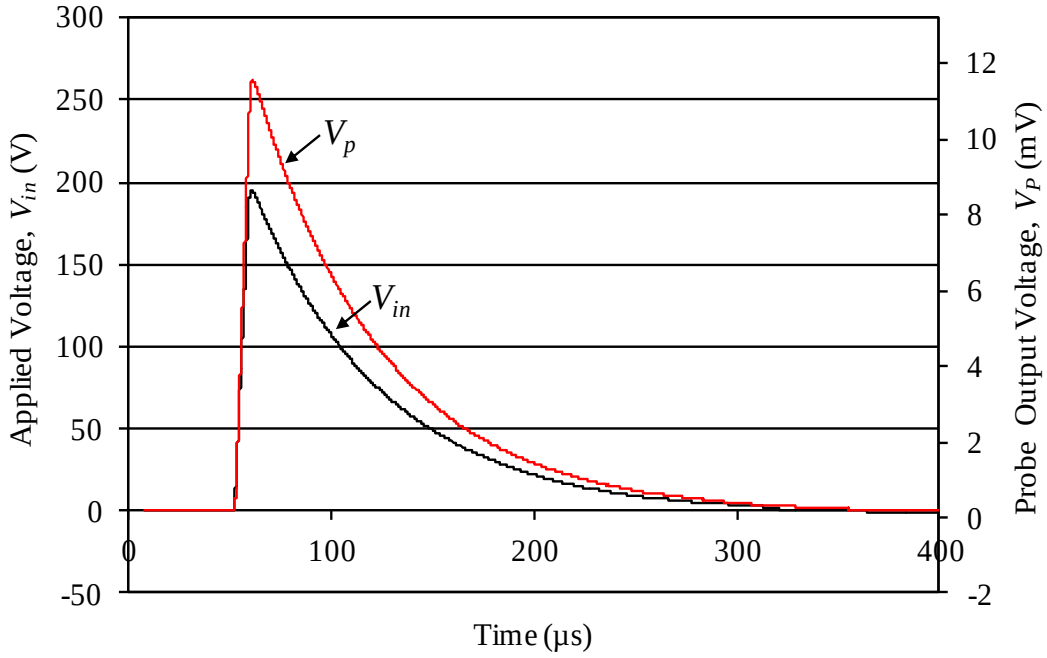

Figure 4.12: Measured probe output voltage obtained from the lightning impulse test.

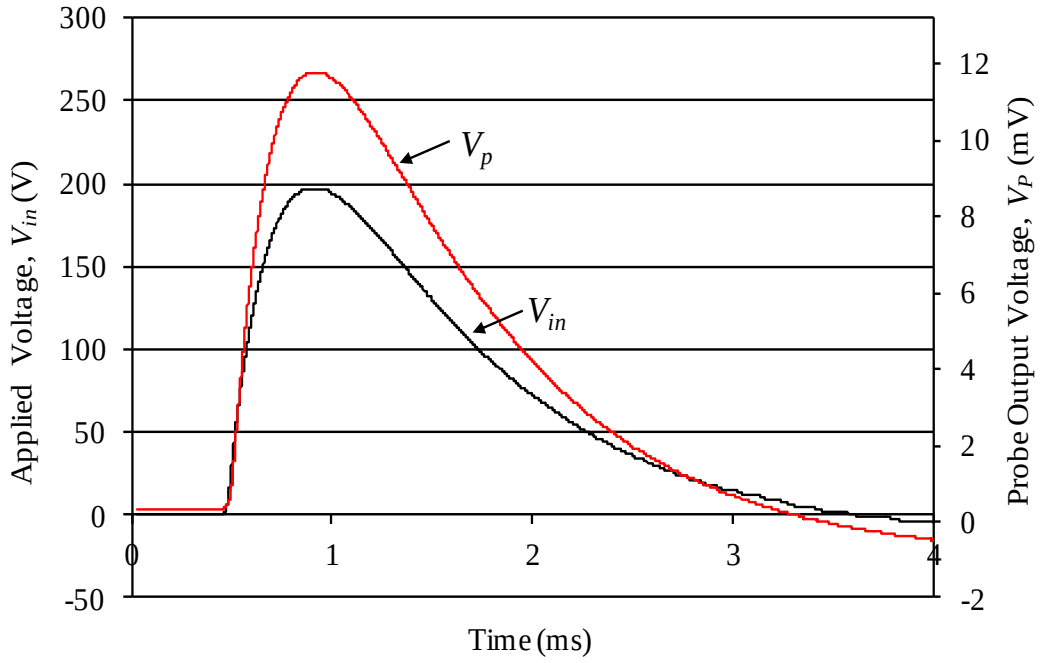

Figure 4.13: Measured probe output voltage obtained from the switching impulse test.

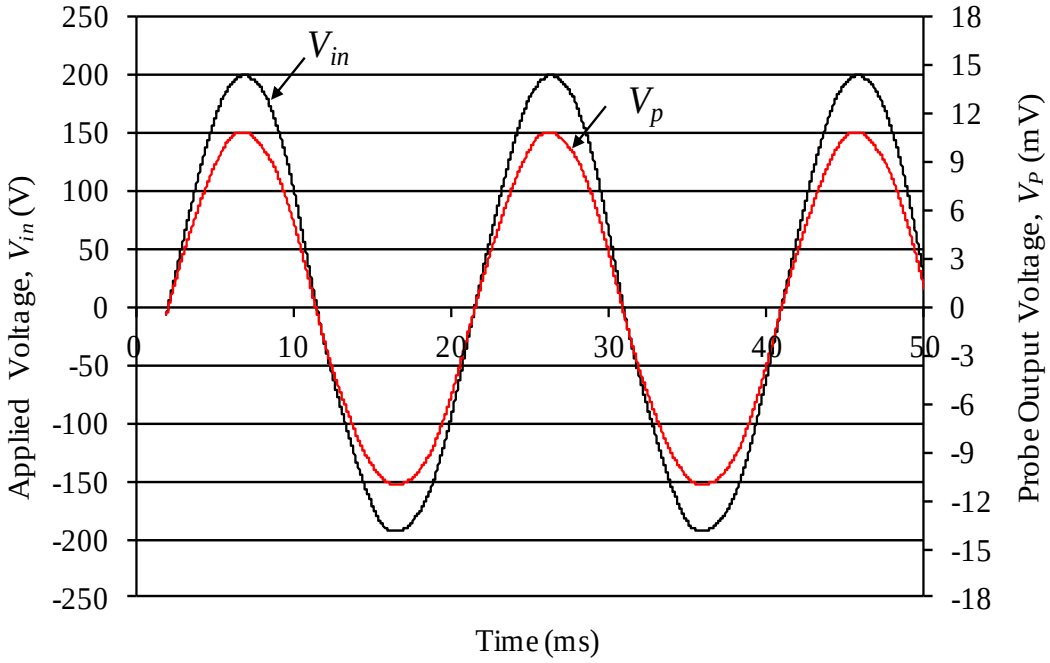

Figure 4.14: Measured probe output voltage obtained from the ac voltage test.

No straightforward comparison can be carried out based on the measured output voltage amplitude obtained from both tests (developed transducer and non-contact probe) due to the differences on the sensing probe surface area (the developed transducer [600 cm^2] and the non-contact probe [79cm^2] respectively). Nevertheless, these results indicated that both devices are suitable to measure various voltage types, including impulse voltages.

4.4.2 Effect of Integrating Capacitor Value and Height of HV Conductor

4.4.2.1 New High Voltage Impulse Transducer

Figure 4.15 reports a set of measured output voltage amplitudes obtained with different integrating capacitor (C_i) values ranging from 2.03nF to 10.85nF and at a fixed height of 0.1m (10cm) above ground. These output voltage amplitudes are plotted against the corresponding amplitudes of their applied voltages. Note that for a given value of C_i, the transducer output voltage is linearly proportional with the applied voltage.

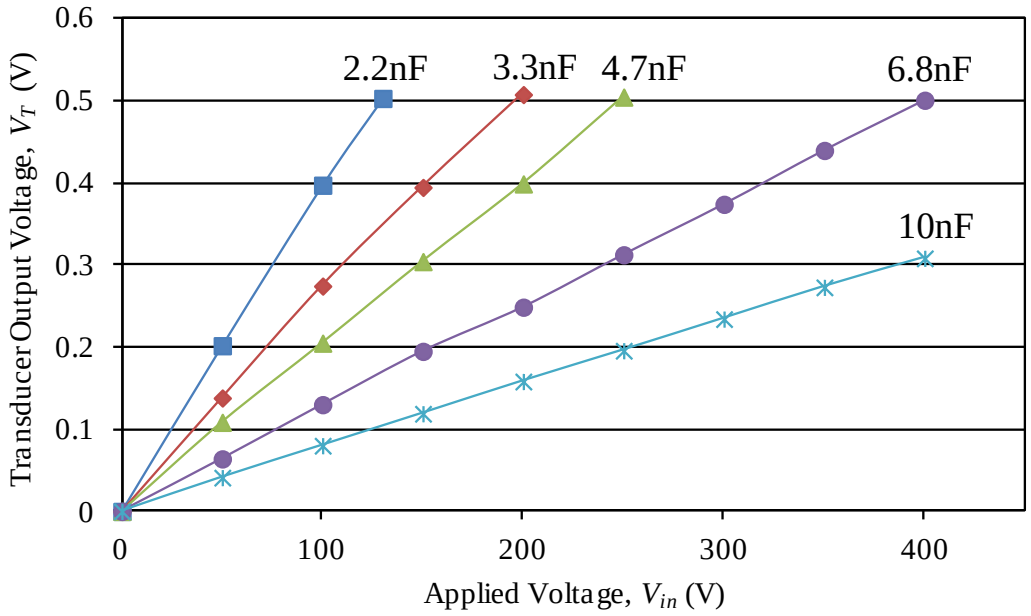

Figure 4.15: Measured transducer output voltage against HV conductor applied voltage for various capacitance values, and at fixed conductor height of 0.1m.

Figure 4.16 and Figure 4.17 shows the dependence of the transducer output on the integrating capacitor (C_i) and conductor height above ground when the applied voltage is set at $100V_p$.

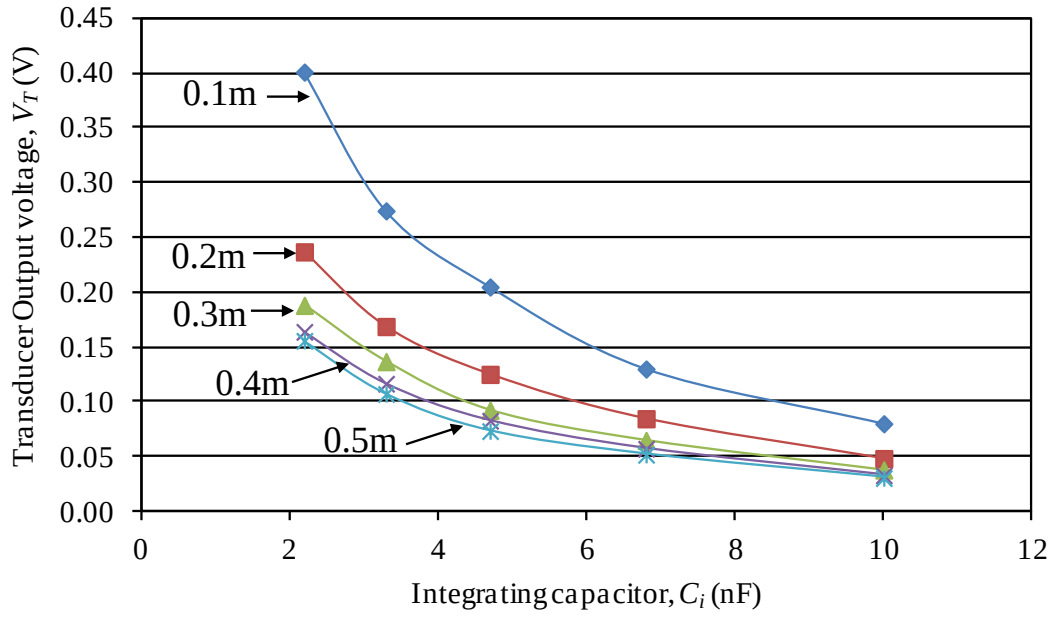

Figure 4.16: Measured transducer output voltage versus capacitor (C_i) for various heights setting but fixed input voltage of $100V_p$.

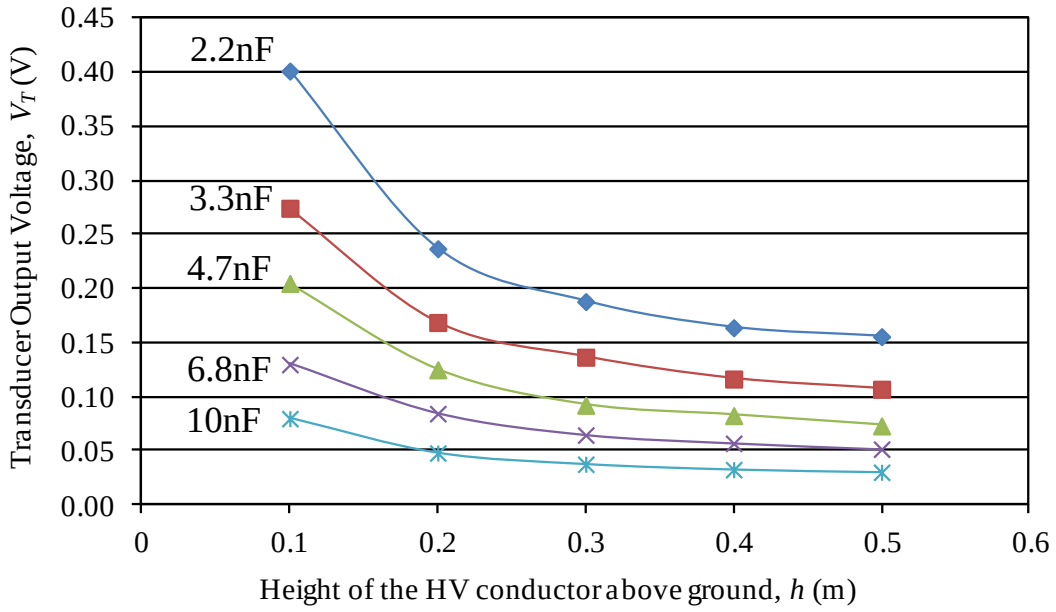

Figure 4.17: Measured transducer output voltage against height above ground for different values of C_i but fixed input voltage of $100V_p$

These figures demonstrate that the output voltage decreases non-linearly when C_i increases, and also when the transducer is placed higher above the ground. These results indicates that the applied voltage, integrating capacitor (C_i) and height above ground are the key practical elements in the measurement system that can be manipulated to control the output voltage of the transducer as explained in the analytical approach in Section 4.5.

4.4.2.2 Non-Contact Capacitive Voltage Probe

For comparison purposes, a set of tests were carried out using the ground fixed non-contact capacitive voltage probe as described in Chapter 2, Section 2.6. Figure 4.18 shows the measured probe output voltage amplitudes plotted against the applied voltage at different heights of the HV conductor and fixed capacitor, C_p of 10nF. Similar to the case with the developed transducer in this research, the output voltage produced by the probe is linear with the applied voltage, but the probe output decreases when the HV conductor height increases. This also indicates that the applied voltage, height and low

voltage arm capacitor (C_p) are parameters that can be used to control the output voltage of the probe.

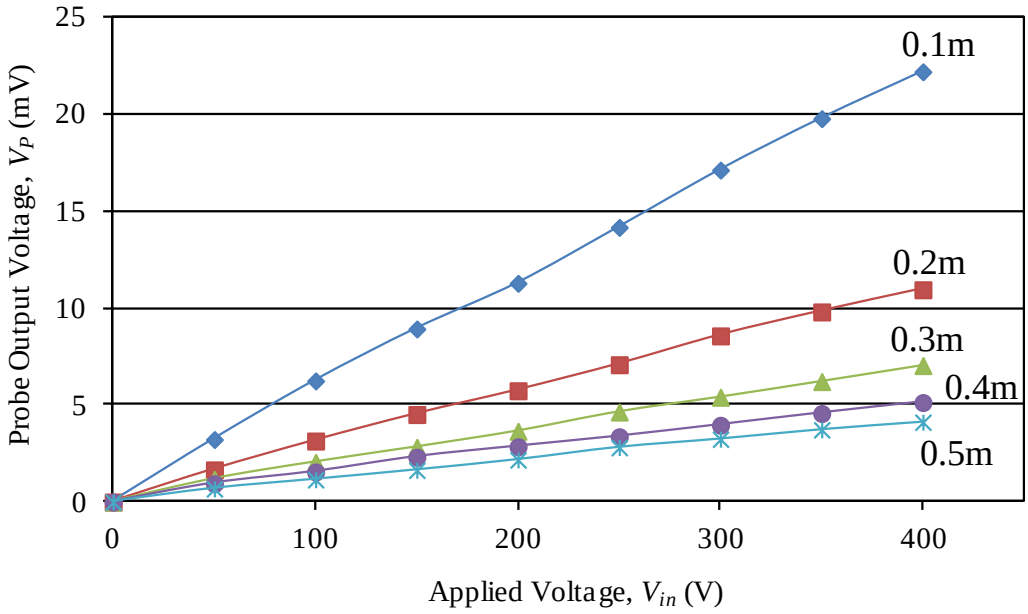

Figure 4.18: Amplitudes of output voltage when applied voltage and heights are varied but fixed value capacitance of 10.85nF is used.

4.5 Analytical Calculation and Modelling Approach

4.5.1 New High Voltage Impulse Transducer

In order to validate the experimental results (as mentioned in Section 4.4.2) that indicated the applied voltage, the integrating capacitor (C_i) and height above ground are the key practical elements in the measurement system that can be manipulated to control the output voltage of the transducer. This was achieved by conducting extensive analysis based on the single-phase measurement configuration or geometry representation as shown in Figure 4.19.

Where,

r_1 is inner radius of the conductor (0.01m),

r_2 is outer radius of the simplified transducer configuration (with an assumption that the transducer is also represented as an outer radius of the conductor,

0.15m),

C_T is the geometric capacitance between the conductor and the transducer,

C_i is the physical integrating capacitor inserted between the conductor and the transducer,

C_G is the capacitance with respect to the ground,

V_{in} is applied voltage,

V_T is the transducer output voltage (wrt the conductor line voltage),

ΔV is the difference in voltage between V_{in} and V_T.

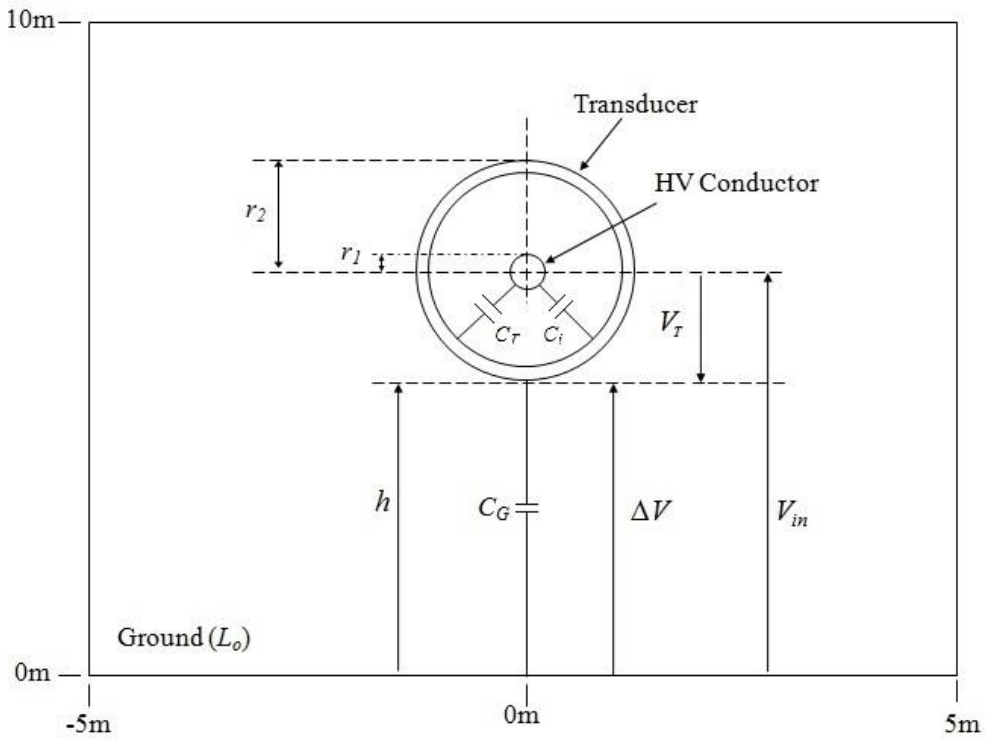

Figure 4.19: Geometry representation based on single-phase measurement set up (not to scale).

The method of images is used to determine the capacitance from the transducer sensing probe to ground (in this case C_G). The ground is replaced by a fictitious conductor, as shown in Figure 4.20, and this represents that the single-phase conductor with the ground is equivalent to a single-phase transmission line.

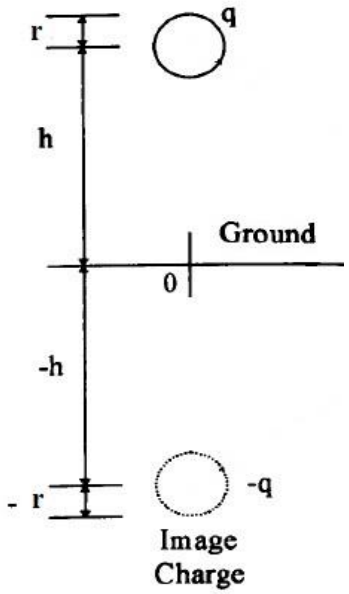

Figure 4.20: Single-phase conductor and its image.

Hence, the expression for the voltage is shown in Equation (4.1) [4.3].

$$V = \frac{1}{2\pi\varepsilon_0}\left(q\ln\frac{1}{r} - q\ln\frac{1}{2h} \right) \tag{4.1}$$

This Equation (4.1) is simplified and expressed as Equation (4.2).

$$V = \frac{q}{2\pi\varepsilon_0}\left(\ln\frac{2h}{r} \right) \tag{4.2}$$

Where 'r' is conductor radius at voltage 'V' with charge 'q' above an ideal ground plane at height 'h' for single-phase configuration.

Then, substituting $C = \frac{Q}{V}$ into Equation (4.2) gives the capacitance of the conductor with reference to ground, as shown in Equation (4.3).

$$C = \frac{2\pi\varepsilon_0}{\left(\ln\frac{2h}{r} \right)} \qquad [F/m] \tag{4.3}$$

From Equation (4.3), the C_G expression can be stated (based on Figure 4.19) as Equation (4.4).

$$C_G = \frac{2\pi\varepsilon_0}{\left(\ln\frac{2h}{r_1}\right)} \qquad [F/m] \qquad (4.4)$$

The geometric capacitance (C_T) can be determined by using the coaxial cable configuration, as stated in Equation (3.10) in Section 3.5, but based on the Figure 4.19, the C_T is stated as below (Equation (4.5)).

$$C_T = \frac{2\pi\varepsilon_0}{\ln\frac{r_2}{r_1}} \qquad [F/m] \qquad (4.5)$$

Equation (4.5) is expressed in units of farad per meter, and to change it to farad the equation is required to be multiplied by the transducer (sensing probe) length of 0.3m, (ℓ_P), as indicated in Equation (4.6).

$$C_T = \frac{2\pi\varepsilon_0}{\ln\frac{r_2}{r_1}} \bullet \ell_P \qquad (4.6)$$

However, in order to simulate the added effect of the integrating capacitance (C_i) inserted between the HV conductor and the sensing probe and in parallel with the geometric capacitance (C_T) based on the actual laboratory measurement environment, an equivalent permittivity value ($\varepsilon_r = \frac{C_i}{C_T}$) is calculated and inserted into the Equation (4.5) and expressed below (Equation (4.7).

$$C_i = \frac{2\pi\varepsilon_0\varepsilon_r}{\ln\frac{r_2}{r_1}} \qquad [F/m] \qquad (4.7)$$

Equation (4.7) is expressed in units of farad per meter, and to change it to farad the equation is required to be multiplied with the transducer (sensing probe) length of 0.3m, (ℓ_P), as indicated in Equation (4.8).

$$C_i = \frac{2\pi\varepsilon_0\varepsilon_r}{\ln\frac{r_2}{r_1}} \bullet \ell_P \tag{4.8}$$

However, this method is an approximation for ease of calculation (as stated above), and the end-effect is neglected. Thus, this equation is only used to determine the equivalent capacitance of C_i based on the equivalent relative permittivity (ε_r).

The transducer output voltage (V_T) can be determined by substituting Equation (4.4) and Equation (4.7) into Equation (3.2), and expressed as Equation (4.9).

$$V_T = \frac{\frac{2\pi\varepsilon_0}{\ln(\frac{2h}{r_1})}}{\frac{2\pi\varepsilon_0}{\ln(\frac{2h}{r_1})} + \frac{2\pi\varepsilon_0\varepsilon_r}{\ln(\frac{r_2}{r_1})}} V_{in} \tag{4.9}$$

The above equation can be simplified and rewritten as shown in Equation (4.10).

$$V_T = \frac{\ln(\frac{r_2}{r_1})}{\ln(\frac{r_2}{r_1}) + \varepsilon_r \ln(\frac{2h}{r_1})} V_{in} \tag{4.10}$$

As can be seen, this output voltage (Equation (4.10)) is based on the measurement configuration involving height (h), applied voltage (V_{in}) and integrating capacitor (C_i) - based on the equivalent permittivity ($\varepsilon_r = \frac{C_i}{C_T}$). Equation (4.6) is used to calculate the C_T in order to determine the equivalent permittivity (ε_r) in Equation (4.10).

Figure 4.21 shows a comparison for the transducer output voltage between analytical methods (Equation (4.10)) and the experiment result (as shown in Figure 4.15) when C_i used is 10.85nF, height is fixed at 0.1m above ground and the applied voltage is varied with $50V_p$ increment.

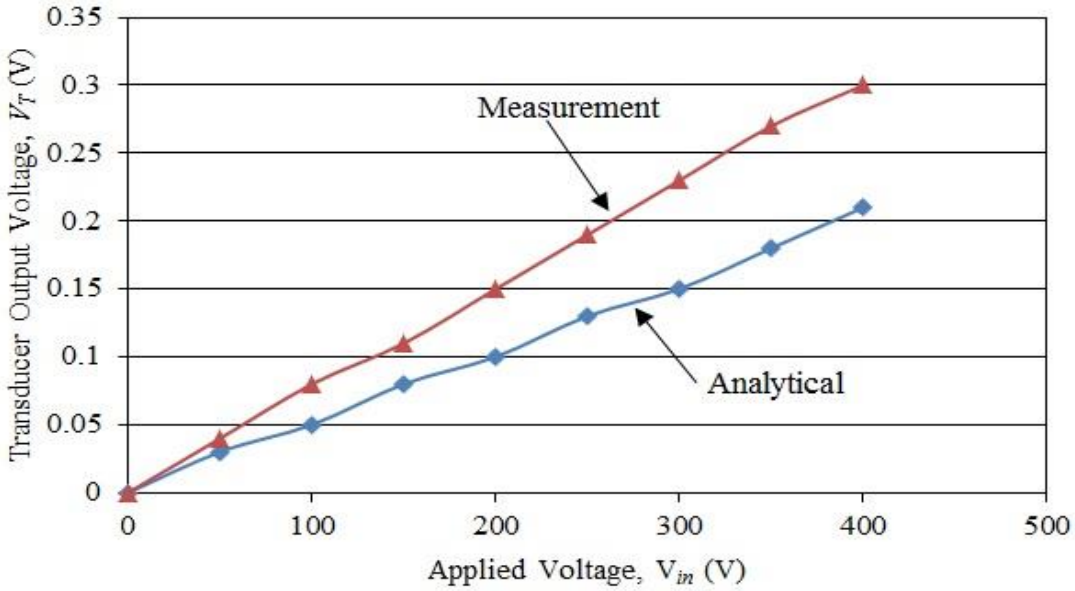

Figure 4.21: Comparison between analytical and measurement results when C_i value of 10.85nF is used, height above ground is fixed at 0.1m but applied voltage is varied.

Figure 4.22 shows a comparison for the transducer output voltage between analytical methods (Equation (4.10)) and the experiment result (as shown in Figure 4.16) when height is fixed at 0.1m and applied voltage is set at $100V_p$. However, the integrating capacitor (C_i) values are varied from 2.03nF to 10.85nF. Only measured values of C_i are used instead of manufacture's values in order to obtain a more accurate result.

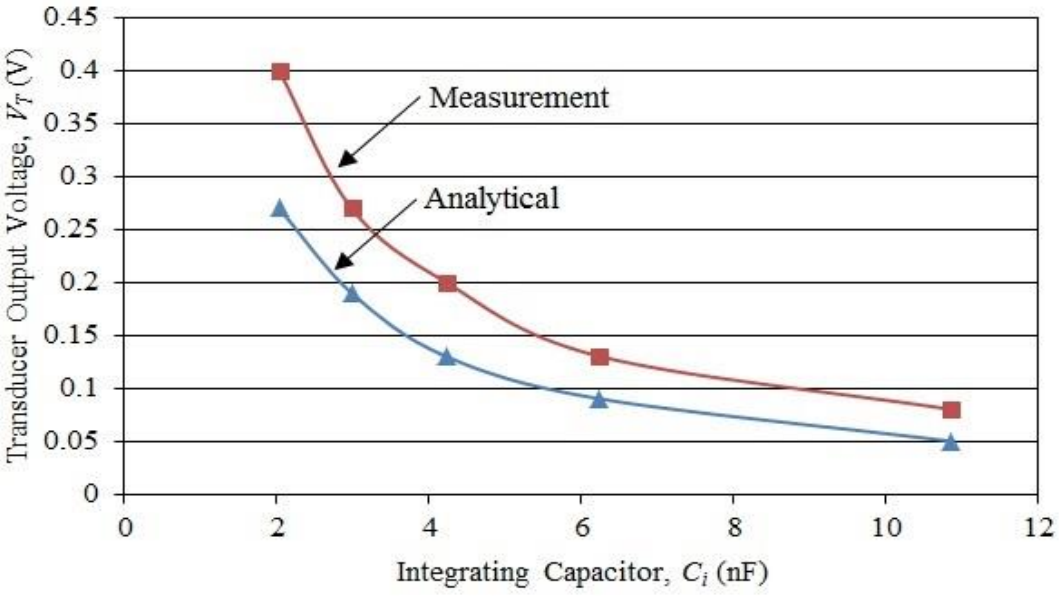

Figure 4.22: Comparison between analytical and measurement results when height and applied voltage are fixed (0.1m and $100V_p$ respectively) but C_i values are varied from 2.2nF to 10nF.

Figure 4.23 shows a comparison for the transducer output voltage between analytical methods (Equation (4.10)) and the experiment result (as shown in Figure 4.17) when C_i used is 2.03nF and applied voltage is set to $100V_p$ but height is varied from 0.1m to 0.5m.

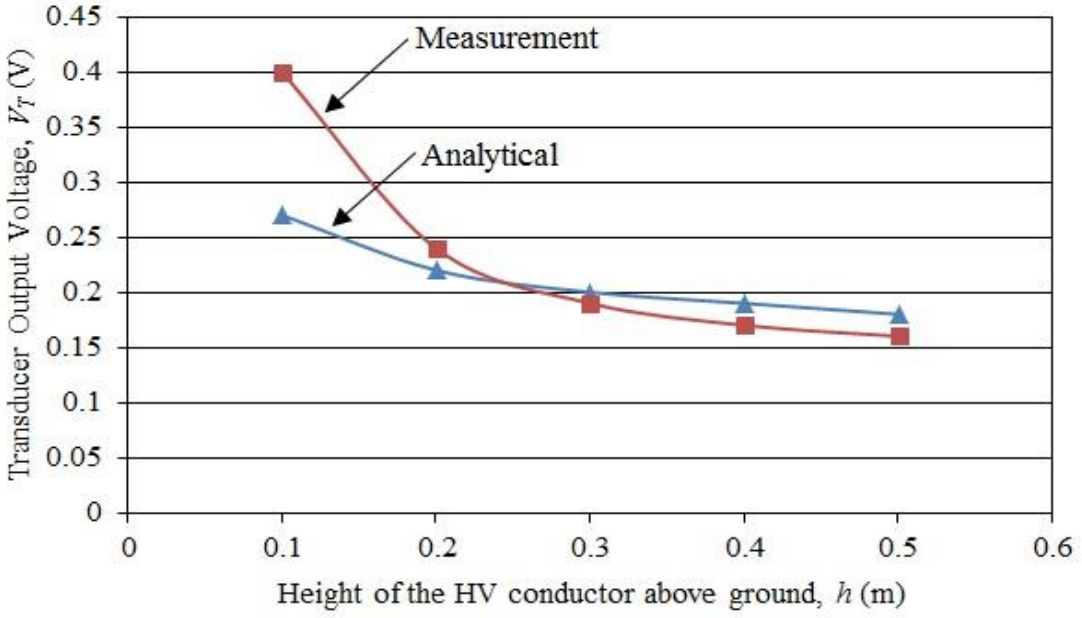

Figure 4.23: Comparison between analytical and measurement results when measured C_i value of 2.03nF is used and fixed voltage of $100V_p$ is applied but height is varied from 0.1m to 0.5m.

The maximum differences between the analytical (as shown in Figure 4.21, Figure 4.22 and Figure 4.23) and the measurement results are approximately 33%. This is due to the fact that the analytical method is based on an approximation that refers to the geometry of the experimental configuration and neglects the end-effects of the transducer geometric capacitance. On the other hand, the experiment is based on the actual environment setup. Hence, external factors such as interference need to be taken into account. Despite this, the analytical and measurement results are still within an acceptable range.

Since the measurement technique is based on the capacitive divider configuration, further analysis can be carried out to determine the value of capacitance to ground (C_G) by using Equation (3.3). In order to obtain calculation data as accurately as possible for

C_G, measured values of C_i are used. Using the measurement results (shown in Figure 4.17), C_G values for each corresponding C_i and height (h) are then calculated and plotted in Figure 4.24. This figure shows that, at a constant height, C_G values are identical, regardless of differing values of C_i but the C_G values decrease as height increases as shown in Figure 4.25.

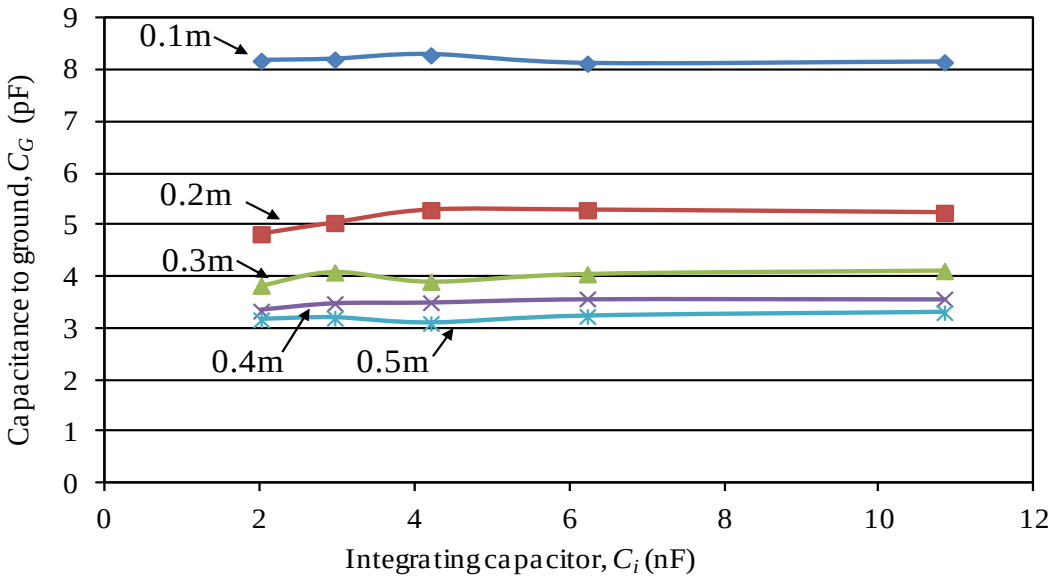

Figure 4.24: Capacitance (C_G) values obtained for each corresponding C_i and height.

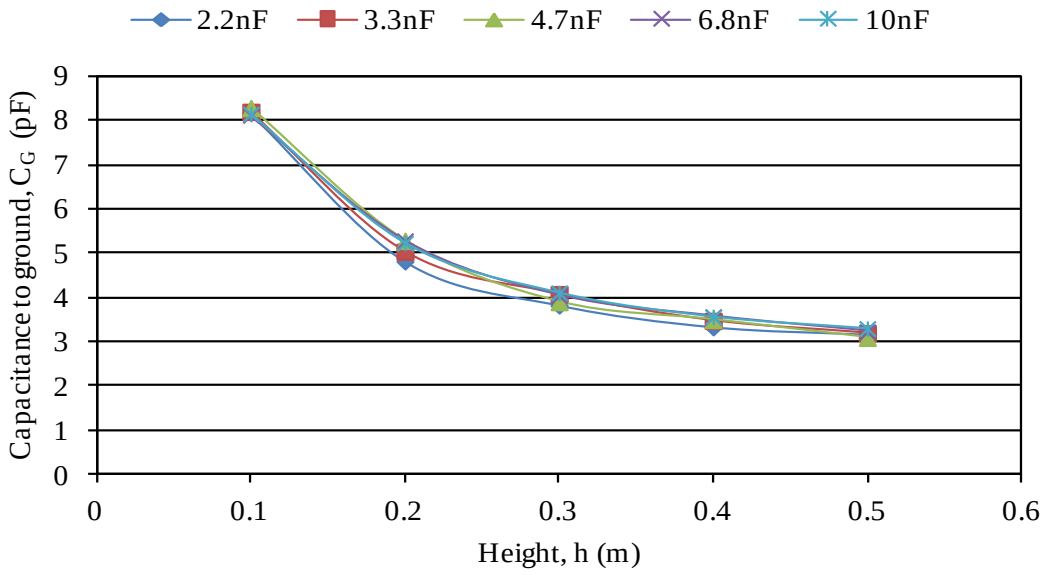

Figure 4.25: Capacitance (C_G) values obtained for each corresponding C_i and height.

For instance, at height 0.1m, C_G is approximately 8pF, even when the value of C_i is varied in the range of 2.2nF to 10nF (as shown in Figure 4.24). On the other hand, for 10nF of C_i, the C_G value drops from 8pF to approximately 5pF when the height is varied from 0.1m to 0.2m (as shown in Figure 4.25). This is due to the change of the measurement configuration as the control elements (such as height and C_i) are varied.

Table 4.1 gives a comparison between the measured data in the laboratory experiments (Figure 4.17) and the computed results (as described in Section 3.5). These results were acquired when the transducer is placed at a height of 0.1m above ground and the applied voltage is set to $100V_p$ while changing the value of C_i within the range of 2.03nF to 10.85nF. The maximum differences between the measured and computed values are approximately 15%. The computed results are slightly lower than the measurement results, which may be due to the limitation of SLIM software as mentioned in Chapter 3.

Table 4.1: Comparison between measured and computed results.

$C_{i\ \text{measured}}$ (nF)	Measured, V_T (V_p)	Computed, V_T (V_p)
2.03	0.40	0.33
2.98	0.27	0.23
4.22	0.20	0.17
6.24	0.13	0.11
10.85	0.08	0.07

In addition, Matlab has also been used to generate a 3D representation that can provide an estimate of the transducer output voltage for any pair of height and C_i value within a range, as shown in Figure 4.26. This 3D representation is generated based on data displayed in Figure 4.16 and Figure 4.17, and Appendix 4.1 shows the Matlab algorithm.

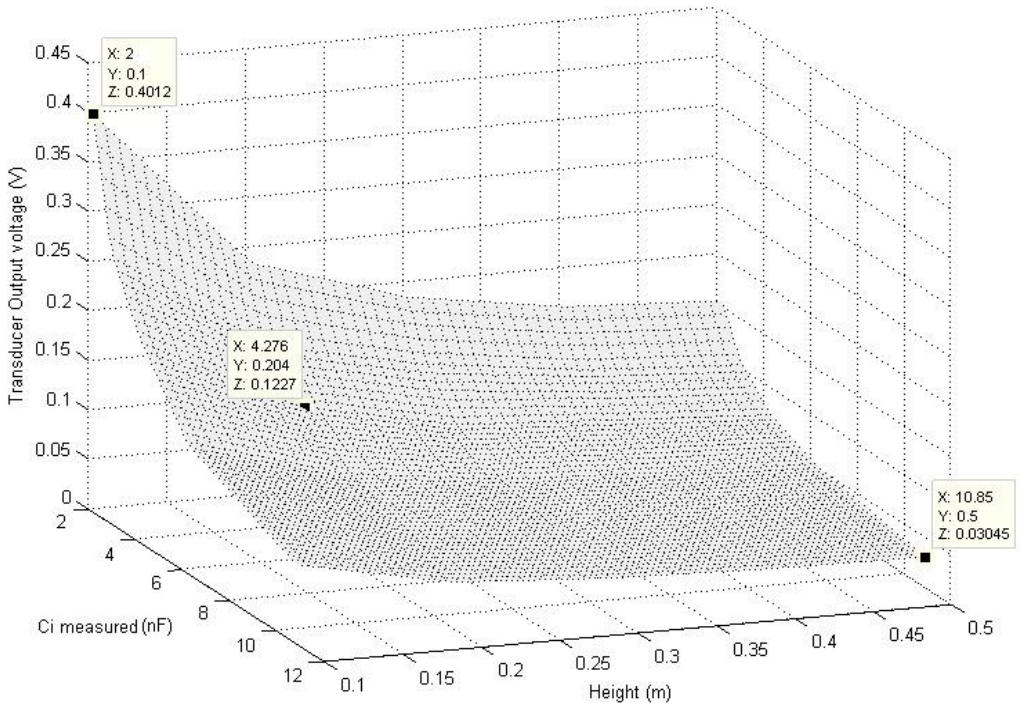

Figure 4.26: 3D representation generated based on results displayed in Figure 4.16 and Figure 4.17.

4.5.2 Non-Contact Capacitive Voltage Probe

Again, for comparison purposes, a set of tests were conducted using the ground fixed non-contact capacitive probe. Table 4.2 compares the value of output voltages obtained from the experiment and the computed output voltages presented in Section 3.2. Both the measured and simulated data correspond to the applied voltage of $200V_p$ and height of the HV conductor at 0.1m above the sensing probe surface. The discrepancy between the two voltage amplitudes (measured and computed) is most likely due to the limitation of the simulation software as mentioned in Chapter 3, Section 3.4 (Appendix 3.1).

In addition, the computed result is calculated based on the maximum electric field obtained at the ground level (Equation (3.1)) and does not take into account the effect of inserting the probe physical low voltage arm capacitor (C_p) and also the amplifier circuit installed underneath the probe that used to amplify the output voltage measured by the probe as described in Chapter 2, Section 2.6.

Table 4.2: Comparison between computed and measured output voltage amplitude for the non-contact probe.

Measured, V_p (mV_p)	Computed, V_p (mV_p)
11.5	6.3

Based on the derivation of the HV divider equation, the capacitance value from the HV line to the sensing probe surface (C_{LP}) can be denoted as (based on Figure 2.10):

$$C_{LP} = \frac{V_p C_P}{V_{in} - V_p} \tag{4.11}$$

Where:

C_{LP} is capacitance between the HV conductor to the sensing probe,

C_p is low voltage arm capacitance soldered onto the PCB,

V_p is probe output voltage,

V_{in} is applied voltage.

Using the measurement data in Figure 4.18 (where the applied voltage is $200V_p$), values of the probe output voltage V_P are substituted into Equation (4.11) with a constant C_p of 10nF to calculate the capacitance C_{LP}; the results are then plotted against height (h), which varies between 0.1m and 0.5m in Figure 4.27.

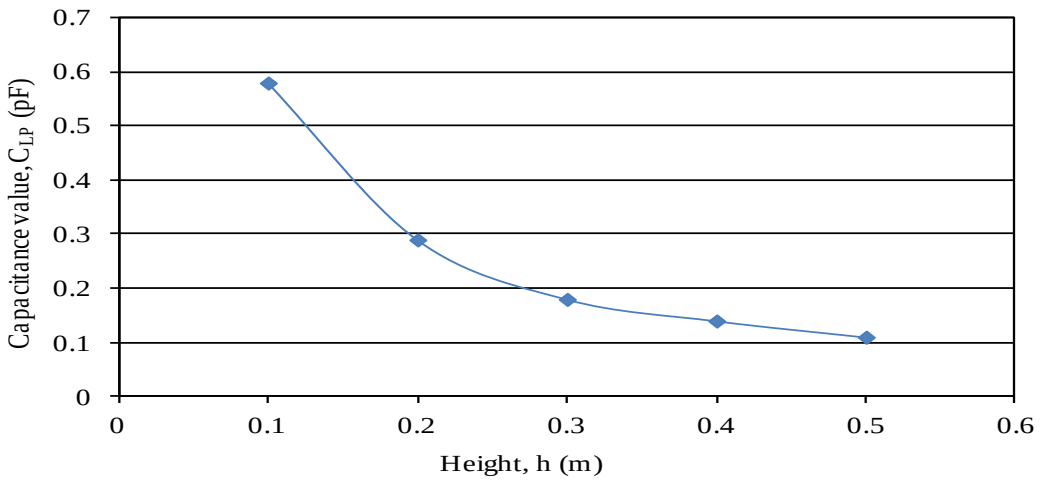

Figure 4.27: Capacitance (C_{LP}) values obtained when heights are varied.

As can be seen, the capacitance (C_{LP}) has a non-linear relationship with height (h), which is identical to the case of the developed voltage transducer (based on Equation (3.3)) as portrayed in Figure 4.22. Therefore, both cases agree with the capacitive divider measurement technique

4.6 CONCLUSION

The laboratory experiments using the developed transducer and the non-contact capacitive voltage probe demonstrate that both types of transducers exhibit similar characteristics, with the amplitudes of the output voltages remaining unchanged regardless of whether impulse or ac voltages are used as the applied voltage supply to the measurement system. The measurement results exhibit close agreement with the simulation results, thus indicating that the simulation model is valid and reliable.

For the laboratory experiments, control of the amplitude of the output voltage generated by the developed voltage transducer can be achieved through three variables:

(a) Amplitude of the applied voltage supplied to the system,

(b) Choice of the value of the integrating capacitor used,

(c) Height of the transducer measured from the ground level.

In particular, it was demonstrated that the amplitude of the output voltage is linearly proportional to that of the applied voltage, but it is non-linear with both the height and value of the integrating capacitance. Conducting additional low voltage experiments using the former non-contact capacitive probe demonstrated that both transducers conform to the capacitive divider measurement technique principles.

CHAPTER 5

CALIBRATION AND TRIAL TESTS OF THE NEW HIGH VOLTAGE IMPULSE TRANSDUCER ON A TEST OVERHEAD LINE

5.1 INTRODUCTION

The developed voltage transducer was tested on an 11kV three-phase overhead line setup at the Cardiff University sports fields, in the area of Llanrumney. This test was conducted to calibrate and investigate the characteristics of the developed transducer when it is operated under real overhead line environment conditions. The preliminary stage of the field experiment involved the use of low magnitude impulse voltages in order to evaluate the transducer. Furthermore, this low voltage test was also conducted to understand and calibrate the measurement setup and field working environment prior to proceeding with the high voltage tests. The low impulse voltages test results are validated with low magnitude ac voltages.

The subsequent stage of the field test involved a high voltage supply, but for safety purposes, the transducer was only tested with a high voltage ac supply generated from an HV transformer, as dealing with HV impulse voltages requires an adequate protection measurement setup (which is very complex to deploy, especially for a field test). Moreover, the impulse generator is heavy, with an approximate weight of 200kg, and raised concerns of possible damage during transport, in addition to health and safety restrictions.

The effects on the value of the output voltage are investigated against the applied voltage magnitude, as is the use of different integrating capacitor (C_i) values. The height of the transducer above ground was constant, as the overhead line conductor height

were fixed throughout the field test. This test was conducted based on the single-phase configuration since there is only a single transducer fabricated in this work. In addition, there is no concern about stray capacitance effects from neighbouring conductors, as it has already been shown that this effect is negligible (as mentioned in Chapter 3, Section 3.5.1.2).

5.2 PHYSICAL MODELLING OF THE FIELD TEST ARRANGEMENT

5.2.1 Two-Dimensional Model of Field Experimental Arrangement

A two-dimensional model was constructed using finite element (SLIM) software. The model is based on the field experimental configuration in order to determine the electric field distribution around the HV conductor and the transducer, hence enabling prediction of the transducer characteristics and performance under real overhead line environment conditions.

The additional presence of a metal fence in the actual experimental environment, approximately 3.0m away from the centre pole of the overhead line and around 2.0m tall was also taken into account. This fence is used to separate the sports field area from the nearby school field, as depicted in Figure 5.1. Hence, the model was extended to accommodate any possible effects of distortion on the computational results of the electric field distribution.

Figure 5.2 shows the 2D model construction based on the field testing configuration, with the diameter of the conductor equal to 6mm and the height of the transducer above ground at 8.5m, as measured from the centre of the HV conductor. This particular single-phase overhead line model is based on the consideration that the transducer is placed at the middle conductor of the actual three-phase overhead lines.

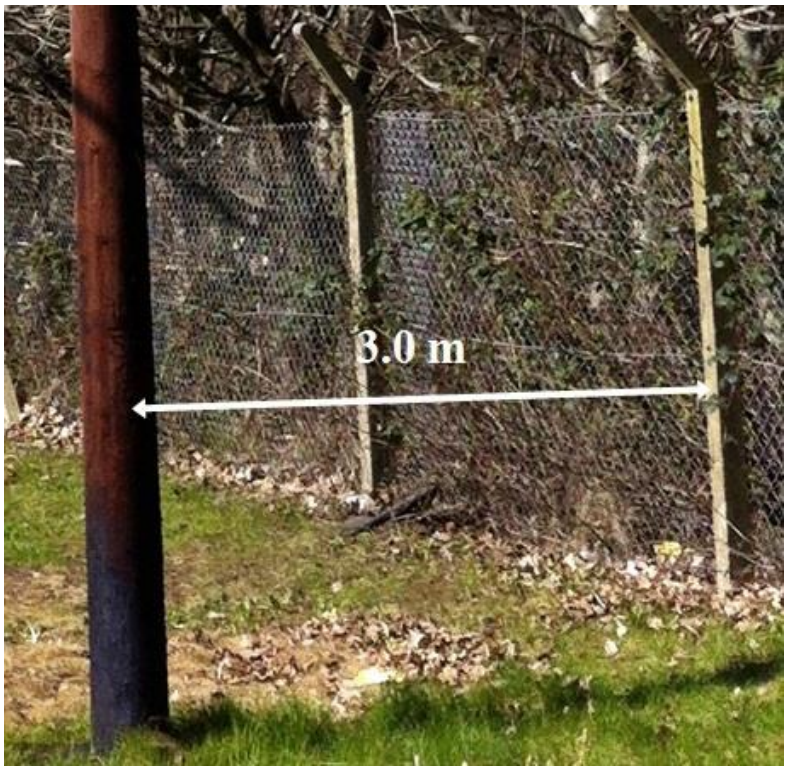

Figure 5.1: Test overhead line and adjacent fence.

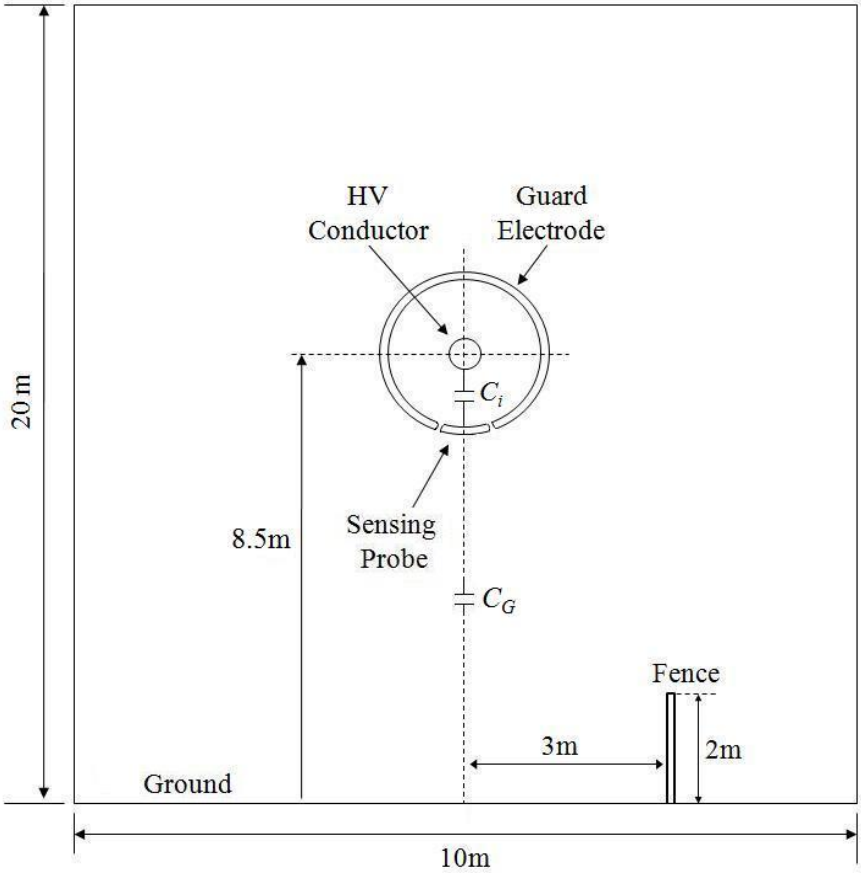

Figure 5.2: 2D modelling based on the field test configuration (not to scale).

Similar to the 2D simulation discussed in Chapter 3, the entire space was meshed into a set of triangular elements and set as free space within the simulation software, with the exception of the HV conductor, the guard electrode, the sensing probe and the metal fence. The HV conductor and the guard electrode were assigned to high potential, while the ground and the metal fence were assigned to zero potential. The sensing probe remained as the floating electrode.

5.2.2 Simulation Results and Analytical Approach

The simulation of the test site model is to compute the equipotential distribution and the electric field around the transducer and the HV conductor, as shown in Figure 5.3. The so computed potential values were used to calibrate the transducer and calculate the geometric capacitance (C_T) of the voltage transducer based on the field experimental configuration.

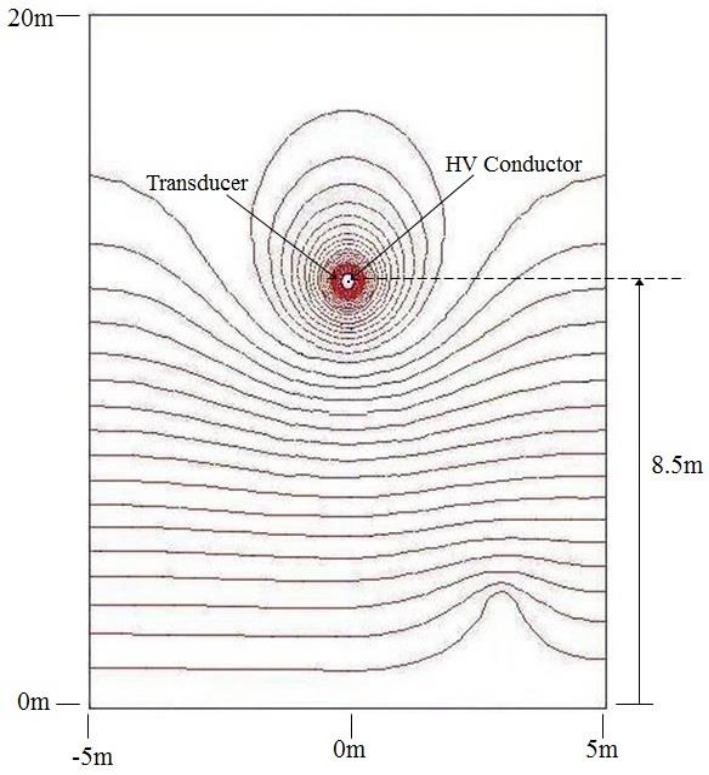

Figure 5.3: The electric potential distribution around the overhead line conductor and the transducer.

As can been seen in the above figure, there is a slight distortion in the equipotential distribution around the metal fence, but no noticeable effect on the equipotential distribution around the transducer was observed, since, the transducer is relatively far away from the fence to be influenced.

Figure 5.4 plots the electric field magnitude along the width of the sensing probe surface when an alternating voltage of 1kV is applied to the HV conductor. As can be seen on the figure, the electric field magnitude increases towards the edge of the sensing probe, with a field peak value of around 5.5kV/m due to the end-effects, as seen in the transducer modelling results described in Section 3.5. This magnitude (as shown in Figure 5.4) is later used to calibrate the transducer.

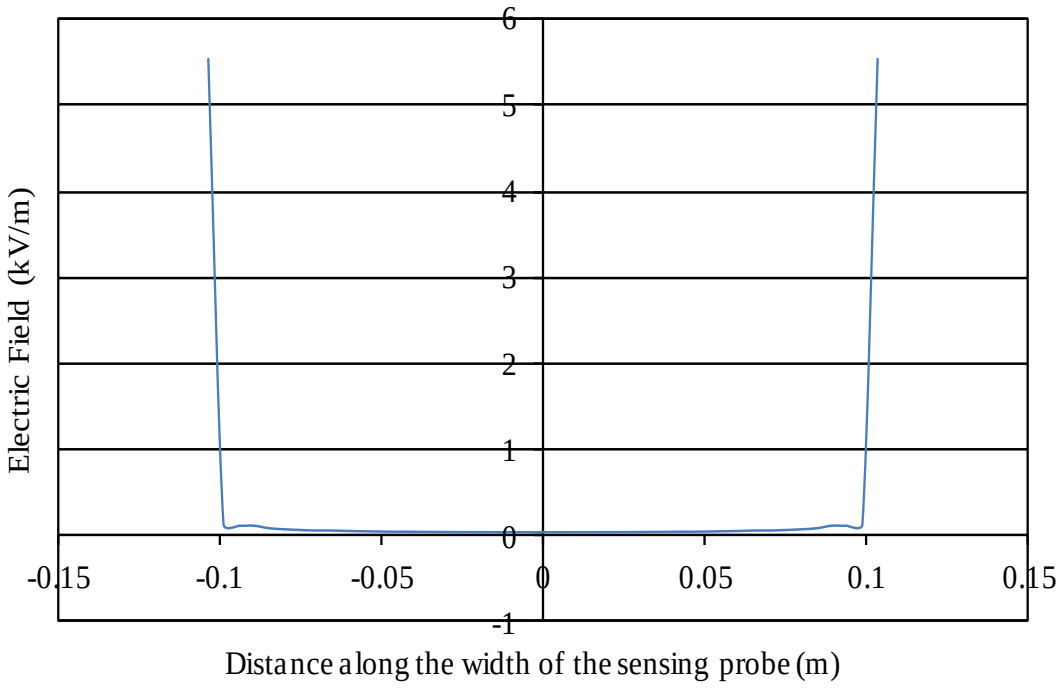

Figure 5.4: Electric field magnitude profiles along the surface of the sensing probe.

A Matlab routine (discussed in Chapter 3, Appendix 3.1) is also used to generate the electric field values on the probe surface to allow a 3D representation with the assumption that the electric field magnitude (from Figure 5.4) is applied to the entire

sensing probe surface, as shown in Figure 5.5. By using the field values of Figure 5.5, the induced charge (Q) on the transducer sensing probe surface is computed through the integration of the field magnitudes over the entire probe surface based on Equation (3.5).

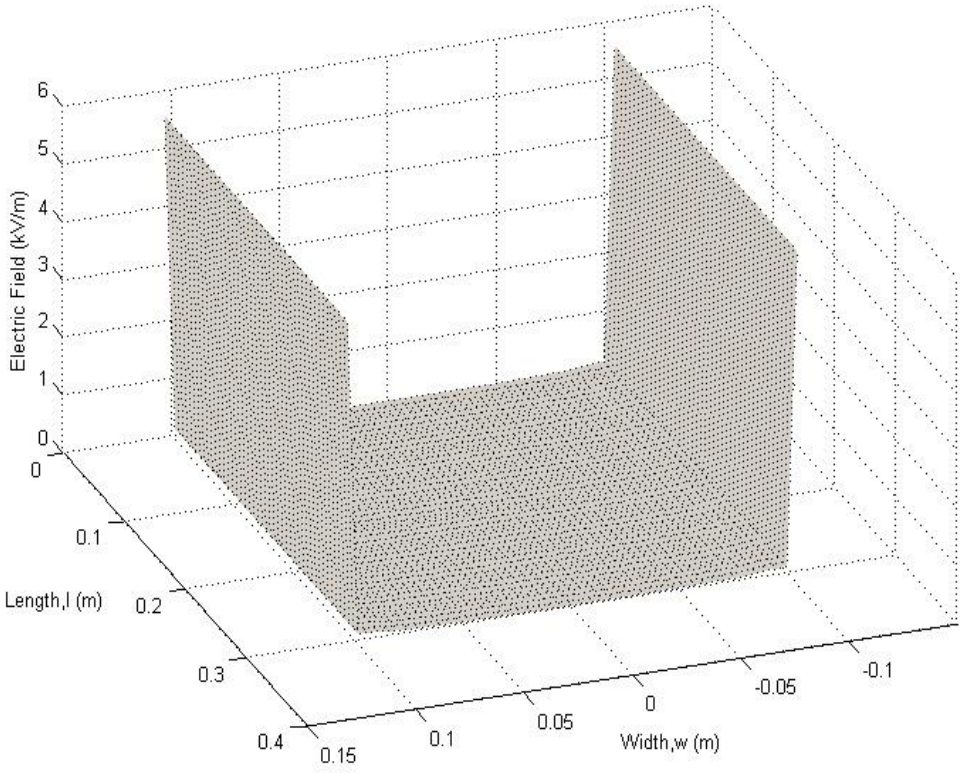

Figure 5.5: The electric field on the surface of the sensing probe.

The computed charge of approximately 97.9pC is obtained. The geometric capacitance (C_T) of the transducer based on the computed electric field (E_{xy}) for the field experiment configuration can be calculated using Equation (3.7), and in this case, it is found to be 18.9pF based on the above charge value. This C_T value is then compared with the C_T values previously obtained from the laboratory experiment model computation, along with the analytical approach (as reported in Chapter 3), and tabulated in Table 5.1. As can be seen in the table, the calculated C_T values are within range for these two models and the analytical result, despite differences in the HV

conductor height above ground in both the field and laboratory 2D models (8.5m and 2.5m respectively). This indicates that the developed models are accurate, because the geometric capacitance should theoretically be similar, as the transducer dimensions remain identical and the model permittivity (ε_0) is still based on free space.

Table 5.1: Comparison of geometric capacitance (C_T) values between the analytical and the 2D computation models (based on laboratory and field experimental configuration).

Model	Geometric Capacitance, C_T (pF)
Laboratory Experiment	19.9
Field Experiment	18.9
Analytical	19

An equivalent permittivity (as explained in Section 3.6) is used in order to simulate the effect of an integrating capacitance (C_i) inserted between the HV conductor and the sensing probe, and to predict the transducer output voltage (V_T). Table 5.2 shows the computed output voltage for the respective C_i, which is obtained when the model is injected with 1kV alternating voltage. In order to produce computed results for the simulation model that are as accurate as possible, the measured values of C_i are used instead of the manufacturer's stated values.

Table 5.2: Computed output voltage values obtained from the simulation.

$C_{i\ \text{Measured}}$ (nF)	$V_{T\ \text{Computed}}$ (V_p)
2.03	0.60
2.98	0.42
4.22	0.30
6.24	0.20
10.85	0.12

Using the results shown in Table 5.2 and substituting these values in Equation (3.3) gives the corresponding capacitance to ground (C_G) value for each C_i, as summarised in Table 5.3. These calculated results give an average capacitance value of 1.25pF and due to at a fixed height, the C_G values are identical, regardless of differing values of C_i as explained in Section 4.5. This average C_G value is subsequently used to determine the suitable integrating capacitor (C_i) value for the field experiment.

Table 5.3: Computed capacitance probe to ground (C_G) values obtained from the field experiment model configuration.

$C_{i\ measured}$ (nF)	$C_{G\ computed}$ (pF)
2.03	1.22
2.98	1.25
4.22	1.27
6.24	1.25
10.85	1.28

Since the highest output voltage permitted as input to the optical fibre system is $1V_{p-p}$ due to the limitations of the LED in the transmitter system, the capacitance (C_i) is one of the key elements that can be used to control the output voltage produced from the transducer. At a fixed height, the capacitance C_G value is constant. Hence, the suitable value of physical C_i that can be used in the actual experiment can then be calculated by manipulation and rearrangement of the capacitive divider equation (Equation (3.2)).

There are two different sets of C_i values that need to be determined, as the field experiments are conducted in two different stages (low and high voltage tests). The low voltage test is carried out by supplying low impulse voltage using the impulse generator, with a maximum output of approximately $400V_p$. Substitution of these data into Equation (5.1) that is derived from Equation (3.2) gives the appropriate C_i value that

can be used for the low voltage field test.

$$C_i = \frac{C_G (V_{in} - V_T)}{V_T} \tag{5.1}$$

Where:

C_i is integrating capacitor inserted between the HV conductor and the sensing probe,

C_G is the capacitance from the sensing probe to ground,

V_{in} is input voltage applied to the HV conductor,

V_T is output voltage measured from the transducer.

In this case, the integrating capacitor (C_i) value is calculated to be approximately 1nF when the applied voltage and the transducer output voltages are set to the maximum level of $400V_p$ and $0.5V_p$ respectively. The same process is repeated to determine C_i for the high voltage test, but in this case, the input voltage is set to $9kV_p$, while the transducer output remains at $0.5V_p$ based on the maximum limit permitted by the optical transmitter. This gives a C_i value of around 22nF. These C_i values are later used in the actual experiment discussed in the next section.

5.3 FIELD TEST

The field tests were divided into two categories, namely the low voltage and the high voltage tests. The low voltage test was performed as the preliminary stage in order to obtain experience with the field working environment and the use of the field testing instruments before proceeding with the high voltage test. Furthermore, the field test aimed to demonstrate that the output from the transducer can be controlled according to measurement specifications by determining the value of the integrating capacitor (C_i) when the height of the HV conductor is fixed (as explained in Section 4.5). A hired lifting crane of model Z45D (as portrayed in Figure 5.6) was used to assist the operator

with the installation of the transducer on the overhead line conductor. Details of the lifting crane's specifications can be obtained in Appendix 5.1. The measurement results obtained from both tests are compared with the computed results.

Figure 5.6: Lifting equipment model Z45D.

5.3.1 Low Voltage Test

Figure 5.7 illustrates the schematic diagram of the low voltage measurement setup. The setup is similar to the low voltage test conducted in the laboratory experiment, as described in Chapter 4, Section 4.2, and includes a surge generator, HV divider, oscilloscope (DSO), optical fibre system and the developed transducer. However, only a single-phase measurement configuration was used in this test, as there is only one fabricated voltage transducer. Figure 5.8 shows the actual field experiment setup, with the transducer (indicated in dashed circle line) placed on the outer phase HV conductor. Figure 5.9 shows the measurement area setup at one end of the overhead line.

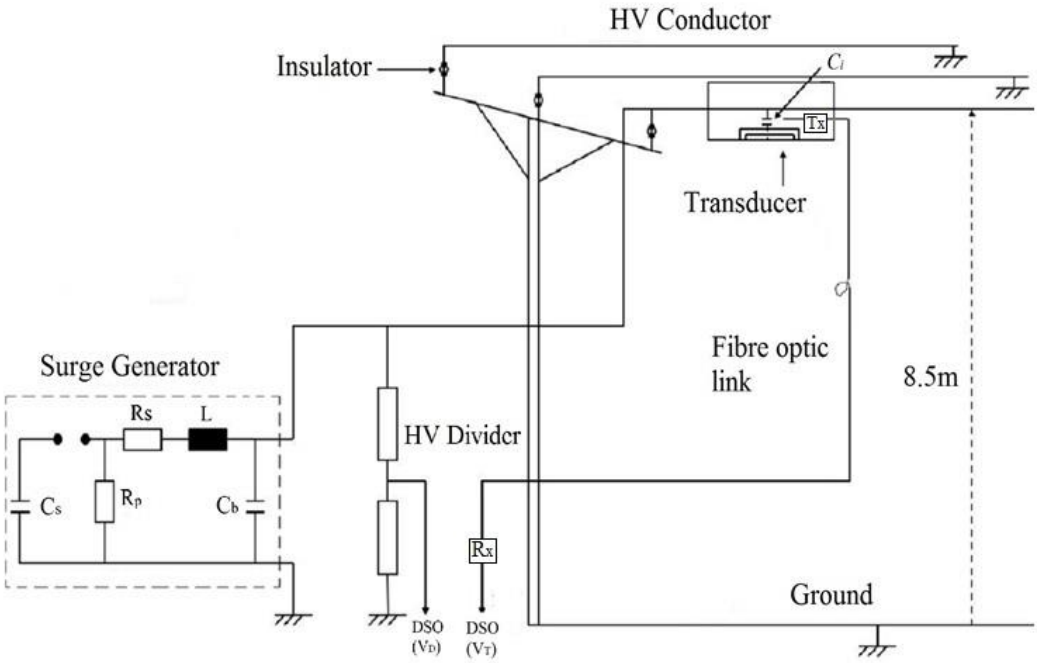

Figure 5.7: Low impulse voltage test for field experiment setup.

Figure 5.8: The actual transducer installed on one phase of the overhead line.

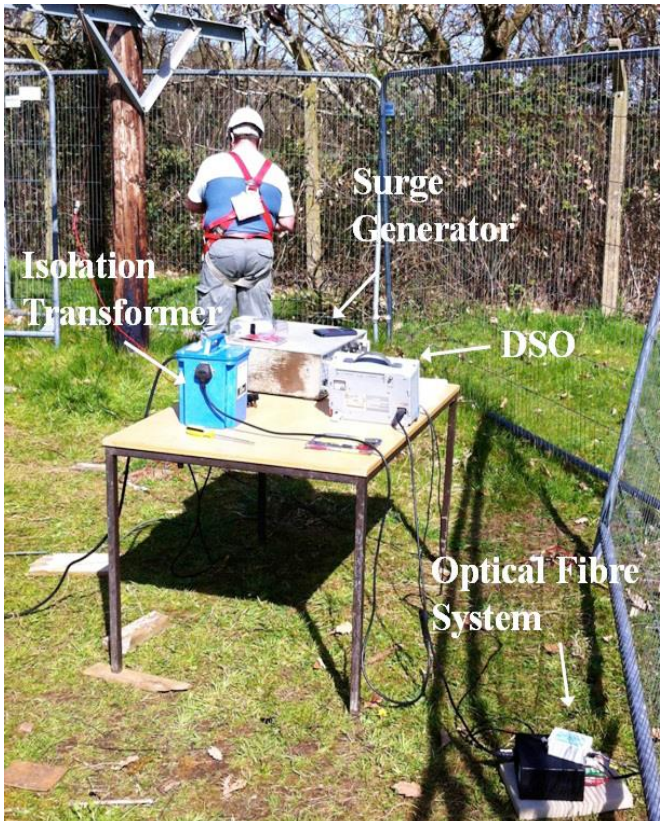

Figure 5.9: Measurement setup deployed at one end of the overhead line.

Each phase was tested individually, and a horizontal distance of 1m markers were placed on conductor of the overhead line (OHL) to ensure that the transducer was installed at the same distance from the pole, as indicated by circles in Figure 5.10. Furthermore, the main reason why the transducer was placed close to the OHL pole at an approximate horizontal distance of 1m (as indicated in Figure 5.10) was to avoid adding any further sag to the existing overhead line conductor, ensuring that the test conducted would not breach the safety ground clearance of the overhead line operation (considering the weight of the current transducer, which is approximately 4.5kg). The outer conductor is labelled as HVC_1, while the middle conductor is HVC_2 and the conductor near to the field fence is indicated as HVC_3.

In order to simulate the single-phase overhead line as tested using the three-phase overhead line, it was vital to ground the other two phases (as shown in Figure 5.7). It

was also essential to ensure that all the ground connections were connected to the same point in order to reduce any ground noise or interference with the measurement results. Both ends of the transducer were shielded with aluminium foil (as previously adopted in the laboratory experiments), and this foil was connected to the HV conductor in order to reduce any fringing effects.

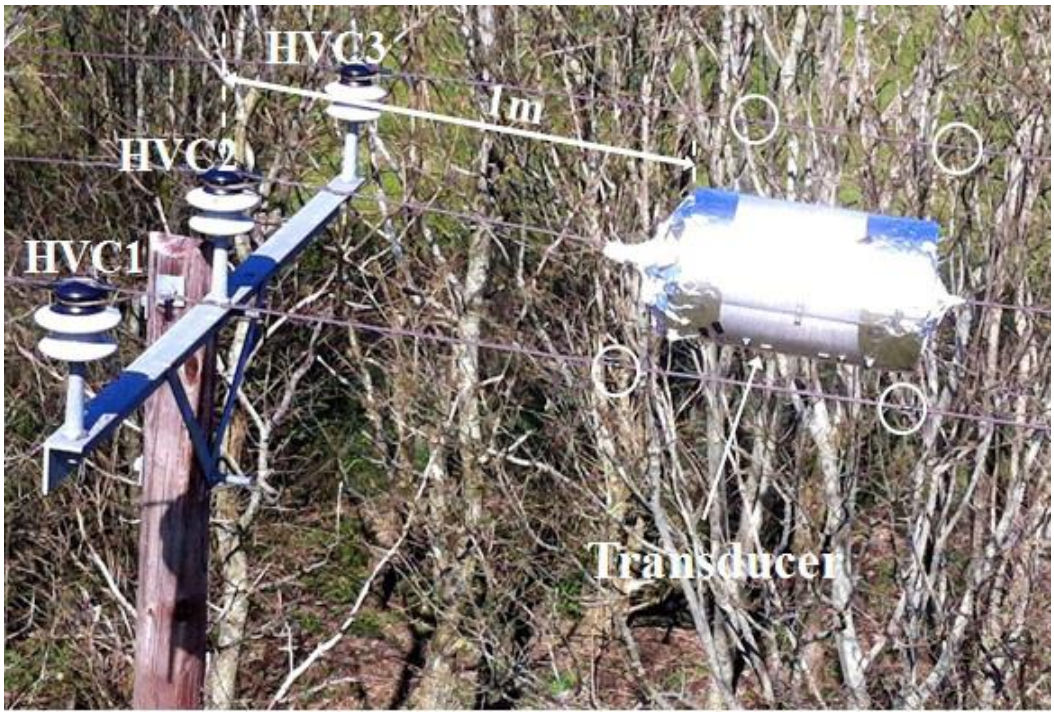

Figure 5.10: The transducer is placed approximately 1m closed to the OHL pole.

An integrating capacitor of 1nF was inserted between the HV conductor and the sensing probe. This capacitance value was obtained from the computational results, as explained in the previous simulation section. The low impulse voltage was injected into the conductor and controlled using the generator. Later, the output voltage amplitude obtained from the transducer was verified with the low ac voltage test.

5.3.2 High Voltage Test

For the high voltage field test, the transducer was only subjected to high voltage ac supply produced from the HV transformer, since dealing with a high impulse voltage supply requires an extensive protection measurement setup (which is very complex to

deploy, particularly in the field test environment).

Figure 5.11 illustrates the schematic diagram of the HV ac field test measurement setup, which consists of a variac, isolation transformer, filtering unit (comprises of inductance (L) and capacitance (C)) and HV transformer. The variac was used to regulate the input voltage from 0 to $240V_{rms}$, while the isolation transformer was used as a protection device to isolate the measurement setup and between the low voltage and high voltage sides. The input voltage was stepped up from 0 to the maximum of $7kV_{rms}$ using the HV transformer.

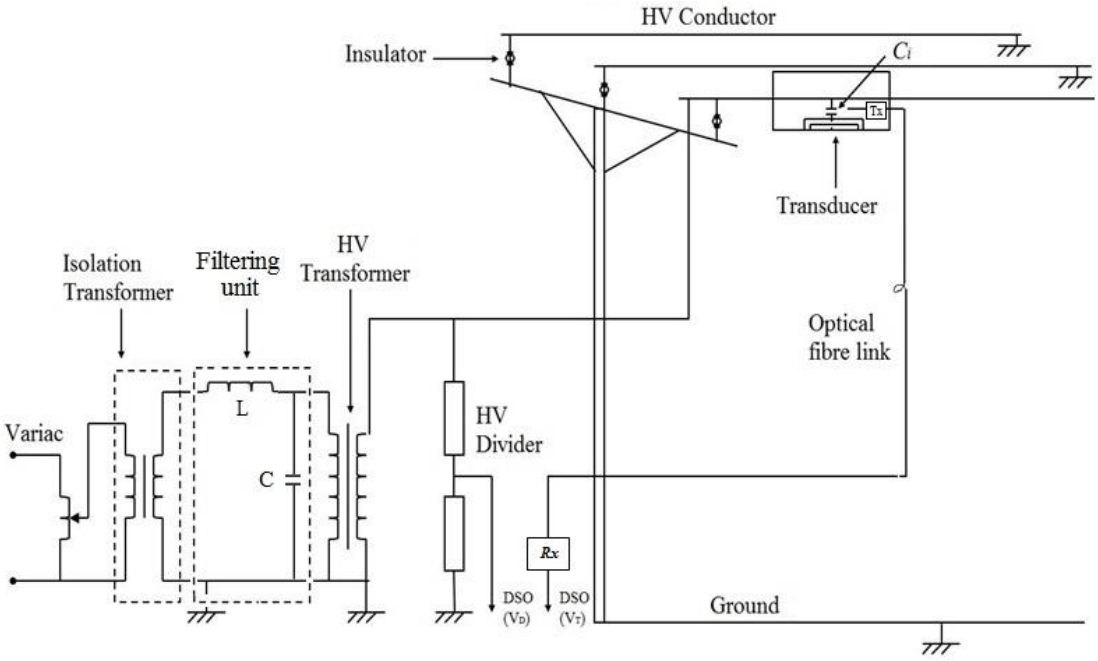

Figure 5.11: Schematic diagram of high voltage field test setup.

Figure 5.12 shows the physical measurement setup. The test procedures were similar to the low voltage test discussed in Section 5.3.1, but the value of the integrating capacitor (C_i) used was 22nF. This C_i value was based on the computed result (as described in Section 5.2.2) obtained for the high voltage field test model. The output voltage obtained from this test was subsequently verified with the computed result.

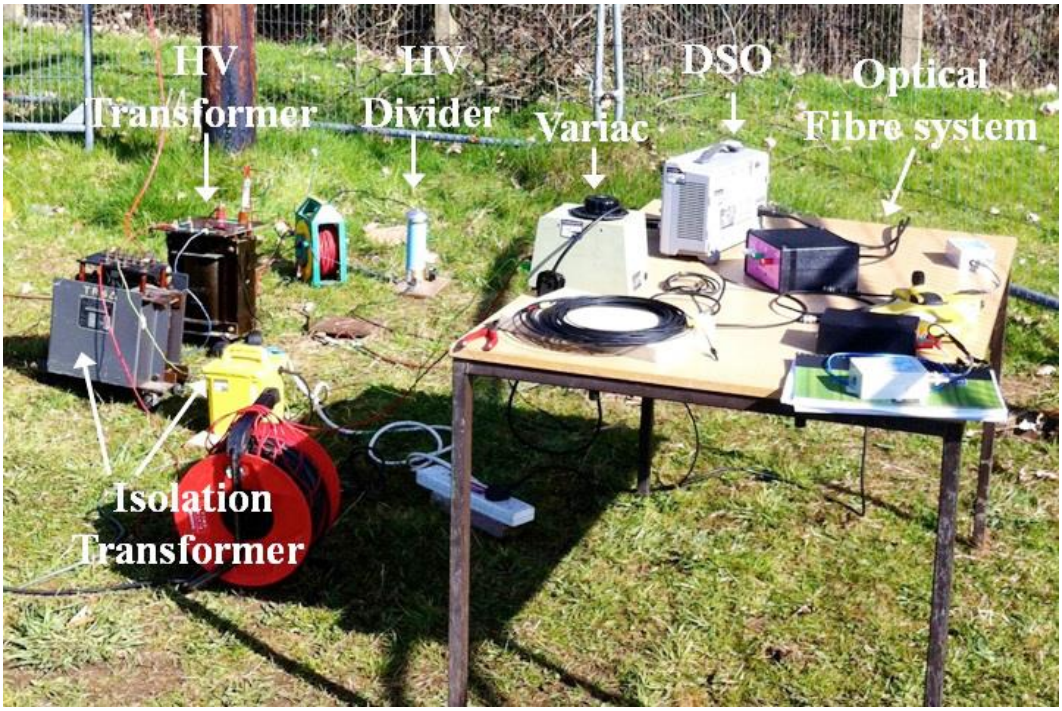

Figure 5.12: The field test measurement setup.

5.4 FIELD EXPERIMENT RESULTS AND ANALYSIS

5.4.1 Low Voltage Test

Figure 5.13 and Figure 5.14 show the corresponding output voltage for each of the three-phase conductors of the overhead line when subjected to the low impulse voltage (lightning and switching impulse shapes respectively). Similar to the laboratory experiment, the impulse voltage field tests are also conducted based on IEC 60060-1 standard. An output voltage amplitude of $0.45V_p$ is measured from the transducer when $300V_p$ voltage is applied and a C_i of 1nF is inserted between the HV conductor and the sensing probe for both impulse tests. The results shown in the figures demonstrate that the output voltage amplitudes have similar shapes, even though the transducer is tested independently at different phases. However, there is an apparent presence of noise (mainly lightning test) due to the applied voltage ($300V_p$), for this particular field test is considered to be too low (owing to the height of the transducer above ground level of 8.5m).

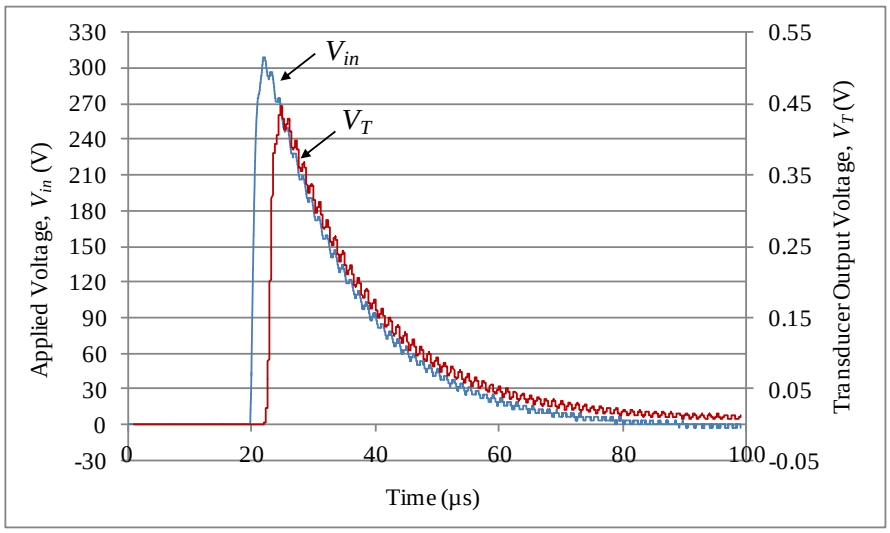

(a) Measured transducer output voltage obtained at HVC1.

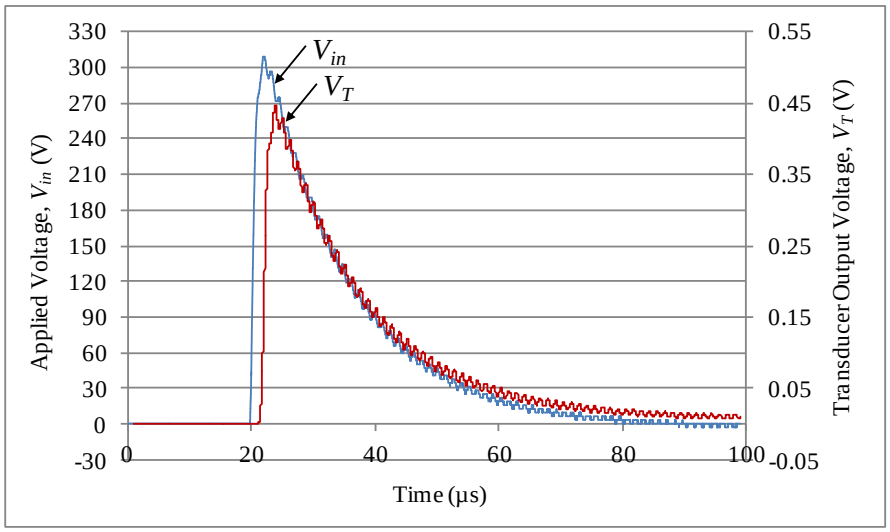

(b) Measured transducer output voltage obtained at HVC2.

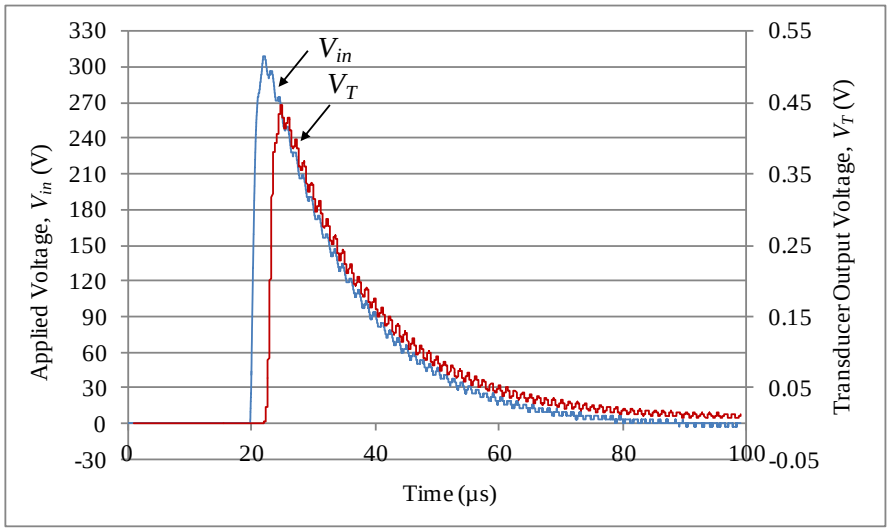

(c) Measured transducer output voltage obtained at HVC3.

Figure 5.13: Measurement results obtained when applied low amplitude of lightning impulse voltage.

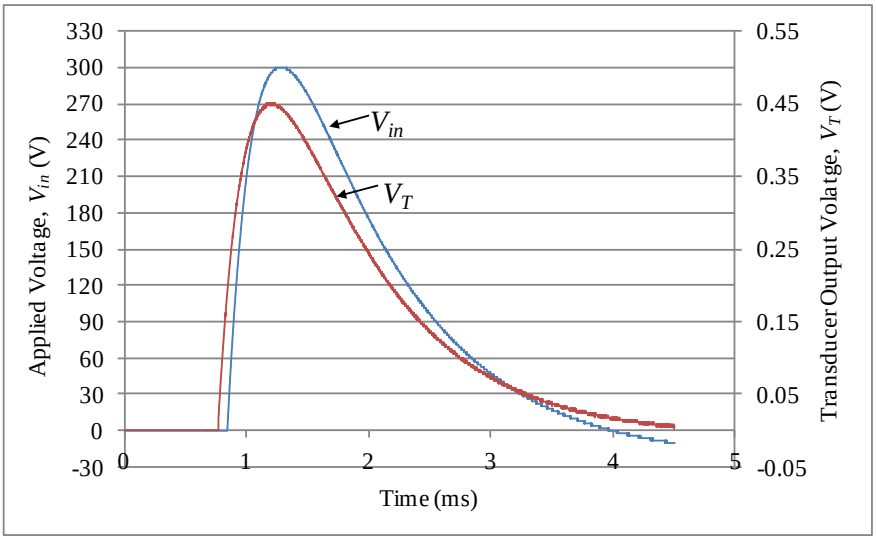

(a) Measured transducer output voltage obtained at HVC1.

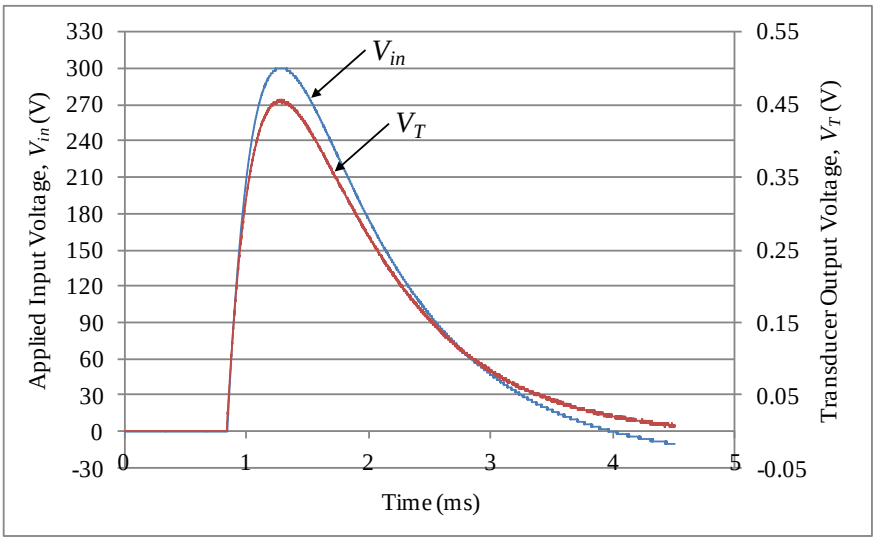

(b) Measured transducer output voltage obtained at HVC2.

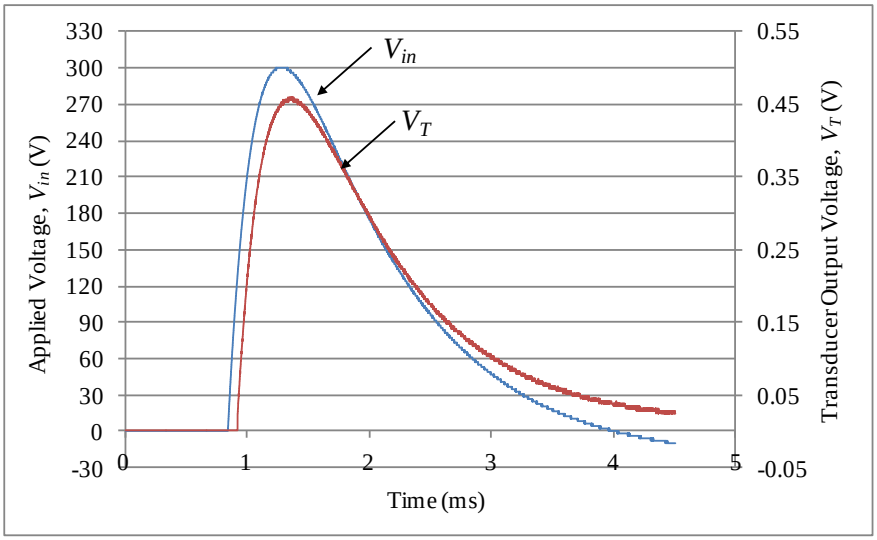

(c) Measured transducer output voltage obtained at HVC3.

Figure 5.14: Measurement results obtained when applied low amplitude of switching impulse voltage.

The results corresponding to the low impulse voltage application are then verified against the results obtained with the low ac voltage (by replacing the impulse generator in the measurement setup with a variac). Figure 5.15 displays the ac measurement results acquired when the transducer is placed on the middle conductor (HVC2). The output voltage amplitude obtained from this ac test shows an output voltage of $0.45V_p$ obtained for a $300V_p$ input supply. The results above indicate that the transducer is capable of measuring different types of voltages consistently. Furthermore, the results also justify the finding (measurement results) established in the laboratory experiments, as discussed in Section 4.4.1.

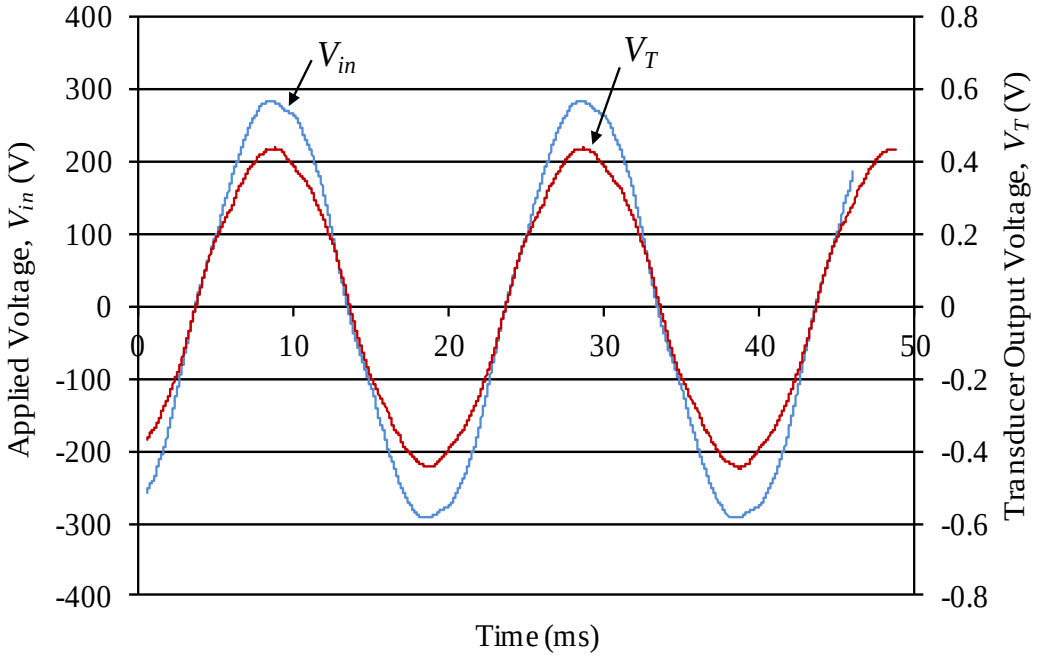

Figure 5.15: Low ac test measurement results obtained when the transducer is placed on the middle conductor (HVC2).

Table 5.4 compares the measured and computed results of the probe's output voltage under ac application. There is a difference of 15% between the output voltages for the two cases, with the one corresponding to the field test having a higher value of $0.45V_p$. This is attributed to noise interference in the outdoor field environment. However, this difference is considered to be well within the acceptable accuracy limits.

Table 5.4: Output voltage comparison between the experiments and computational results.

Result	Output Voltage, V_T (V_p)
Field test	0.45
Computed	0.38

5.4.2 High Voltage Test

Figure 5.16 shows the output voltage obtained from the transducer against the input voltage when a C_i of 22nF and a height of 8.5m above ground of the HV conductor are used. The result demonstrates that the transducer output voltage has a linear relationship with the amplitude of the input voltage, which is consistent with the results produced in the laboratory experiments. A sample of sinusoidal waveforms for the input and output voltages (when C_i and height above ground is 22nF and 8.5m respectively) is illustrated in Figure 5.16; this is obtained when the AC applied voltage is set to $10kV_{p-p}$, with a corresponding transducer output voltage of approximately $0.65V_{p-p}$. This result is acquired when the transducer is placed on the middle conductor of the three-phase overhead line. The measurement results were subsequently compared with the computed results based on the developed field experiment model, as shown in Table 5.5. There is a difference of 7% between the measured and the computed result, which is considered to be within the acceptable range.

Table 5.5: Comparison between the field test result and the modelling result.

Result	Output Voltage, V_T (V_{p-p})
Field testing	0.65
Computed	0.60

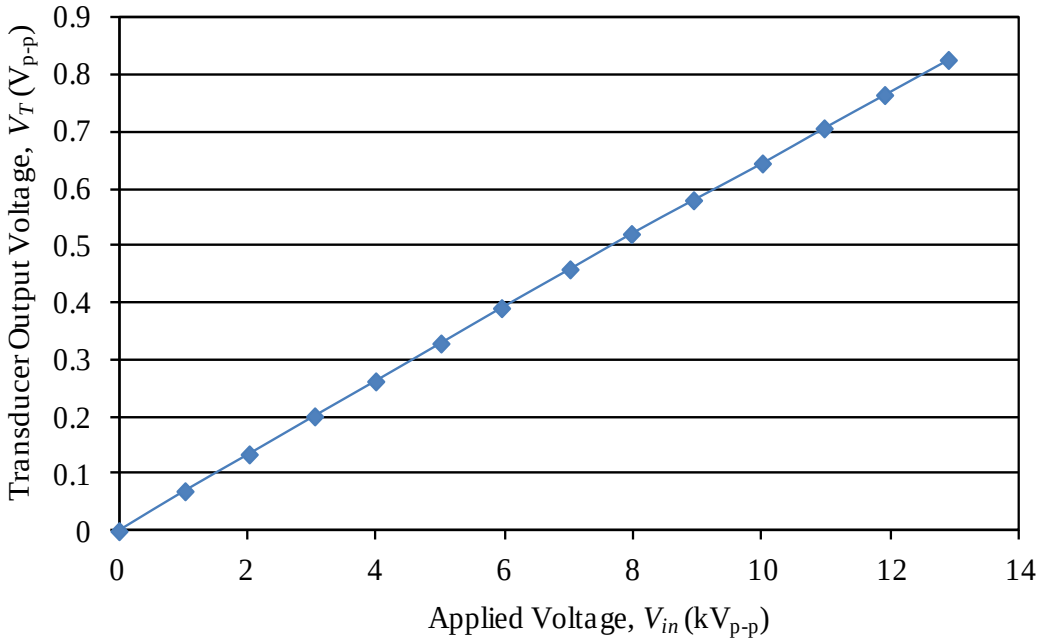

Figure 5.16: Transducer output voltage against the applied voltage.

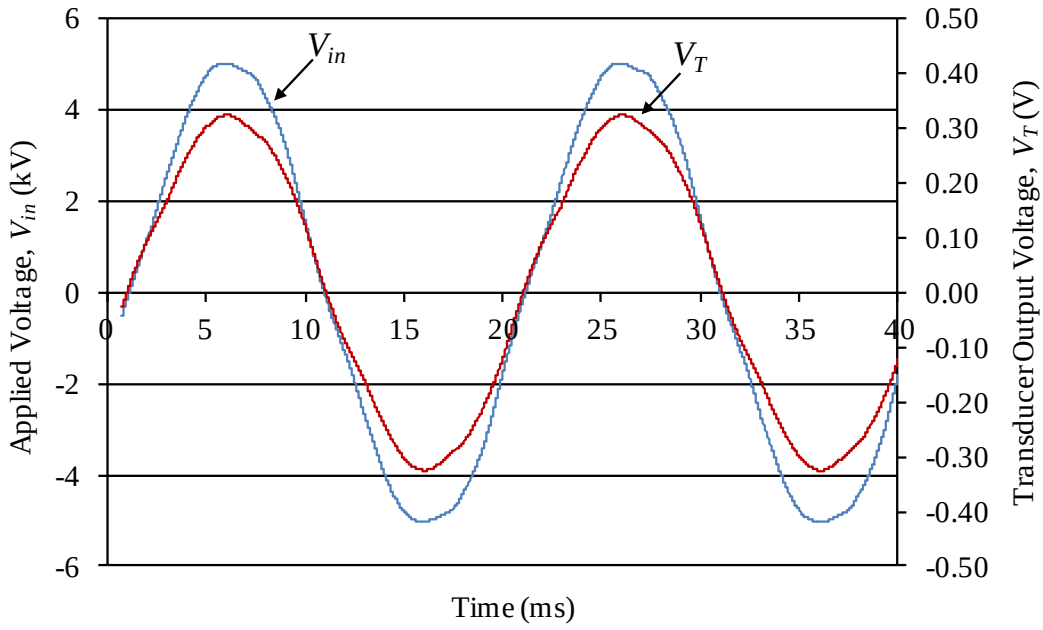

Figure 5.17: Measured output obtained from the ac high voltage test when the transducer is placed at the middle conductor.

5.5 CONCLUSION

Prior to the field tests, a 2D modelling simulation was constructed based on the field test configuration. The modelling simulation was used to determine a suitable value of capacitance C_i (considering that C_i is one of the controllable components in the measurement system that could be inserted between the sensing probe and the HV conductor). This was necessary in order to prevent damage to the fibre optic transmitter, which only allows a maximum of $1V_{p-p}$. Furthermore, the modelling simulation was also developed to observe a possibility of interference caused by the nearby metal fence that separated the test field from the school field. No interference occurred because the transducer is far away from the metal fence at approximately 8.5m.

The field tests were divided into two stages, namely the low and high voltage tests. The low voltage test was conducted as a preliminary test to understand the field environment and the measurement equipment. A physical capacitance (C_i) value of 1nF is used for the test, and this value is selected based on the modelling computation result for low voltage test configuration. The overhead line conductors were tested individually owing to the fact that only one transducer is fabricated in this work and in each case, the transducer is placed near to the OHL pole (approximately 1m) in order to avoid additional sagging of the conductor (considering the transducer weighs around 4.5kg).

An initial test was conducted with low amplitude impulse voltages (lightning and switching respectively) using the low-voltage surge generator. There was no difference in the output voltage amplitude or the impulse voltage patterns obtained from each phase. The measured amplitude was later cross-checked with an ac voltage test. The results obtained from the low voltage field tests agreed with the measurement results acquired from the laboratory test, indicating that the developed transducer is capable of measuring different types of input voltages.

Only a high voltage ac test using a high voltage transformer was performed for high voltage field tests, since dealing with a high impulse voltage supply requires complex protection measurements and setup, and involves additional hazards. The results of the high voltage tests show that the output voltage obtained from the transducer is linearly proportional with the input voltage. This finding also agrees with the results obtained from the laboratory tests. The field experimental results obtained from both tests are evaluated against the computational modelling results, with only small differences noted between the models and the measurement results (probably due to the presence of stray capacitance in the measurement setup). The differences are within the acceptable limits, indicating that the developed transducer is suitable for application on high voltage overhead conductors.

CHAPTER 6

FURTHER DESIGN REFINEMENT OF THE NEW HIGH VOLTAGE IMPULSE TRANSDUCER

6.1 INTRODUCTION

The developed voltage transducer is designed to measure steady state and surge overvoltage, particularly on 11kV overhead lines, which are mostly located in rural areas. The transducer can also be used on substation busbars. However, there are aspects of the transducer design open for improvement. The developed transducer is perceived to be practically heavy, as it is approximately 4.5kg and bulky in size. Therefore, refinement should aim at a better and more compact design of the voltage transducer in order to improve its portability and weight for the transportation and installation process. Since the transducer is placed on the OHL conductor instead of the ground, it is vital not to violate the OHL's ground clearance in order to ensure the safety and performance of the OHL operation, as detailed in Section 2.2.1.

As an initial point of refinement, the originally developed transducer model design is remodelled into two different models of smaller dimensions. A numerical method computational software package described in Chapter 3 is used to model and compute the electric field distribution around the refined transducer and the HV conductor. From the computed results, the effects of the reduction of the sensing probe dimensions (surface area) on the electric field magnitude along the width of the sensing probe and the geometric probe capacitance (C_T) of the refined transducer design are analysed and compared with the computed results obtained from the original model. This geometric capacitance is then verified through analytical calculation.

The computed results of the developed transducer demonstrate significant end-effects at

the edges of the sensing probe, as shown in Section 3.5, and there is a concern that these effects may possibly initiate corona or partial discharges. Therefore, a new improved transducer design is proposed that would incorporate an additional floating electrode (Figure 6.8, Section 6.4) around the sensing probe in order to alleviate this problem. This additional floating electrode is intended as a foil and would have the same potential as the sensing probe, helping to prevent the sensing probe from sensing unwanted electric fields. Furthermore, the additional floating electrode could also provide extra guarding by providing more distance between the sensing probe and the guard electrode, rather than depending solely on the air gap.

The single-phase model configuration described in Chapter 3 is developed for the improved transducer model, and the electric field magnitudes on the probe surface are computed based on the model. Comparisons are made between the improved and original models in terms of the magnitude of end-effects at the sensing probe edges, along with assessment of the geometric capacitance of the transducer before and after adding the floating electrode. However, the improved transducer models are yet to be physically constructed, and their development is thus proposed for future work as outlined in Chapter 7.

6.2 MODELLING OF REFINED MODELS

The original transducer (as described in Chapter 3) is remodelled into two smaller models in order to obtain a more compact transducer design. The developed (original) model is labelled “Model A,” while the other two smaller models are labelled “Model B” and “Model C” respectively. The dimensions of Model B are half of those of Model A, while the dimensions of Model C are a quarter of those of Model A, as shown in Figure 6.1, where “d” and “r” represent diameter and radius of the transducer respectively.

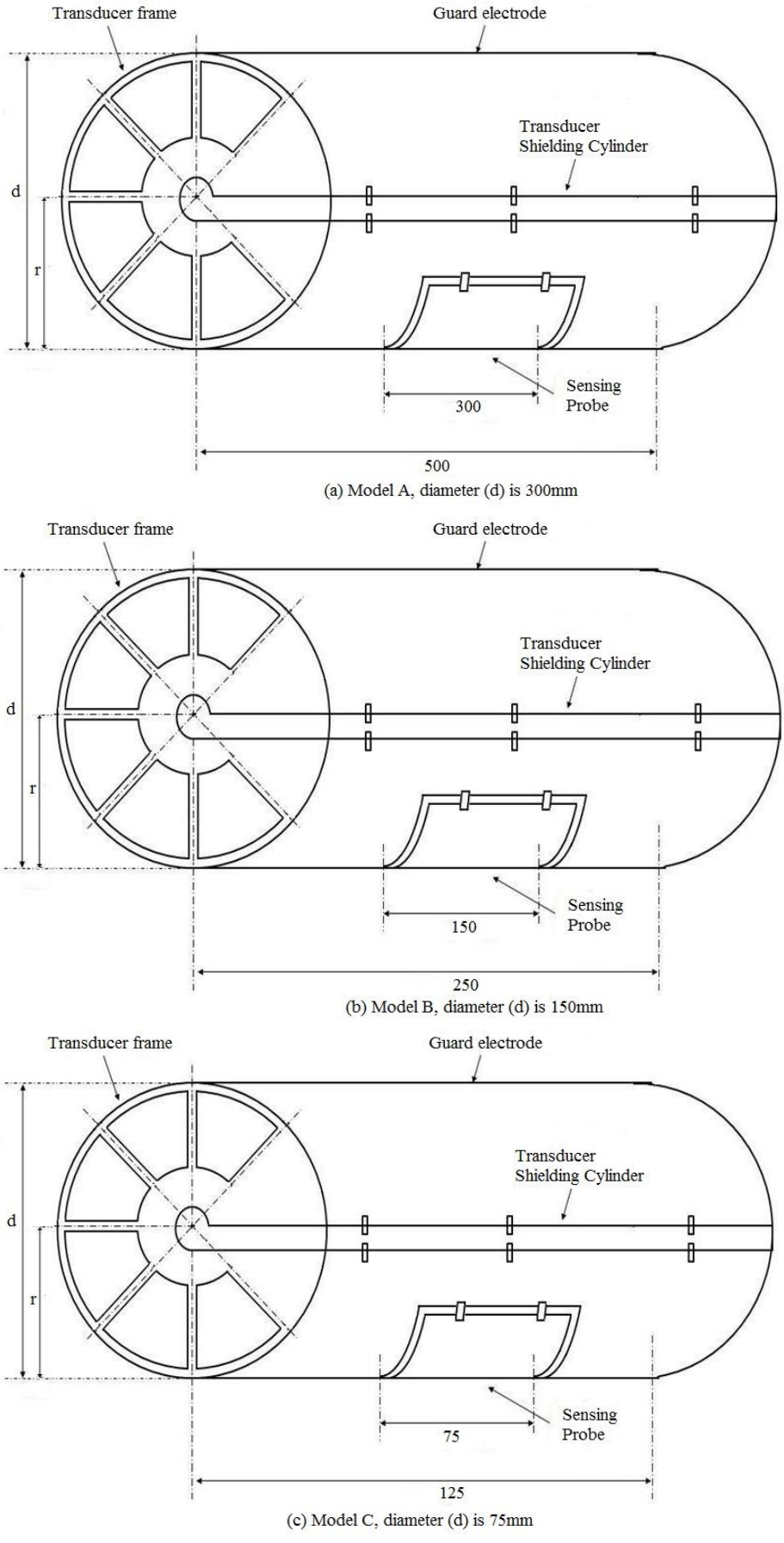

Figure 6.1: (a) Model "A", (b) Model "B" and (c) Model "C" (dimension in mm and not to scale).

The sensing probe areas for both models are also reduced correspondingly, as tabulated in Table 6.1.

Table 6.1: Sensing probe surface area for respective models.

Model	Sensing probe surface area, (cm^2)
A	600
B	150
C	37.5

The refinement models are simulated in 2D and 3D using SLIM and Coulomb respectively. The software is used to compute the electric field distribution around the transducer sensing probe and the HV conductor. The value of the electric field is then used to calibrate the transducer by calculating the geometric capacitance of the voltage transducer. The single-phase laboratory configuration (as developed in Chapter 3 and shown in Figure 3.5 and Figure 3.8) is used for 2D and 3D modelling respectively in order to allow for a direct comparison (based on the simulated results) between the original model (Model A) and the refined models (Model B and Model C).

6.2.1 Refined Model Based on Two-Dimensional Modelling

Modelling simulation procedures similar to those described in Section 3.4 are repeated in this work, and a Matlab routine (as described in Chapter 3) is also used to assist with the integration of the electric field magnitudes over the entire probe surface to determine the charge (Q) on the sensing probe surface. Figure 6.2 compares the computed electric field magnitudes along the width of the sensing probe obtained from the refined Model B and Model C against Model A (original model). As can be seen on the figure, the computed electric field magnitudes on the sensing probe obtained from Model C are higher than those Model A and Model B, due to the fact that the sensing

probe surface of Model C is closer to the HV conductor as a result of its smaller dimensions.

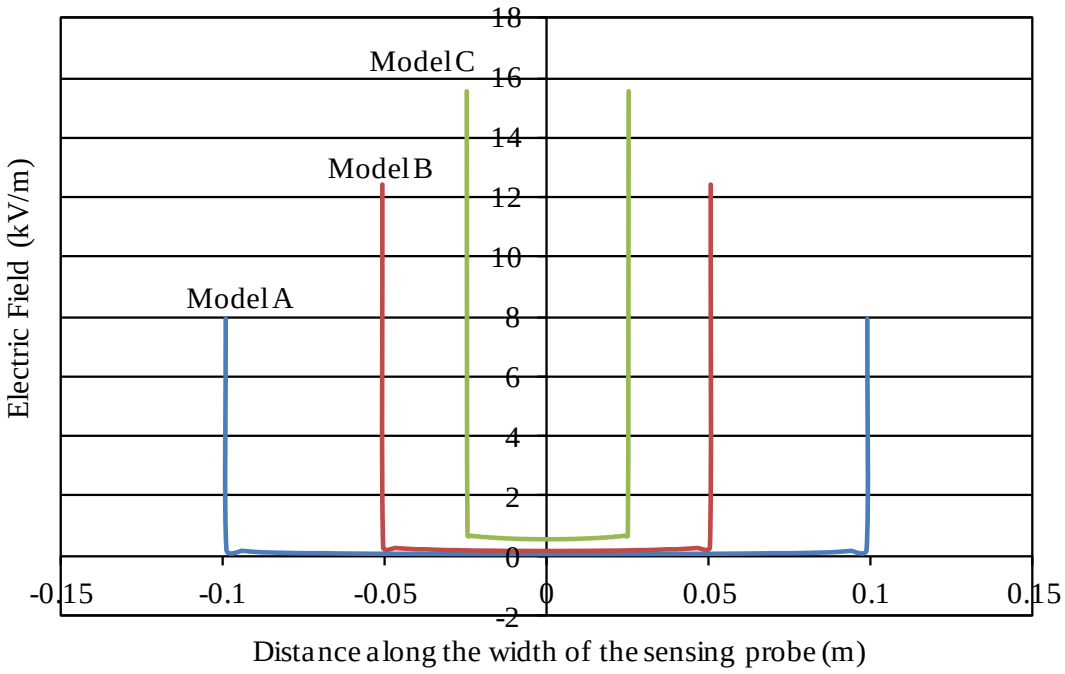

Figure 6.2: Comparison of the electric field magnitudes between the refined and the original models for 2D modelling.

The relationship between the electric field magnitude and the transducer dimensions (as shown in Figure 6.1) is non-linear, as shown in Figure 6.3. This figure is expressed by plotting the electric field obtained at the centre of the sensing probe against the distance of the sensing probe from the centre of the HV conductor which also represent radius (r) of the transducer. These results are obtained when the models are injected with 1kV alternating voltage. The refined models also show the high field magnitudes due to end-effects at the sensing probe edges, which are similar to the original model computation results (as discussed in Chapter 3). Figure 6.4 illustrates the electric field magnitudes over the surface of the sensing probe, which were generated using Matlab based on the computed results of Model B.

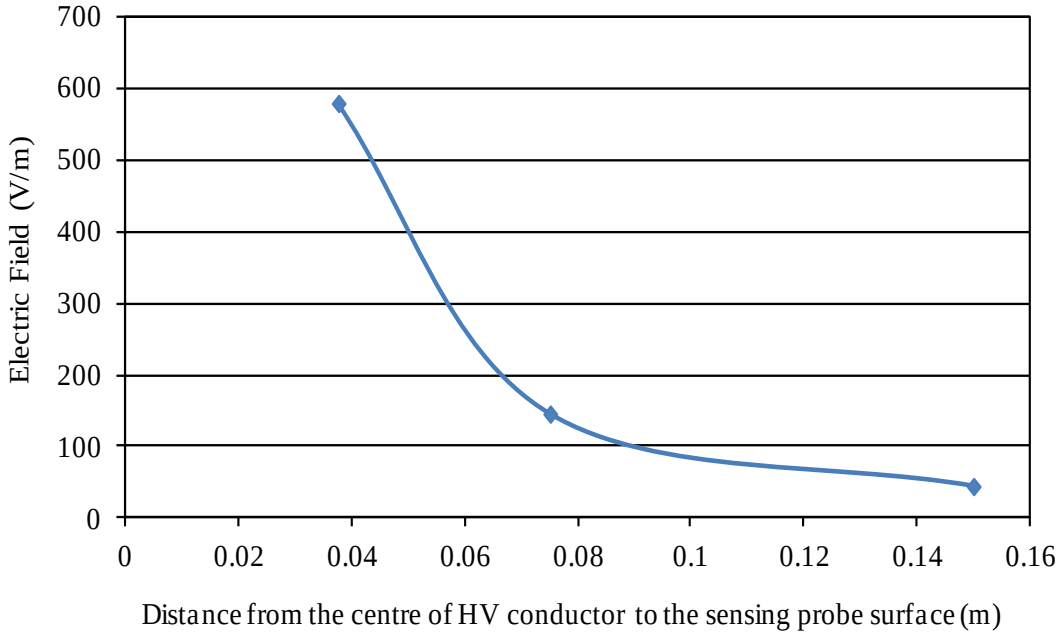

Figure 6.3: Electric field at the centre of the sensing probe against radius of the transducer.

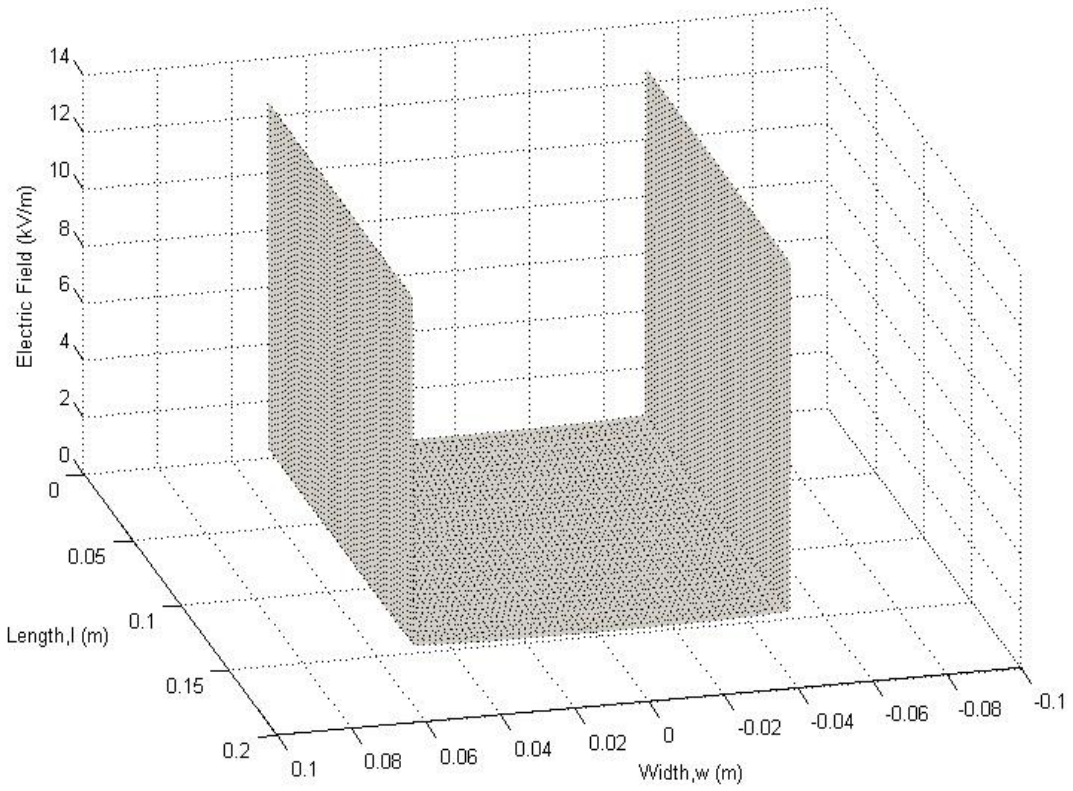

Figure 6.4: Electric field magnitudes on the surface of the sensing probe for Model B.

Table 6.2 summarises the charges induced on the sensing probe surface for each model. Based on this charge value, the geometric capacitances (C_T) for all models were determined and are given in Table 6.3. The results demonstrate that C_T values decrease when the dimensions of the transducer are reduced. These geometric capacitances of the 2D model are compared with the 3D model computational and analytical results in Section 6.3.

Table 6.2: Comparison of the electric field integration on the sensing probe surface area.

Model	Charge Q on the sensing probe surface (nC)
A	0.13
B	0.06
C	0.02

Table 6.3: Geometric capacitance corresponding to each modelling.

Model	Geometric capacitance, C_T (pF)
A	19.9
B	9.1
C	4.9

6.2.2 Refined Models Based on Three-Dimensional Modelling

The simulation procedures for the 3D model (as described in Section 3.4.2) are performed here, with the entire physical boundaries being defined and the model surfaces were meshed into triangular elements to enable computation and analysis of the electric field distribution on the sensing probe surface. Figure 6.5 compares the electric field magnitudes obtained from the centre of the sensing probes of the two refined models (Model B & Model C) against the original model (Model A).

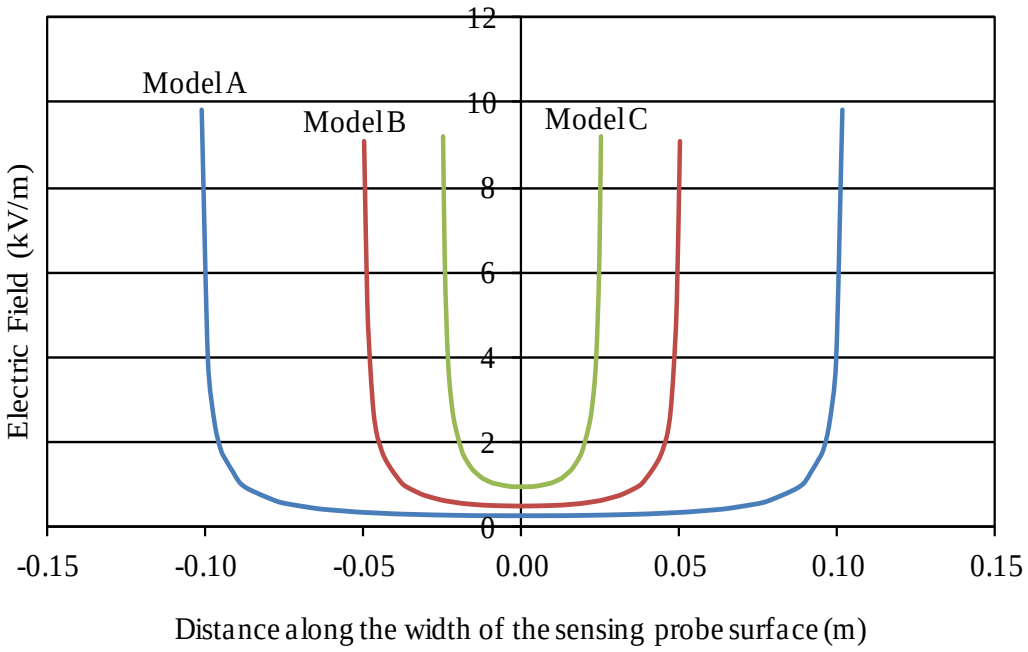

Figure 6.5: Comparison of the electric field magnitudes between the refined and the original models for 3D modelling.

Similar to the 2D modelling results described in the previous section, the electric field magnitudes of Model C are higher than those of Model A and Model B, as the sensing probe surface of Model C is nearer to the HV conductor (due to its smaller dimensions). The 3D refined models also indicate end-effects at the edges of the sensing probe. These magnitudes are obtained when the models are supplied with 1kV alternating voltage. The electric field magnitude decreases as the dimensions of the transducer increases (as the sensing probe surface is further away from the HV conductor), as illustrated in Figure 6.6. This figure is plotted based on electric field magnitude obtained at the centre of the transducer sensing probe against the distance of the sensing probe from the centre of the HV conductor (radius (r) of the transducer as shown in Figure 6.1).

Table 6.4 summarises the charges induced on the sensing probe surface for each model (refined and the original models). The charge values are determined based on the integration of electric field magnitudes on the sensing probe surface (as shown in Figure

6.5). Table 6.5 gives the comparison of the capacitance (C_T) values of the refined models and the original model as obtained from the 3D simulation. As shown in Table 6.5, the geometric capacitance value decreases when the transducer dimension is reduced.

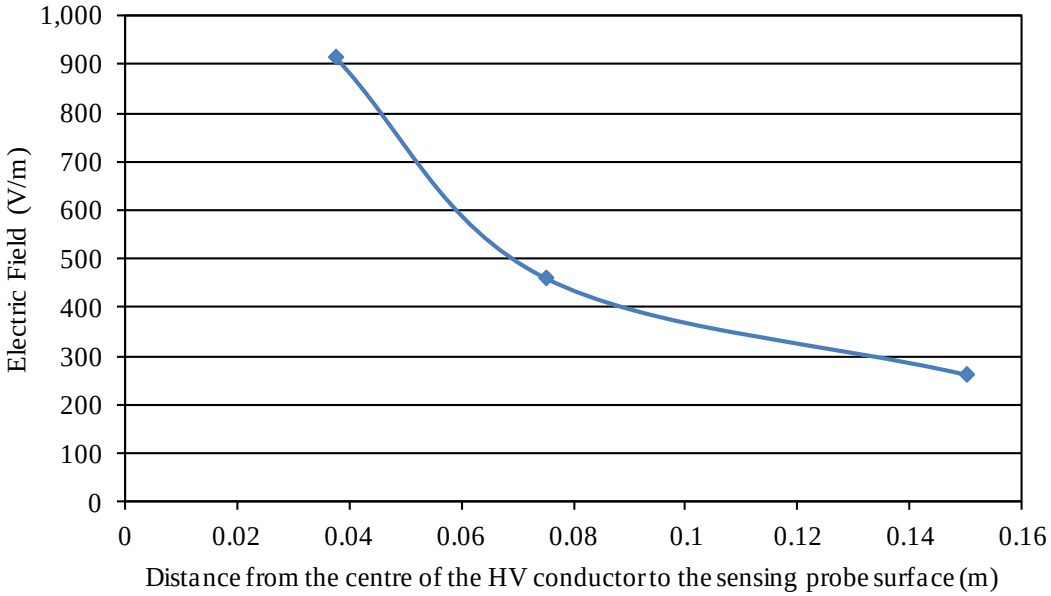

Figure 6.6: Electric field at the centre of the sensing probe against the transducer radius.

Table 6.4: Induced charge (Q) on the probe surface for the three probe models.

Model	Charge (Q) on the sensing probe surface (nC)
A	0.86
B	0.36
C	0.18

Table 6.5: Comparison of the C_T for the 3 models using 3D modelling.

Model	Geometric capacitance, C_T (pF)
A	21.7
B	10.5
C	6.1

6.3 ANALYSIS OF REFINED MODELS

The simplified analytical calculation approached (as explained in Chapter 3, Section 3.6) are used to calculate the geometric capacitance (C_T) of the refined transducer designs. Table 6.6 compares the computed C_T values of the models and the analytical calculation using Equation (3.13). As can be seen in the table, the computed geometric capacitances of the refined models are within an acceptable range when compared with the C_T values obtained from the analytical calculation. The 3D models produced a higher geometric capacitance than the 2D models due to the higher accuracy of Coulomb software, as the former takes into account the full dimensions of the transducer and the HV conductor. The benefit of this feature allows for enhanced analysis of electric field distribution on the entire surface area of the sensing probe. The 2D model, on the other hand, only computes the field based on the cross-section, and assumes the transducer and HV conductor length to be infinite. Moreover, the geometric capacitance values computed from the models (mainly the 3D computational) are much higher due to the fact that the analytical approach is based on the simplified coaxial cable approach, with the assumption that the end-effects at the sensing probe edges are neglected. Nonetheless, the computed and analytical results agree that a smaller transducer resulted in a lower value of geometric capacitance.

Table 6.6: Comparison of the capacitance (C_T) of the computed and analytical calculations for all models.

Model	Geometric capacitance, C_T (pF)		
	SLIM (2D)	Coulomb (3D)	Analytical
A	19.9	21.7	19
B	9.1	10.5	9.7
C	4.9	6.1	5.10

The developed transducer (Model A) is considered to be a bit bulky, but it offers an adequate space for storing the optical fibre system, which is comprised of a bulky battery pack (as described in Chapter 2). The battery pack can be difficult to store inside the new refined models (Model B and Model C), as their dimensions are smaller. Therefore, the existing optical fibre system needs to be redesigned or a new optical system needs to be developed and constructed to fit into the new refined transducer configuration.

Model C has better portability when compared with the others model (Model A and Model B) since it has the smallest dimensions, which results in a reduction of the sensing probe surface area. Owing to this, the charges induced on the sensing probe surface are also reduced, based on Equation (3.5). There is a concern about the accuracy of the measurement results, based on the ability of the sensing probe to sense an adequate electric field magnitude.

When the transducers (especially Model C) deal with severe weather conditions such as heavy wind, the straight vertical position of the transducer to the ground can be altered to a slightly adjacent position (by swinging the transducer around). As a result, this changes the geometry of the measurement configuration and possibly causes a reduction in the accuracy of the measurement result. Nonetheless, this swing effect can be avoided by positioning the transducer closer to the overhead line pole (described in Chapter 5). Therefore, it is better to construct and test these refined models in order to understand the implication of reduction of the sensing probe surface on the output voltage measurement. However, due to time constraints, this is proposed as future work.

6.4 IMPROVED MODEL OF THE TRANSDUCER

As demonstrated in Section 3.5, significant end-effects at the edges of the sensing probe are detected due to the fact that the air gap separating the sensing probe from the guard

electrode is not adequate to isolate the probe from sensing the electric field from the nearby guard electrode (considering there is only a 1mm gap separating them), as shown in Figure 6.7. Therefore, a new, improved design is developed through the installation of an additional floating electrode between the sensing probe and the guard electrode, as shown in Figure 6.8.

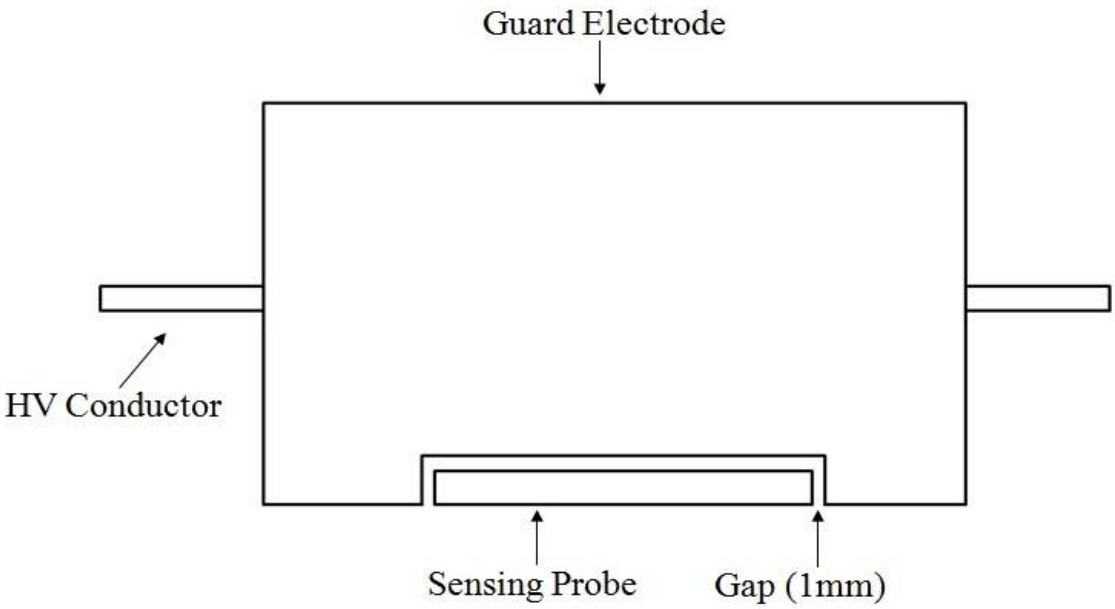

Figure 6.7: The developed voltage transducer (not to scale).

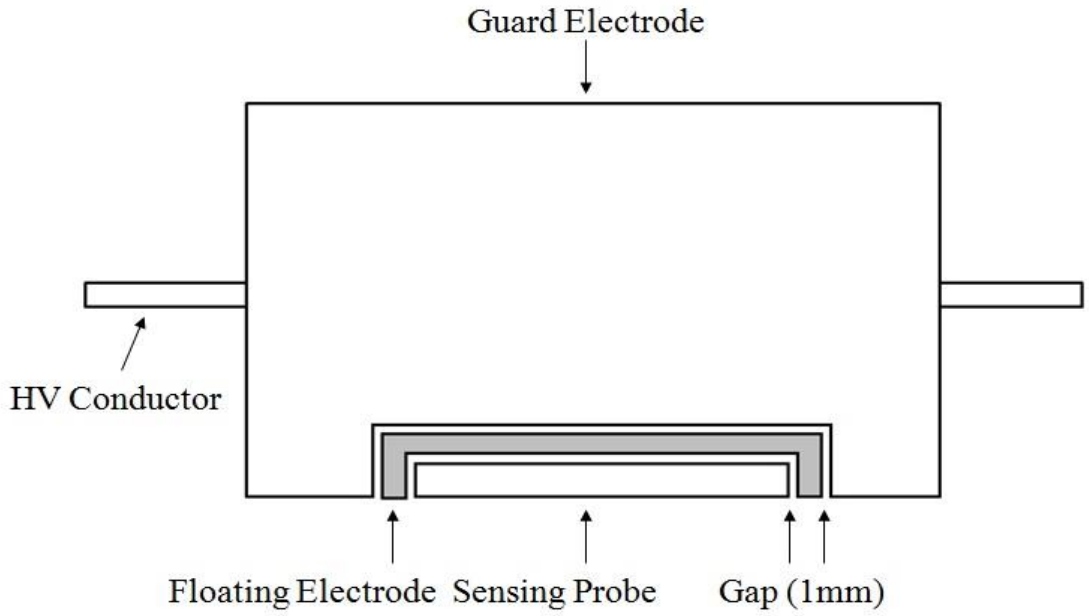

Figure 6.8: The improved transducer model (not to scale).

The additional floating electrode is set to have the same potential as the sensing probe, as it is assigned as a foil in order to reduce the end-effects. Moreover, this floating electrode can also provide wider gaps between the sensing probe and the guard electrode, which previously depended solely on the small air gap. The width of the floating electrode is 5mm and a gap of 1mm is incorporated into the design of the improved transducer model in order to separate the floating electrode from the sensing probe and the guard electrode.

Only the 3D model is conducted for this improved work due to the limitations of the SLIM software, which is unable to identify and differentiate between the additional floating electrode and the sensing probe (as both of them have the same potential). Simulation procedures are similar to the 3D model process mentioned in Chapter 3. Figure 6.9 compares the electric field magnitudes of the developed transducer (Figure 6.7) and the improved model with an additional floating electrode (Figure 6.8), with magnitudes being taken along the width of the sensing probe surfaces.

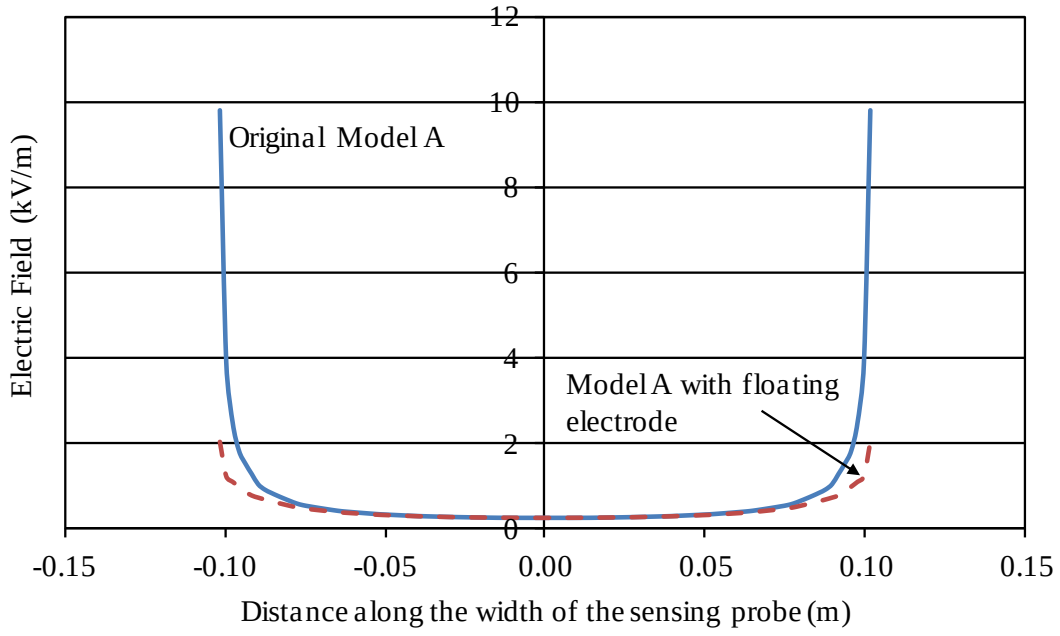

Figure 6.9: Comparison of the electric field magnitudes between the original and the improved model obtained from 3D modelling.

The computed results demonstrate a significant reduction of electric field at the edge of the sensing probe in the improved model simulation. The field magnitude at the probe edge was reduced significantly from 10kV/m to approximately 2kV/m. This field magnitude is generated when the models are injected with 1kV alternating voltage. Using these computed field magnitudes obtained from the improved model (as shown in Figure 6.9), the induced charge on the sensing probe surface is estimated to be 0.32nC. Table 6.7 compares the geometric capacitance (C_T) values of the developed transducer and the improved model. The geometric capacitance is calculated using the computed electric charge on the probe surface, as presented above (Figure 6.9).

Table 6.7: Comparison of the C_T of the developed and improved models.

Geometric Capacitance, C_T (pF)	
Developed	Improved
21.7	7.2

From the table, it is noted that the geometric capacitance (C_T) value of the improved model is almost 67% smaller than that of the developed model, as the improved model significantly reduces end-effects at the sensing probe edges. Therefore, concern about partial discharge at the probe edges can be disregarded for this model. There is no comparison made in the physical measurement, as the improved transducer model has not been constructed in this work. This procedure is proposed as a future work in the next chapter.

6.5 CONCLUSION

The developed transducer is refined by remodelling it into two smaller designs, namely Model B and Model C. These models are created in order to study the merits of designing a more compact transducer based on the original model. This allows for a more lightweight transducer, and prevents the possibility of violating the operational safety of the overhead lines, as the developed transducer uses the HV conductor as the measurement reference.

Single-phase overhead lines are constructed using SLIM and Coulomb for the simulation of 2D and 3D modelling computation in order to compute the electric field around the HV conductor and the sensing probe for these two models. This electric field is subsequently used to calibrate and determine the geometric capacitance (C_T) of the voltage transducer. The computed results obtained from both models demonstrate that a smaller transducer model (Model C) produces a lower value of geometric capacitance. Low output voltage is predicted to be produced from the small refinement model (Model C) since the induced charge computed on the sensing probe surface is reduced correspondingly to the transducer sensing probe surface area, consequently affecting the geometric capacitance value of the transducer model (as tabulated in Table 6.4 and 6.5 respectively). In keeping with the developed transducer's computational results, the refined transducer models also indicate end-effects at the sensing probe edges, which have the potential to initiate partial discharges. In order to reduce the end-effects, an improved design is proposed for the developed transducer that incorporates an additional floating electrode around the sensing probe.

The computed results obtained from the improved model simulation show that the electric field magnitude at the probe edges is vastly reduced, from 10kV/m to approximately 2kV/m. This indicates that the addition of the floating electrode manages

to reduce the end-effect, as the electrode provides extra space between the sensing probe and the guard electrode. An equal potential is assigned for both the electrode and the sensing probe, thus preventing the sensing probe from picking up any unwanted field around the probe edges. As a result, the risk of partial discharge is reduced, and a smaller value of geometric capacitance is produced when compared with the originally developed model. Unfortunately, physical construction of these refined and improved models has not been completed due to time constraints. Thus, the construction of these models is proposed as a future work in Chapter 7.

CHAPTER 7

GENERAL CONCLUSION AND FUTURE WORK

This research aims to design, develop and construct a compact, portable and low cost voltage transducer that can be used to measure different types of voltages including monitor faults by measuring impulse voltages, particularly on 11kV overhead lines. A comprehensive literature review is completed by outlining various approaches of OHL monitoring techniques, along with advantages and disadvantages of individual techniques used to ensure that overhead lines are maintained in an appropriate working condition.

Overhead lines are the backbone of the electrical power distribution network, as they are the medium used to transmit and distribute electrical power from power stations to end users. However, overhead lines are exposed to adverse weather condition (such as heavy wind, snow and ice), pollution and tree initiated faults. Furthermore, surge voltages caused by transient overvoltage originating either from lightning strikes to the lines or switching operations on the power transmission networks also contribute to faults occurring on overhead lines. The occurrence of overvoltages can cause a decline in the health of overhead line conductors by accelerating the aging and reducing the current-carrying capability of the conductor. It is, therefore, paramount that measurements and condition monitoring of voltages on the conductors and terminals be assessed as accurately as possible in order to maintain a safe and economic operation of HV substations and overhead line equipment.

There are a number of measurement devices available on the market that can be used to monitor and measure impulse voltages on overhead lines, such as HV dividers, and voltage transformers. However, there are still challenges that need to be addressed, such

as time consumption during installation and maintenance of the transformer, which require the line to be disconnected or switched off. This procedure can interrupt line operation and cut into energy providers' profits. Installation or maintenance work also can result in end users being temporarily cut off from their electricity supply. In addition, the large size and cost of the divider makes implementation inconvenient on a wider commercial scale, as HV dividers require a proper housing in order to protect them from vandalism or theft when placed on the ground.

A non-contact capacitive voltage probe which was previously developed and constructed at Cardiff University was thoroughly assessed in this present research for a thorough understanding of the capacitive divider measurement technique with ground as the measurement reference. The design of this former probe is based on a circular shape, and the sensing plate is surrounded by an earthed plate that is designed to reduce end-effects at the sensing plate perimeter. The material used to fabricate this probe is aluminium, and there is an enclosure underneath the sensing plate used for housing the low voltage arm capacitor and other electronic circuits such as buffer and amplifier circuits. Unfortunately, the probe has limitations when dealing with three-phase overhead line measurement due to stray capacitances caused by neighbouring conductors. Furthermore, it is also necessary to position the probe at its optimum position in order to obtain accurate results, and this involves simulation prior to installation of the probe in a real field test environment.

A new design of a voltage transducer is, therefore, proposed and developed in this work. Similar to the former non-contact voltage probe, the new transducer is based on the capacitive probe measurement principle, with the major change that an HV conductor is used as the measurement reference instead of the ground. The proposed transducer construction is based on a cylindrical-shape for ease of installation at the HV conductor,

and also to avoid any sharp edges that could lead to partial discharge. By using the HV conductor as the measurement reference, the issue of stray capacitances from neighbouring conductors and the need to determine the best position for the transducer in order to obtain accurate measurements are avoided.

Two commercial numerical software packages known as SLIM and Coulomb were used to assist in the development and calibration of the new voltage transducer in two-dimensional (2D) and three-dimensional (3D) model environments respectively. The software is utilised for the simulation of electric field distribution around the HV conductor and the developed transducer. The electric field magnitudes computed on the sensing probe surface are crucial for the calibration of the transducer. An integration of the field magnitude is used to quantify the charges on the entire sensing probe surface, and the charge is later used to determine the geometric capacitance of the new transducer.

The model simulation is developed using a single-phase overhead line configuration. For the setup in the laboratory experiment, the transducer is placed at 2.5m above ground level, whilst an alternating input voltage of 1kV is applied to the HV conductor. The equipotential distribution obtained from the SLIM simulation illustrated contour lines that projected away from the HV conductor towards the ground. This indicated that the electric field around the conductor is expected to be high. The profile of electric field magnitudes along the width of the sensing probe portrays some end-effects in the form of increasing field magnitudes towards the edges of the sensing probe at approximately 8kV/m and 10kV/m (from the computation of 2D and 3D models respectively). The respective geometric capacitance (C_T) obtained for 2D and 3D models are 19.9pF and 21.7pF respectively. There is a slight difference between these two values of geometric capacitance, probably due to the higher accuracy of the 3D

model as opposed to the 2D model, since Coulomb software uses the full dimensions of the transducer and the HV conductor, whereas SLIM incorporates an assumption that the length of the developed model is infinite.

A three-phase overhead line model is also developed using SLIM. Computation for this model aims to analyse the effects of stray capacitances between the OHL and the transducers, as they are in close proximity. The geometric capacitance between the HV conductor and the sensing probe must be sufficiently high in order to minimise the effects of stray capacitances from the neighbouring transducer and the conductor. Simulation procedures are performed by alternately injecting voltage at one of the conductor phases and simultaneously setting the others to ground; repetition of the simulation to each phase results in a simple matrix of finite element model. The matrix demonstrates that the developed voltage transducer, as opposed to the non-contact probe, would not be significantly affected by the issue of adjacent phase stray capacitances when dealing with the three-phase overhead line. This is because the transducers face the ground and are setup close to the HV conductor instead of the ground. Therefore, the effects of stray capacitances on the nearby transducer can be disregarded, as can the need to establish optimum positioning during installation of the transducer.

A series of carefully selected laboratory experiments were carried out in order to analyse actual characteristics and perform calibration of the developed voltage transducer, thus ensuring its practicality prior to installation of the transducer in the real overhead line environment. The results obtained from the experiment were then compared with the computed results obtained from the computational models. The laboratory experiments were conducted by injecting low impulse voltage amplitudes onto the HV conductor using the impulse generator, and the experimental setup is based

on the single-phase overhead line configuration. The amplitude of the output voltage obtained from this test was then verified with an ac voltage test. Furthermore, the effects of varying input voltage, transducer height above ground and integrating capacitor (C_i) values inserted between the HV conductor and the sensing probe were quantified.

Based on the experimental results, the amplitude of the output voltage remains at a similar level despite changing the input supply from impulse to ac voltage. The transducer output voltage is linearly proportional to the input voltage, but decreases when the transducer is placed further away from the ground and with increasing increments of the integrating capacitor (C_i) value. Therefore, these results and analysis undertaken demonstrated that input voltage, height of the transducer above the ground and integrating capacitor are the main variables that can be used to control the output voltage produced by the developed transducer. These results were verified with an extensive analytical calculation based on approximation that refers to the geometry of the experimental configuration and neglects the end-effect of the transducer geometric capacitance. The difference between the analytical and measurement results are within an tolerable range approximately 33% due to analytical is based on simplification and also the analytical is not considered the end-effect between the sensing probe and the guard electrode. Further analysis was also carried out using the capacitive divider equation in order to determine capacitance probe to ground value (C_G) from the sensing probe to the ground surface.

Field experiments are conducted on the three-phase test overhead line located in Llanrumney, Cardiff. The field experiments aimed to determine the characteristics of the developed transducer when it is operated in the real overhead line environment. Modelling of the HV conductor geometry with the attached transducer is carried out

before proceeding with the actual test in order to determine a suitable integrating capacitor value that can be inserted between the HV conductor and the sensing probe to ensure the fibre optic transmitter input specifications are not exceeded. The model is also developed in order to investigate any interference to the electric field distribution around the HV conductor and the transducer caused by the nearby metal fence.

At the preliminary stage, the outdoor field experiment is initially carried out using low amplitude voltage in order to understand better the field measurement setup and working environment. Each phase is tested individually based on a single-phase overhead line configuration. The procedures for low voltage tests are similar to the laboratory experiment, in that the HV conductor is injected with a low impulse voltage amplitude and the output voltage amplitude obtained from the transducer is verified with the low voltage ac test. Based on the results of the experiment, it is noted that the amplitude of the output voltage produced by the transducer remains unaffected when the input voltage is changed from impulse to ac voltage. This observation agrees with the results acquired during the laboratory experiments. The output voltage waveforms produced by the transducer for each individual phase are considerably similar to each other, thus indicating that no interference (such as stray capacitances caused by the nearby HV conductors) exists in the measurement results.

A high ac voltage test is also conducted in the field experiment using a step up HV transformer. The HV experiment results demonstrated a linear relationship between the output voltage and the input voltage, and this finding agrees with the results obtained from the laboratory tests.

The developed transducer is considered to be suitable for measuring impulse voltages on the overhead lines based on the results obtained from the model simulation, laboratory and field experiments. However, the transducer is still perceived to be

practically heavy and bulky in size. Therefore, refinement design work is incorporated into this research, concentrated on reducing the size of the transducer for practical purposes. The refinement work involved single-phase modelling of SLIM and Coulomb simulations of two smaller models (Model B and Model C), where Model B is half and Model C a quarter of the dimensions of the original model (Model A) of the developed transducer. The effect of this reduction in size of the transducer dimensions (and particularly the sensing probe surface area) on the magnitude of the geometric capacitance of the transducer was quantified. As the size is reduced, the geometric capacitance of the model also decreases in both SLIM and Coulomb simulations. Analysis with the electric field magnitude also demonstrated that the closer the sensing probe of the transducer is to the voltage source (i.e., the HV conductor), the higher the electric field is.

The developed transducer model simulation also demonstrated the presence of high end-effects at the sensing probe edges. Hence, an improved model which incorporates an additional floating electrode around the probe to overcome this weakness was proposed. This floating electrode is set at the same potential as the sensing probe in order to prevent the probe from sensing the nearby electric field potential. In addition, the additional floating electrode can also provide a wider gap between the guard electrode and the sensing probe rather than depending solely on the small air gap. The improved model computations demonstrated that insertion of this floating electrode results in a significant decrease approximately 80% in the magnitude of the electric field at the probe edges from 10kV/m to 2kV/m (obtained from the computation of 3D model). This has the added benefit of reducing the risk of initiating partial discharge. Due to time constraints, it was not possible to fabricate the refined and improved models and tests them in this work. However, their fabrication is proposed as a future work, as discussed

in the next subsection.

FUTURE WORK

This research has identified the following areas for future investigation:

a) Construction of the refined and improved probe design.

Two refined models have been designed and simulated in Chapter 6 in order to investigate the effects of reducing the dimensions of the transducer (particularly the sensing probe) on its geometric capacitance, which is crucial for calibration purposes. The refined models have smaller dimensions than the present developed transducer, but it is assumed that there is no change in the transducer's ability to measure impulse voltages on the overhead lines.

It is also believed that the design of the improved model can result in a decrease of the end-effects at the sensing probe edges. The computed results generated from the model demonstrated that inserting an additional floating electrode in between the sensing probe and the guard electrode vastly reduces end-effects, which subsequently eliminates the risk of initiating partial discharge.

Physical construction of the refined and improved transducer models is yet to be conducted, and it is thus proposed that these models be constructed and tested in a laboratory environment in order to validate the computational results obtained thus far. The two models can also be combined in order to create a better voltage transducer for monitoring faults on the OHL.

b) Protection unit.

As the transducer is used to measure impulse voltages on overhead lines, it is crucial that a protection unit system be integrated in order to protect the electronic devices located inside the transducer (such as the fibre optic system). The proposed protection

unit should be simple, reliable and inexpensive in its implementation. An example of one such protection unit is a surge suppressor unit that consists of three main components: a Gas Discharge Tube (GDT), a Metal Oxide Varistor (MOV) and spark gap.

c) Integration with current transducer.

Design of the new transducer is based on a cylindrical shape, which facilitates the possibility of integrating a current transducer (such as a Rogowski coil) for current measurement. This would enable the system to measure both voltage and current at the same time, thus enhancing the condition monitoring of overhead lines.

d) Wireless data transfer.

A fibre optic system is currently used to transfer measurement data from the transducer to the receiving end. This present method of data transfer has several disadvantages, such as the requirement of a long fibre optic link, which is costly. Wireless communication methods such as Bluetooth, zigbee or Wi-Fi could be adapted to improve the method of data transfer by wirelessly transferring measurement data. This would do away with the need for any physical connection between the measuring and monitoring sides.

e) Energy harvesting.

The transducer is a stand-alone unit located on overhead lines. Thus, the transducer could utilise energy harvested from the high voltage conductor to power its electronic devices rather than relying on battery power. The decoupling method could be used to harvest the energy by converting the electromagnetic field generated by the conductor into charge. This charge could then be stored in rechargeable batteries.

REFERENCES

[1.1] J.H. Evans, "Overhead Line Fault Current Indicators- Are They Cost Effective", IEE Colloquium on Improving Supply security on 11kV Overhead Networks, London, UK, pp. 14/1-14/5, 22 May 1990.

[1.2] C.A. Spellman, "Condition Monitoring of High Voltage Surge Arresters", PhD Thesis, Cardiff University, pp. 5.11-5.20, September 1999.

[2.1] K.S Hung, W.K. Lee, V.O.K. Li, K.S. Lui, P.W.T. Pong, K.K.Y Wong, G.H. Yang and J. Zhong, "On Wireless Sensors Communication for Overhead Transmission Line Monitoring in Power Delivery Systems", First IEEE International Conference on Smart Grid Communications, Gaithersburg, MD, pp.309-314, October 2010.

[2.2] H.M. Ryan, "High Voltage Engineering and Testing", 2nd Edition, IEEE Power and Energy Series 32, The Institution of Electrical Engineers, ISBN: 085296-775-6, pp. 349-350.

[2.3] E. Kuffel, J. Kuffle and W.S. Zaengl, "High Voltage Engineering Fundamentals", Newnes, ISBN: 0-7506-3634-3, pp. 49, 460, 2001.

[2.4] G. Stroud and J. Elphick, "Remote Condition Monitoring- An Asset Management Viewpoint", The IEE Railway and Control & Automation Professional Networks, IEE Seminar on Railway Condition Monitoring: Why?, What, How?, Atkins Rail, London, February 2005.

[2.5] R. Ambikairajah, B.T. Phung, J. Ravishankar, T.R. Blackburn and Z. Liu, "Smart Sensors and Online Condition Monitoring of High Voltage Cables for the Smart Grid", Proceeding of the 14th International Middle East Power Systems Conference, Cairo University, Egypt, pp. 807-811, December 2010.

[2.6] A. S. Kumar, R.P. Gupta, K. Udayakumar and A. Venkatasami, "Online Partial Discharge Detection and Location Techniques for Condition Monitoring of Power Transformers: A Review", International Conference on Condition Monitoring and Diagnosis, Beijing, China, pp. 927-931, April 2008.

[2.7] M. J. Moser, H. Zangl, T. Bretterklieber, G. Brasseur, "An Autonomous Sensor System for Monitoring of High Overhead Power Supply Lines", Journal of Elektrotechnik & Informationstechnik, Vol. 126, Issue 5, pp. 214-219, May 2009.

[2.8] M. Landry, R. Beauchemin, A. Venne, " De-icing EHV overhead transmission lines using electromagnetic forces generated by moderate short-circuit currents", IEEE 9th International Conference on Transmission and Distribution Construction, Operation and Live-Line Maintenance, Montreal, Canada , pp. 94-100, October 2000.

[2.9] M.J. Moser, T. Bretterklieber, H. Zangl and G. Brasseur, "Strong and Weak Electric Field Interfering: Capacitive Icing Detection and Capacitive Energy harvesting on a 220-kV High-Voltage Overhead Power Line", IEEE Transactions on Industrial Electronics, Vol. 58, No. 7, pp. 2597-2604, July 2011.

[2.10] R.K. Aggarwal, A.T. Johns, J.A.S.B Jayasinghe and W. Su, "An Overview of the Condition Monitoring of Overhead Lines", Elsevier, Electric Power System Research,Vol. 53, pp. 15-22, December 1998.

[2.11] Jaensch G, Hoffman H and Markees A, "Locating defects in high-voltage transmission lines", Proc. of IEEE 8th Intl. Conf. ESMO 98, Orlando, USA, pp 179-186, April 1998.

[2.12] P.J. Moore, I.A. Glover, “Remote Diagnosis of Overhead Line Insulation Defects”, IEEE Power Engineering Society General Meeting, Vol.2, Denver, Colorado, USA, pp. 1831-1835, January 2005.

[2.13] T.W. Stringfield, D.J. Marihart, R.F. Stevens, “ Fault Location Methods for Overhead Lines”, Transactions of the American Institute of Electrical Engineers Power Apparatus and Systems, Part 3, Vol. 76, Issue 3, pp.518-529, 1957.

[2.14] P.J. Moore and D.B. Grace, “Remote Sensing of Overhead Line Conductor Temperature Using an Infra-red Sensor”, Proceeding of the 5th Conference on Advances in Power System Control, Operation and Management, pp. 385-389, Hong Kong, October 2000.

[2.15] S. Muhr, S. Pack and S. Jaufer, “Usage and Benefit of an Overhead Line Monitoring System”, International Conference on High Voltage Engineering and Application, pp. 557-561, China, November 2008.

[2.16] D.A Douglass, D.C. Lawry, A. Edris and E.C. Bascom, “Dynamic Thermal Ratings Realize Circuit Load Limits”, IEEE Computer Applications in Power, Vol. 13, Issue 1, pp. 38-44, January 2000.

[2.17] S.M. Mahajan and U.M. Singareddy, “A Real-Time Conductor Sag Measurement System Using a Differential GPS”, Vol. 27, Issue. 2, pp.475-480, April 2012.

[2.18] T.O Seppa, “Accurate ampacity determination: Temperature – Sag Model for Operation Real Time Ratings”, IEEE Transactions on Power Delivery, Vol. 10, No.3, July 1995, pp. 1460-1470.

[2.19] T.V. Santhosh, A.K. Ghosh, B.G. Fernandes, “Remaining life prediction of I&C cables for reliability assessment of NPP systems”, Nuclear Engineering and Design, Elsevier, Vol. 245, pp. 197-201.

[2.20] Q. Su, “Insulation Condition Assessment of HV Cables”, International Conference on Condition Monitoring and Diagnosis, pp. 1127-1131, April 2008.

[2.21] L. Mariut, E. Helerea, G. Lungoci and S. Abagiu, “ Thermal Analysis of Underground Power Cables – A Monitoring Procedure”, International Conference on Applied and Theoretical Electricity (ICATE), pp. 1,6, 25-27, Oct. 2012.

[2.22] S. Grzybowski, P. Trnka and J.C. Fulper, “Aging of High Voltage Cables by Switching Impulse”, IEEE Electric Ship Technologies Symposium, pp. 165-168, May 2007.

[2.23] W.Z. Fam, “A Novel Transducer to Replace Current and Voltage Transformers in High-Voltage Measurements”, IEEE Transactions on Instrumentation and Measurement, Vol. 45, Issue. 1, pp. 190-194, February 1996.

[2.24] N.H. Ahmed and N.N. Srinivas, “On-Line Partial Discharge Detection in Transformer”, IEEE International Symposium on Electrical Insulation, Vol. 1, Virginia, USA, pp. 39-42, June 1998.

[2.25] M.D. Judd, S.D.J. McArthur, J.R. McDonald and O. Farish, “Intelligent Condition Monitoring and Asset Management. Partial Discharge Monitoring for Power Transformers”, Power Engineering Journal, Vol. 16, Issue. 6, pp. 297-304, December 2002.

[2.26] S. Meijer, P. Cichecki, P.D. Agoris, J.J. Smit and H.F. Reijnders, “UHF Sensors for Partial Discharge Diagnostics of Power Transformers”, Proceedings of the International Conference on Electrical Engineering and Informatics, pp. 769-772, June 2007.

[2.27] I.A. Metwally, “Failures, Monitoring and New Trends of Power Transformers”, IEEE Potentials, Vol.30, Issue. 3, pp.36-43, May-June 2011.

[2.28] Z. Shi, Y. Meng, W. Yang, D. Ding, S. Jia, M. Rong and Y. Cheng, "On-line Condition Monitoring System of Medium-Voltage Switchgear", Asia Pacific Transmission and distribution Conference and Exhibition, Vol.3, pp. 2290-2294, October 2002.

[2.29] C. Walton, S. Carter, M. Michel and C. Eastham, "Avoidance of MV Switchgear Failure Case Studies of On-Line Condition Monitoring" 20th International Conference on Electricity Distribution, Paper 0422, CIRED, June 2009.

[2.30] D. Birtwhistle and I.D. Gray, "A New Technique for Condition Monitoring of MV Metalclad Switchgear", Fifth International Conference on Trends in Distribution Switchgear: 400-145kV for Utilities and Private Networks, pp. 91-95, November 1998.

[2.31] J. Mettam, "Insulation Aging in 12kV Switchgear-A Users Perspective", Proceedings of the 4th International Conference on Properties and Applications of Dielectric Materials, Vol. 2, pp. 772-775, July 1994.

[2.32] A.I. Ibrahim and H.W. Dommel, "A Knowledge Base for Switching Surge Transients", International Conference on Power system Transients, paper 50, June 2005.

[2.33] M. Sanaye-Pasand, M.R. Dadashzadeh and M. Khodayar, "Limitation of Transmission Line Switching Overvoltages using Switchsyn Relays", International Conference on Power system Transients, paper 87, June 2005.

[2.34] A. Hayati Soloot, A. Gholami, E. Agheb, A. Ghorbandaeipour and P. Mokhtari, "Investigation of Transmission Line Overvoltages and their Deduction Approach", World Academy of Science, engineering and Technology, 2009.

[2.35] G.W. Chang, H.M. Huang and J.H. Lai, "Modelling SF6 Circuit Breaker for Shunt Reactor Switching Transient Analysis", International Conference on Power System Technology, Vol.2, pp. 1315-1320, Singapore, November 2004.

[2.36] J. Wang, T. Jing and Y. Bai, "A Novel Contactless Overvoltage Monitoring Method based on the Principle of Electrostatic Coupling", Asia-Pacific Power and Energy Engineering Conference, pp. 1-6, March 2010.

[2.37] J.D. Morgan, "High Voltage Testing", IEEE Potentials, Vol.7, Issue 2, pp.14-17, August 2002.

[2.38] British Standard, "Guide on High-Voltage Testing Techniques Part 1: General", BS923-1:190, IEC 60-1:1989.

[2.39] K. Feser, W. Pfaff, G. Weyreter and E. Gockenbach, "Distortion-free Measurement of High Impulse Voltages", IEEE Transaction on Power Delivery, Vol.3, Issue. 3, pp. 857-866, July 1988.

[2.40] J.W. Skooglund, W.H. Kolb and T.L. Dyer Jr., "Measuring Equipment and Techniques used for High-Voltage Impulse Tests on Lines and Substations", Transactions of the American Institute of Electrical Engineers Power Apparatus and Systems, Part 3, Vol. 73, Issue 1, pp. 223-228, January 1954.

[2.41] K. Bohnert, P. Gabus and H. Brandle, "Fiber-Optic Current and Voltage Sensors for High-Voltage substations", 16th International Conference on Optical Fiber Sensors, Technical Digest, Japan, pp. 752-754, October 2003.

[2.42] F. Rahmatian and N.A.F Jaeger, "An Integrated Optics Sensor for High-Voltage Measurement Applications", Canadian Conference on Electrical and Computer Engineering, Vol.2, Vancouver, Canada, pp. 672-675, September 1993.

[2.43] H.M. Ryan, "High Voltage Engineering and Testing", 2nd Edition, IEE Power and Energy Series 32, ISBN: 085296 775 6, pp. 611, 2001.

[2.44] Micro Optics, “Optical Fibre sensor Guide Fundamental and Application”, Optical Sensing, www.microoptics.com, (http://www.micronoptics.com/uploads/documents/Updated_Optical_Fiber_Sensors_Guide_130529.pdf).

[2.45] D. Chatrefou, M. Pristchepa and D. Uhde, “Application of Optical Sensors for Measurement of High Frequency Overvoltages in Power Transformers”, IEEE Power Engineering Society Winter Meeting, Vol.3, Singapore, pp. 2257-2268, January 2000.

[2.46] M.A.A. Jamani, “Data Analysis and Processing for Transient Voltage Measurement in HV Substation”, BEng Final Year Project Report, Cardiff University, July 2006.

[3.1] C.A. Gerrard and J.R Gibson, “Remote Monitoring of Conditions on High Voltage Power Systems”, IEE Colloquium on Field Modelling: Applications to High Voltage Power Apparatus, pp. 9/1-9/3, London, January 1996.

[3.2] J.M Feldman, N. Reinhardt and K. Kuehn, “A Hotstick Instrument for the Estimation of the Potential HVDC Conductor”, IEEE Transmission Power Delivery Conference, Vol. 7, No.3, pp. 1533-1541, Dallas, USA, September 1991.

[3.3] P. Hammond, “Electromagnetism for Engineers”, An Introductory Course, 3rd Edition, ISBN: 0-08-0325831-1, pp. 29,30,39,40.

[4.1] L. Callegaro, P.P. Capra and A. Sosso, “Optical Fiber Interface for Distributed Measurement and Control in Metrology Setups: Application to Current Sensing with fA Resolution”, IEEE Transactions on Instrumentation and Measurment, Vol. 50, No. 6, pp. 1634-1637, Dec 2001.

[4.2] K. Gyung-Suk, S. Jae-Yong and A. Haddad, “A New Wideband High Voltage Measurement System with an Integrated Optic Link”, WSEAS Transaction on Circuits and Systems, Vol. 4, Issue 9, ISSN: 1109-2734, September 2005.

[4.3] S. Sivanagaraju and S. Satyanarayana, “Electric Power Transmission and Distribution”, Pearson Education, ISBN: 978-81-317-0791-3, pp. 5.12, 1999.

APPENDIX 3.1

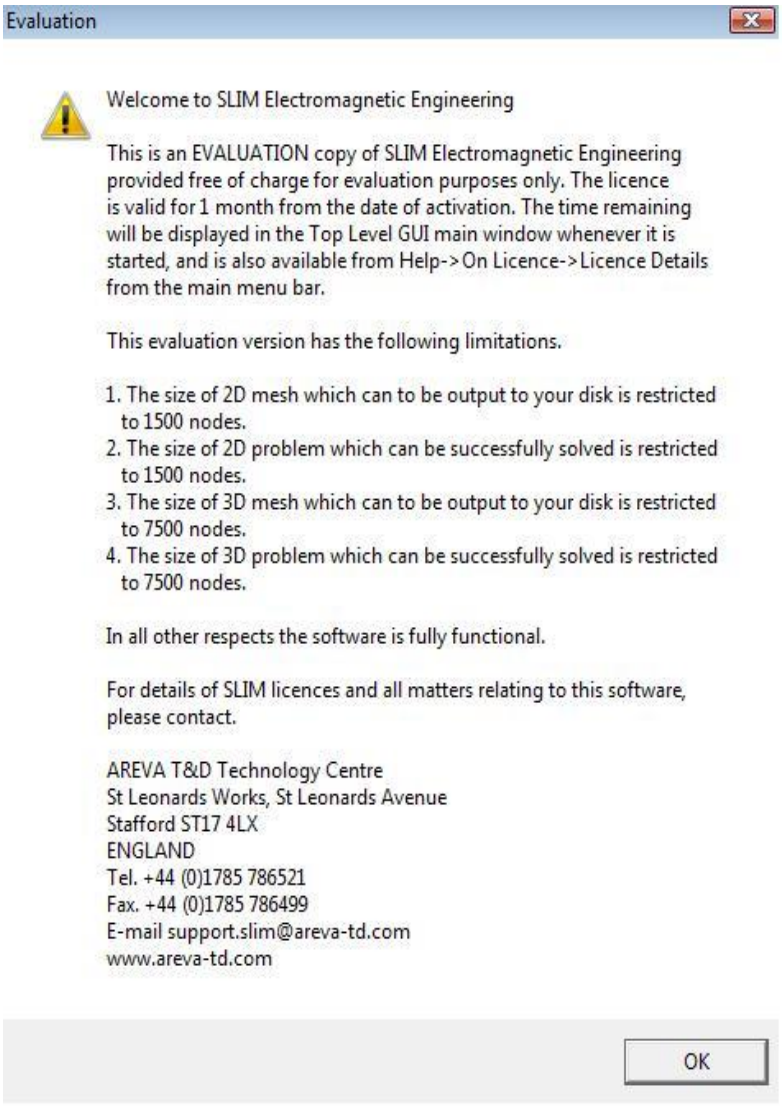

Figure A3.1: SLIM modelling limitation.

APPENDIX 3.2

Matlab routine used to extrapolate and generate a 3D representation and calculate the integration value of electric filed distribution on the sensing probe surface.

```
%% Calculation to measure the electric field
%% Reading the data from excel file.
data = xlsread('data.xls');
%% Extract the data and assign them into x-coordinate(x), y-
coordinate(l)
%% and electric field(e) readings respectively.
x = data(:,1); %%assign the data from the first coloum.
l = linspace(-0.2,0.2,length(x));%%assign the start point and
last point of the length then divided the lenght by following the
size of the x data.
e = data(:,2);%%assign the data from the second coloum.
%% Generate meshgrid to produce 3D plot
[X,L]=meshgrid(x,l);
[E,L1]=meshgrid(e,l);
surf(X,L,E); %%produce surface.
xlabel('Width,w (m)')
ylabel('Length,l (m)')
zlabel('Electric field (V/m)')
%% Integrate electric field over the area
%% Apply double integration using trapezoidal method twice.
I_x=trapz(x,e);
Ix=trapz(x,E);
I =trapz(l,Ix)
```

APPENDIX 4.1

Matlab routine used to extrapolate and generate a 3D representation

```
data = xlsread('analysis_2.xls');
N = length(data);

[Ci,H]=meshgrid(data(1,2:N),data(2:N,1));
Vout = data(2:N,2:N);

gap = 50;
Ci_gap = (data(1,N)-data(1,2))/gap;
H_gap =  (data(N,1)-data(2,1))/gap;

[Ci2,H2] = meshgrid(data(1,2):Ci_gap:data(1,N),data(2,1):H_gap:data(N,1));
Vout2 = interp2(Ci,H,Vout,Ci2,H2);

surf(Ci,H,Vout)
xlabel('Ci measured (nF)')
ylabel('Height (m)')
zlabel('Transducer Output Voltage (V)')

figure
surf(Ci2,H2,Vout2)
xlabel(''Ci measured (nF)')
ylabel('Height (m)')
zlabel('Transducer Output Voltage t (V)')



grid on
```

APPENDIX 5.1

Nationwide Platforms
All you need in access rental

Z45D

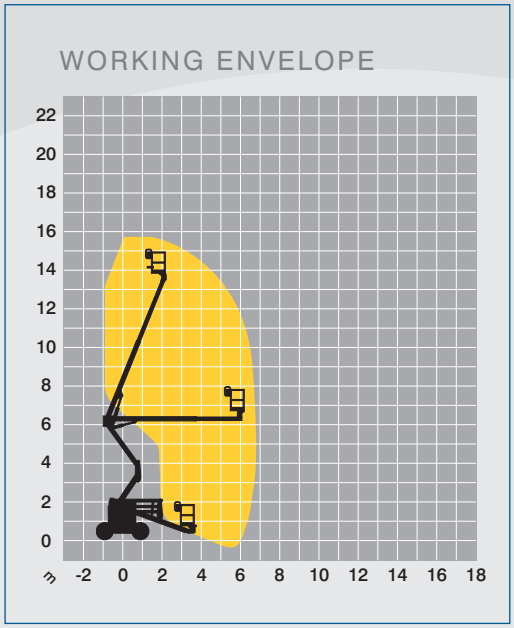

Working height	**15.91m**
Platform height	**13.91m**
Outreach	7.60m
Platform size	1.82 x 0.76m
SWL-high	227kg
Power	Diesel
Rotation	359°
Closed height	2.08m
Closed width	2.23m
Closed length	5.48m
Weight - 4 x 4	6,350kg
Weight - 4 x 2	6,260kg
Options	4x4/Jib
	Foam Filled Tyres
	Generator

The photograph above may not be the machine described, but will be a machine of a similar specification.

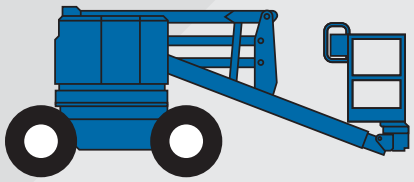

Call us on 0845 745 0000 or visit our website at www.nationwideplatforms.co.uk

Proc. of the IEEE International Conference on Smart Instrumentation, Measurement and Applications (ICSIMA)
26-27 November 2013, Kuala Lumpur, Malaysia

The Development of a Voltage Transducer for Faults Monitoring on High Voltage Overhead Lines Using Numerical Methods

M.F. Hussin[#1], N. Harid[*2], A. Haddad[*2]

[#]*Electrical Department, University Kuala Lumpur*
British Malaysian-Institute, Batu 8, Jln Sg. Pusu,
53100, Gombak, Malaysia
[1]mohdfahmi@bmi.unikl.edu.my

[*]*High Voltage Energy Systems Research Group*
School of Engineering, Cardiff University
The Parade, Cardiff,
CF243AA, U.K
[2]Harid@cardiff.ac.uk
[2]Hadad@cardiff.ac.uk

***Abstract*—Conventional transducers are widely used for high voltage measurement and monitoring purposes. However, these transducers are known to have several drawbacks. This limits their widespread deployment in large numbers especially in high voltage applications such as substation equipment or overhead lines located in rural areas. Hence, a voltage transducer is proposed based on a novel exploitation of the electrical field distribution around the high voltage conductor. Numerical methods are used to determine the electric field distribution around the high voltage conductor and the transducer. The computed electric field is used to calibrate the proposed transducer. The computational results obtained are validated using a simplified analytical method.**

Keywords—overhead line; voltage transducer; numerical methods; faults monitoring

I. INTRODUCTION

Overhead lines and underground cables are two of the common media used for electrical energy transfer, as they are practical and economical, particularly the overhead lines, which has low installation and maintenance costs. However, the overhead lines is expose and susceptible to faults [1]. Faults occurring on high voltage overhead lines (OHL) are normally caused by surge voltages or faulty equipment in the substation system. The surge voltages are caused by transient overvoltage originating either from lightning strikes to the lines or switching operations on the power transmission network [2]. In addition, the OHL also exposed to adverse weather condition, pollution and tree initiated faults. These faults can accelerate the aging of the conductor insulation material and leads to the high voltage system failure [3]. Therefore, it is crucial that measurement and monitoring of the voltage on the OHL to be assessed accurately in order to maintain safe and reliability operation of high voltage (HV) substations and OHL equipment.

Conventional transducers such as voltage transformers and voltage dividers are commonly used for decades to step down high voltage magnitudes to a safe measurable level and ability to provide reliable voltage measurement. Nevertheless, the conventional transducers are tends to be bulky in size hence resulting time-consuming during installation and requires sophisticated set-up procedures. In addition, their frequency response is not adequate for the measurement of fast transient. Moreover, increases in power distribution system voltages which up to several hundred kV and load growth have led to increase operating stresses on the transformer insulation, which are becoming increasingly complex and costly [4].

In this paper, an improvement configuration of cylindrical-shaped capacitive voltage transducer is proposed based on the previous developed transducer presented in paper [5]. This transducer is used for faults monitoring on high voltage overhead lines and is capable of measuring different types of voltage sources, including impulse voltages. The transducer utilizes the capacitive divider measurement principle, but it uses the HV conductor as the measurement reference instead of the ground. The relative merits of the transducer lie in its simple construction feature for ease of installation, low cost and reliability.

Commercially available numerical methods software packages were used to model and aid in the development of the transducer. The software enables simulation of the electric field distribution around the HV conductor and the transducer. The simulated results obtained from the modeling simulation were verified using Matlab computation and simplified analytical calculation.

II. CONFIGURATION OF VOLTAGE TRANSDUCER

The transducer configuration is based on the previous transducer configuration (cylindrical-shaped) as presented in [5] but the transducer cylinder length is increased from 300mm

978-1-4799-0843-1/13/$31.00 ©2013 IEEE

to 500mm. The purpose of this length increment is to fully guard by the sensing probe. In contrast to the previous designs the guard electrode only guarded sides of the sensing probe. This improvement will provide better safeguard to the sensing probe. In addition, the guard electrode is also used to reduce the end-effects at the sensing probe edges by creating more uniform distribution of the electric field. The guard electrode and the sensing probe are separated with an air gap of 1mm.

Fig. 1 illustrates the improved configuration of the cylindrical-shaped voltage transducer consist of the transducer frame, the transducer shielding cylinder, the guard electrode and the sensing probe. The transducer frame is used to hold the entire structure of the voltage transducer whereas the transducer's shielding plate is included in the design to alleviate the transducer installation during the experiment. The sensing probe acts as the sensing device of the electric field on the probe surface.

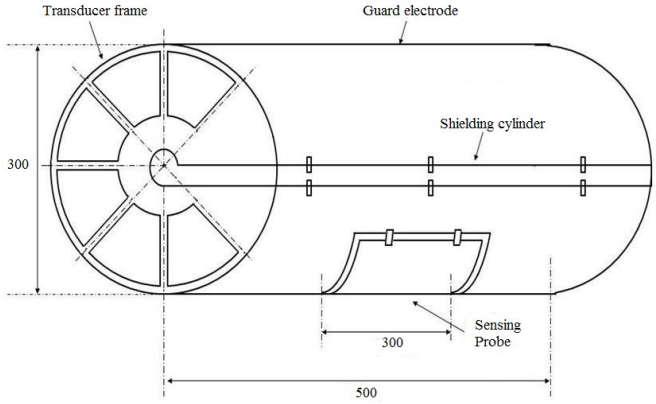

Fig. 1. Configuration of the cylindrical-shaped voltage transducer (dimension in mm and not to scale).

III. MODELLING OF VOLTAGE TRANSDUCER

Numerical method software packages such as finite (FEM) and boundary (BEM) element method known as SLIM and Coulomb are used to model the transducer in two and three-dimensional models respectively. This modelling simulation is essential for determining the electric field distribution around the HV conductor and the transducer, facilitating the transducer development and enabling prediction of transducer characteristics and performance. Furthermore, the computation of the electric field distribution was used to calibrate the transducer and determine the geometric capacitance (C_T) of the voltage transducer. The simulation models were based on the single phase laboratory experiment configuration for ease of comparison between 2D and 3D modelling respectively. Such investigations allow comparison of the computational results and selecting an appropriate approach for the calibration process.

A. *Two-dimenional Model of Voltage Transducer*

The finite element software (SLIM) was used to model the transducer in an X-Y geometry modelling representation. The model was used to simulate a vertical section of the HV conductor, with the transducer placed around it in close proximity. Fig. 2 shows the 2D model as simulated in SLIM, with the boundary area spanning 10m by 10m and the transducer placed at 2.5m above the ground level, which is measured from the centre of the HV conductor.

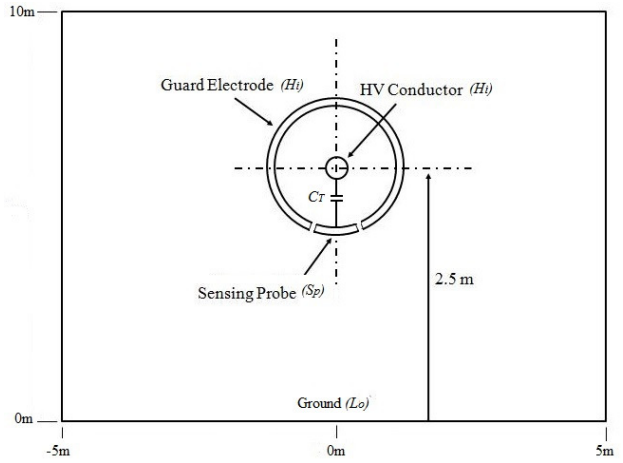

Fig. 2. Single-phase modelling based on laboratory experiment configuration (not to scale).

Within the simulation software, the entire space is meshed into a set of triangular elements and set as free space (labelled as "Air") except for the HV conductor, the sensing probe and the guard electrode. The HV conductor and the guard electrode are subjected to high potential (H_i) while the ground is assigned to low potential (L_o). The sensing probe (S_p) is represented by a foil which acts as a floating electrode. An initial simulation was carried out using the generated model in free space to evaluate the geometric capacitance (C_T) of the transducer with respect to ground surface.

B. *Three-dimensional Model of Voltage Transducer*

The boundary element method (Coulomb) is used to model the transducer in 3D configuration as shown in Fig. 3, with a defined measurement for the length of the transducer, the HV conductor and the sensing probe. Fig. 4, shows the enlarged view of the voltage transducer and the HV conductor as identified within the dashed circle lines in Fig. 3.

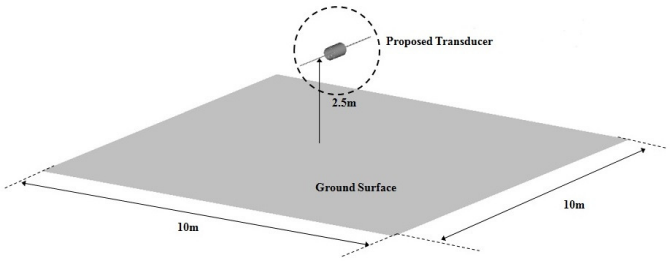

Fig. 3. 3D model configuration computed in Coulomb.

The initial stage of the 3D modeling process involved specifying the coordinates of various key nodes of the geometry. The physical boundaries with their assigned potentials were then defined, and the surfaces were meshed into triangular elements. This enables simulation to be carried out and compute the electric field profile on the sensing probe surface. Similar to the 2D modeling, the initial simulation was

used to evaluate the geometric capacitance (C_T) of the transducer, and this capacitance is subsequently compared with the results from the 2D modeling, as well as the analytical results.

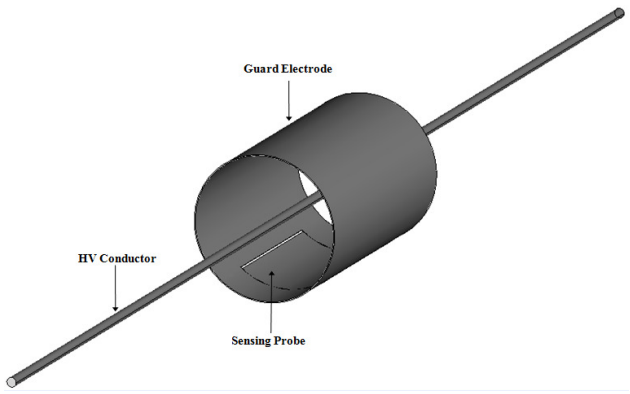

Fig. 4. Zoom in detail of the voltage transducer and the HV conductor.

IV. Simulation Results

A. *Two-dimensional Model Simulation Results*

The computed equipotential distribution around the transducer and the HV conductor using SLIM is displayed in Fig. 5. As can be observed, the equipotential contour lines indicate that the electric field around the conductor is expected to be high.

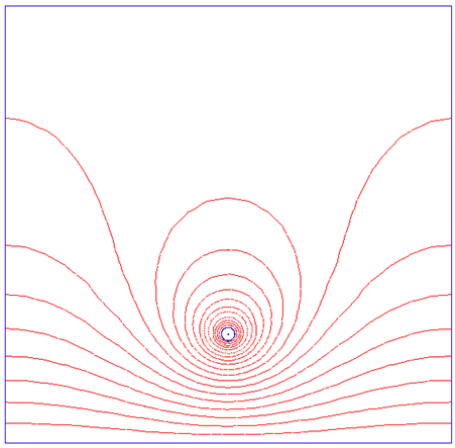

Fig. 5. The equipotential distribution generated around the HV conductor and transducer.

Fig. 6 plots the electric field magnitudes along the width of the sensing probe surface when the input voltage is set to 1kV alternating voltage on the HV conductor. These magnitudes are used to calibrate the transducer and calculate the geometric capacitance of the transducer. Noted, end-effects could be seen in the form of increasing field magnitudes appearing towards the edges of the sensing probe, with the peak value reaching approximately 8kV/m. This is mainly caused by the proximity of the sensing probe edges to the guard electrode.

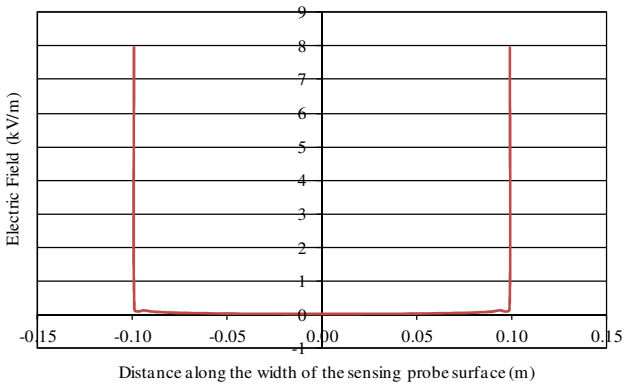

Fig. 6. Electrical field magnitude along the width of the sensing probe.

This modelling simulation incorporates the assumption that the length of the guard electrode, the HV conductor and the sensing probe are infinite since the simulation is constructed in 2D geometry. In order to generate the corresponding result for the whole sensing probe surface, a Matlab routine is developed to generate the field values, as depicted in Fig. 7. Using the field values of Fig. 7, the induced charge (Q) on the probe surface is computed through the integration the electric field magnitudes over the entire probe surface area and the computed charge determined is approximately 0.13nC.

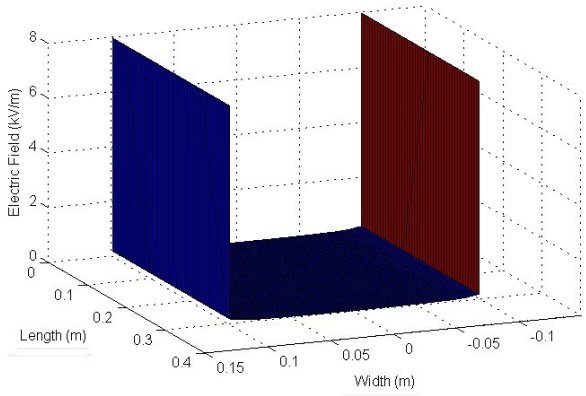

Fig. 7. Matlab generated electric field distribution on the probe surface.

B. *Three-dimensional Simulation Results*

Using the 3D software, the magnitudes of the electric field on the sensing probe surface were computed. As expected, it was found that high magnitude electric fields are concentrated towards the edges of the sensing probe, which are attributed to the end-effects discussed in the case of the 2D simulation above. The electric field magnitude profile computed at the centre of the sensing probe surface is shown in Fig. 8.

As can be observed in the figure, the end-effects at the edges of the probe is present and is approximately 10kV/m. The total induced charge (Q) computed on the probe surface using this result is 0.86nC. The higher value obtained with the 3D model is due to the accuracy of the simulation model,

which included the actual length of the sensing probe and the HV conductor.

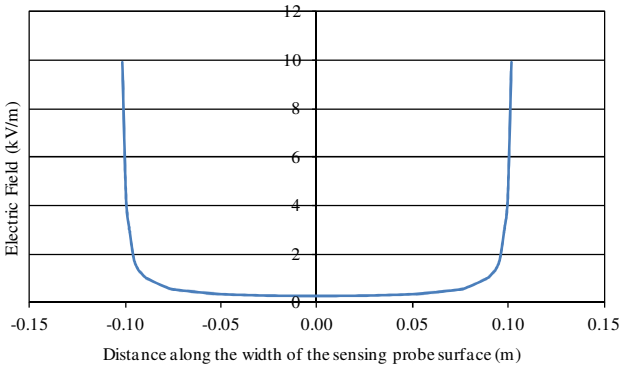

Fig. 8. Electrical field magnitude obtained at the centre of the sensing probe.

V. COMPUTATIONAL AND ANALYTICAL APPROACH

From the single-phase measurement configuration, the electric charge (Q) induced on the sensing probe surface can be determine using the electric field measurement, and is given by (1).

$$Q = \int_0^{\ell} \int_0^{w} E(x, y)\varepsilon_0 dx.dy \qquad (1)$$

Where, *E(x,y)* is the electric field at coordinates x and y on the sensing probe surface, ε_0 is the permittivity of free space (8.854 e^{-12} F/m), ℓ is length of the sensing probe (0.3m) and w is width of the sensing probe (0.2m). The computed geometric capacitance of the transducer, C_T can be estimated as in (2).

$$C = \frac{Q}{V} \qquad (2)$$

Where V is the output voltage obtained from the transducer.

Using the computed electric charge value obtained on the probe surface as presented above for two- and three-dimensional modelling, the computed geometric capacitance of the transducer is calculated using (1) and (2) to be 19.9pF for the 2D model, and 21.7pF for the 3D model.

These computed geometric capacitance values are then verified against the simplified analytical calculation. The simplified analytical approach is based on the coaxial cable configuration with the assumption that end-effects can be neglected. In this case, the per unit length capacitance can be determined using (3).

$$C = \frac{2\pi\varepsilon_0}{\ln\frac{b}{a}} \quad [\text{F/m}] \qquad (3)$$

Where, ε_0 the permittivity of free space, and 'a' and 'b' representing the radius of the HV conductor (0.01m) and the transducer (0.15m) respectively. In order to obtain the equivalent capacitance between the sensing probe and HV conductor, the per unit length capacitance needs to be scaled to the dimensions (length, ℓ and width, w of the sensing probe) of the sensing probe as shown in (4).

$$C_s = \frac{C\ell w}{2\pi b} \qquad (4)$$

However, due to end-effects at the edges of the sensing probe, the extra capacitance within the gap between the sensing probe and the guard electrode needs to be taken into consideration, and is approximated by (5).

$$C_{gap} = \frac{\varepsilon_0 A}{d} \qquad (5)$$

Where C_{gap} is the capacitance between the sensing probe and the guard electrode, ε_0 is the free space permittivity and A=2 t ($\ell + w$) is the total surface areas at the sides of the sensing probe, with t plate thickness. The thickness of the sensing probe is 2mm and the gap distance, *d*, between the sensing probe and the guard electrode is 1mm.

The total geometric capacitance (C_T) of the transducer is the combination of the sensing probe surface capacitance (4) and the air gap capacitance (5), and is defined as

$$C_T = C_s + C_{gap} \qquad (6)$$

Using the transducer's geometry, *Cs* was calculated to be 1.3pF and C_{gap} is 17.7pF which gives the total geometric capacitance of the transducer as 19pF.

Table 1 shows comparison of the geometric capacitance of the voltage transducer between the simulation models and the analytical results. These results compare reasonably well but the modelling simulation results are slightly higher than the analytical due to the fact the analytical approach is based on the simplified coaxial cable method, with the assumption that the end-effect of electric field fringing at the sensing probe edges are neglected.

Table 1. Comparison of the geometric capacitance between the modelling and analytical results.

Method	Geometric Capacitance, C_T (pF)
2D Model	19.9
3D Model	21.7
Analytical	19

VI. CONCLUSION

A cylindrical-shaped voltage transducer is proposed in this work to monitor faults and measure voltages on HV overhead line conductors. An improved transducer configuration is model using SLIM and Coulomb. The simulation and numerical results of the electric field magnitudes on the sensing probe surface were used to calibrate the transducer. The 3D modeling produced an accurate computational result compared with the 2D due to the 3D computation considered the actual length of the transducer and HV conductor. In contrast to the 2D which only assumed the transducer and HV conductor length is infinite. Nevertheless, both modelling results are

within acceptable range when compared with the analytical result. These results can be particularly useful for the development and construction of the voltage transducer for monitoring the high voltage overhead lines.

REFERENCES

[1] M. Muhr, S. Pack, and S. Jaufer, “Usage and Benefit of an Overhead Line Monitoring System,” International Conference on High Voltage Engineering and Application, 2008, pp. 9-13.

[2] E. Kuffel, W.S. Zaengl and J. Kuffel, High Voltage Engineering Fundamentals, ISBN: 0-7506-3634-3,Newness, 2001, pp. 49-52, 460.

[3] S. Grzybowski, P. Trnka and J.C. Fulper, “Aging of High Voltage Cables by Switching Impulse”, IEEE Electric Ship Technologies Symposium, pp. 165-168, May 2007.

[4] M. J. Moser, H. Zangl, T. Bretterklieber, G. Brasseur, “An Autonomous Sensor System for Monitoring of High Overhead Power Supply Lines”, Journal of Elektrotechnik & Informationstechnik, Vol. 126, Issue 5, pp. 214-219, May 2009.

[5] Hussin, M. F., Haddad, A.; Harid, N., "Voltage transducer for monitoring of high voltage overhead lines," Universities Power Engineering Conference (UPEC), 2010 45th International, 2010, pp.1-5.

Voltage Transducer for Monitoring of High Voltage Overhead Lines

M.F Hussin
Cardiff University
mohdfahmiH@cf.ac.uk

A. Haddad
Cardiff University
haddad@Cardiff.ac.uk

N. Harid
Cardiff University
haridn@Cardiff.ac.uk

***Abstract*- In this paper, a voltage transducer is proposed based on the distribution of electric field around high voltage overhead line conductors. Finite-element software is used to compute the electric field distribution around the high voltage lines and the transducer. A cylindrical-shaped voltage transducer is designed and constructed in this work. Laboratory experiments are carried out using the transducer and the effects of varying the integrating capacitors and the transducer height above ground on the output voltage are investigated. A good linearity of output voltage compared with the simultaneous measurement of a calibrated standard high voltage capacitive divider is established. The experiment also observed a relative change in the output voltage when the sensor height is varied in a certain way. These preliminary experiments have demonstrated the feasibility of the transducer to measure the voltage of line conductors. Further enhancement is in progress to enable its use under real overhead lines conditions.**

I. INTRODUCTION

Overhead lines are the backbone for electrical power transfer, as they provide the best economic and practical solution for energy transport [1]. Overhead lines, nevertheless, suffer more faults than underground cables at low voltages up to 11kV due to the vulnerability of lines to wind, snow, ice or falling trees. Faults occurring on high voltage (HV) overhead lines are commonly caused by overvoltages which originate from lightning strikes to the HV line and switching operation on the power transmission [2]. Therefore, it is essential that measurement and monitoring of the voltage on HV lines are assessed accurately to maintain safe and economic operation of HV substation and overhead line equipment.

Conventional transducers such as, voltage transformers and voltage dividers are widely used for voltage measurement and monitoring purposes. They can provide accurate and reliable voltage measurement. However, they have several drawbacks in terms of their size and cost; these are the key factors that limit their deployment in large number for monitoring and measuring voltage of overhead lines in rural areas [3, 4].

In this paper, a cylindrical-shaped voltage transducer prototype is designed and constructed for measurement of voltages on HV distribution lines. This transducer uses the same principle implemented by a contactless capacitive probe but connected to the HV line instead of to the ground [5]. In between the transducer and the HV line, an integrating capacitor, C_i is inserted to allow a differential measurement. Consequently, another capacitance, C_G is formed between the sensing probe and ground. This type of transducer is advantageous in terms of its simple construction, high reliability and low cost, and it is easy to assemble.

A two-dimensional model of the probe is simulated using commercial finite-element software. The software is used to assist the development of the transducer and enable computation of the electric field distribution around the HV line conductor and the transducer. The obtained simulation results obtained are further verified using a simplified analytical modelling.

Laboratory experiments using the transducer are carried out to validate the simulation results. The effects of using different values of integrating capacitor, C_i and transducer height on changes in the value of output voltage are investigated in the experiments. Initial investigations established a good linearity of the transducer compared with a simultaneous measurement with a calibrated standard high voltage capacitive divider. A relative change in the output voltage is also observed when the transducer height is varied in a certain way. These preliminary experiments have demonstrated the feasibility of the transducer to measure the voltage of line conductors.

II. VOLTAGE TRANSDUCER CONFIGURATION

Figure 1 illustrates the configuration of the cylindrical-shaped voltage transducer developed and constructed in this work.

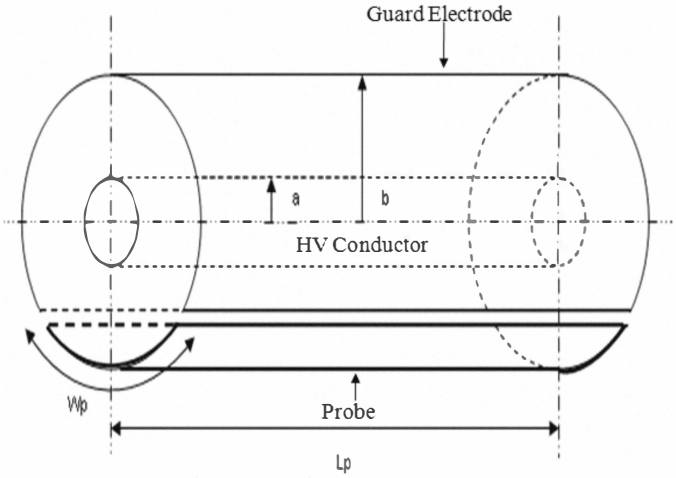

Fig. 1. The design of the cylindrical-shaped voltage transducer.

The parameters of the transducer configuration are listed below:

- The radius of the HV conductor (a) is 0.01m.
- The radius of the transducer (b) is 0.15m.
- The sensing probe length (Lp) is 0.30m.
- The sensing probe width (Wp) is 0.20m.

III. MODELLING OF TRANSDUCER GEOMETRY

An X-Y geometry model of the voltage transducer and the high voltage conductor were developed and the electric field distribution around them is computed using finite-element (FE) software (SLIM). This model is used to simulate a vertical section of the HV conductor with the probe placed around it in a close proximity [6].

Figure 2(a) shows the laboratory experiment environment, noting that the transducer is placed at a certain height above ground (2.5m), measured from the centre of the HV conductor. Figure 2(b) illustrates the 2D mesh for the above geometry representation simulated using SLIM. Within the simulation software, the entire space is meshed as air or free space except for the HV conductor, the sensing probe and the guard electrode. As shown in Figure 2(b), the HV conductor and the guard electrode are subjected to high potential (Hi) while the ground is assigned to low potential (Lo). The sensing probe is represented by a foil which acts as a floating electrode.

The initial simulation is carried out using the generated model in free space, to compute the capacitance (C_p) between the HV conductor and probe plate. To simulate the insertion of an integrating capacitor (C_i), an equivalent permittivity is calculated from the coaxial between the conductor and the probe using its equivalent capacitance. The model shown in Figure 2(C) is used for these simulations. This is further explained in section VII.

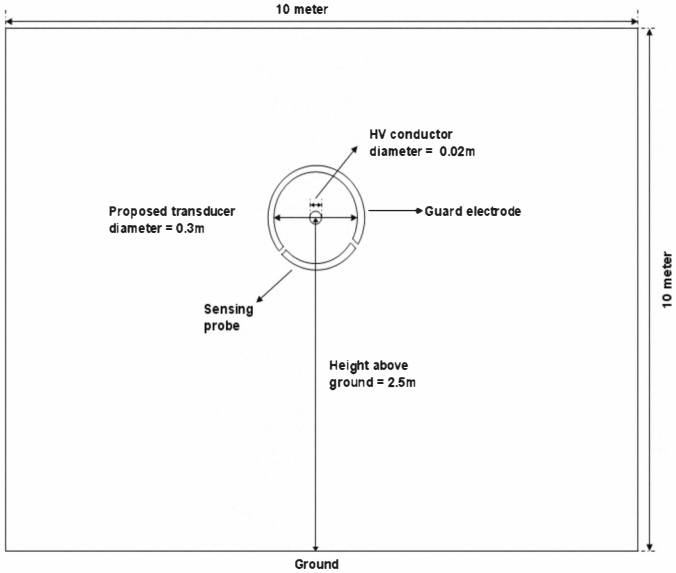

Fig. 2(a). The X-Y geometry representation based on the laboratory experiment environment but not in actual scale.

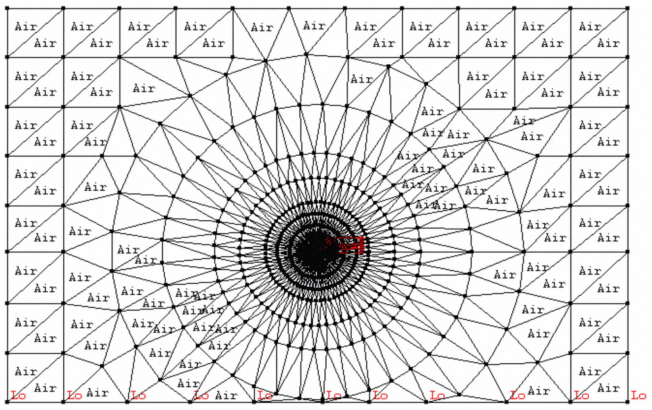

Fig. 2(b). The X-Y geometry representation converted to 2D mesh model.

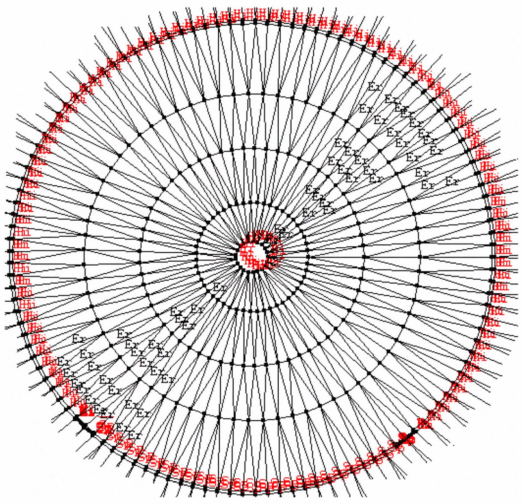

Fig. 2(c). Permittivity ε_r is created on the entire area between the HV conductor and the probe.

V. MEASUREMENT SETUP

A diagram of the measurement setup used for the laboratory experiments is shown in Figure 3. The setup comprises a variac, an isolation transformer, an inductor (L), a capacitor (C), an HV transformer, an HV divider and the proposed transducer. The variac is utilised to regulate the input voltage whereas the isolation transformer is used to isolate the ground reference between the low voltages supply and the HV sides for safety precaution. The inductor and capacitor are inserted as a filtering unit in order to minimise higher harmonics. The HV transformer steps up the incoming supply to the desired output voltage. Voltage measurements are carried out with the proposed transducer and the HV standard divider.

The integrating capacitor (C_i) is placed between the HV conductor and the sensing probe. The output voltage across C_i is subsequently transmitted via a fibre optic system and monitored using the oscilloscope. The value of C_i is varied within the range of 2.2nF to 10nF. The transducer height is also changed from 1.5m to 2.5m with 0.5m steps.

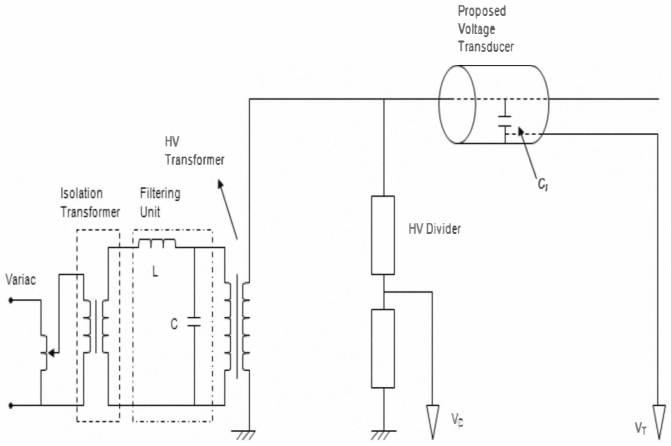

Fig. 3. The laboratory measurement setup of the proposed transducer.

VI. RESULTS

A. *Simulation Results*

Figure 4 shows the equipotential distribution computed using the X-Y geometry model based on Figure 2(a) configuration. Figure 5 shows the electric field magnitudes along the width of the inner surface of the sensing probe when the input voltage is set to 1kV and the average electric field value is around 200V/m. These magnitudes are used for calibration of the transducer. As can be seen, some end effects in the form of increasing field magnitudes appear towards the edges of the sensing probe. However, in the model it is assumed that the length of the transducer is infinite since the model is in 2D geometry. A Matlab routine is used to generate a 3D representation, as shown in Figure 6. It is assumed that the electric field along the inner surface of the sensing probe is applied along the transducer length. The charge Q induced on the probe surface is computed through the integration the electric field over the entire probe surface area and is found to be approximately 0.1nC.

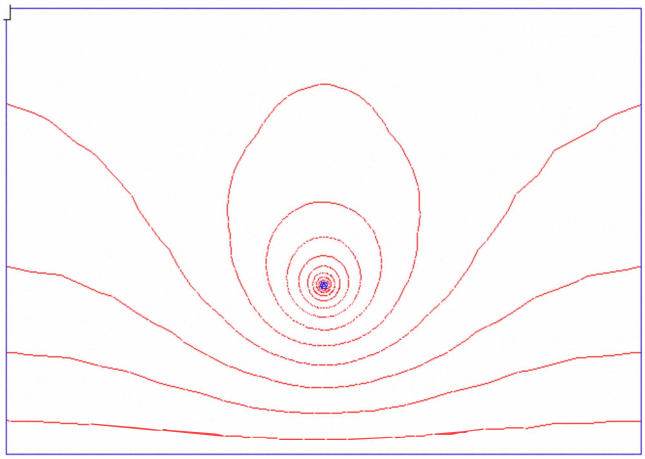

Fig. 4. The equipotential contour at 8% intervals for the X-Y geometry model.

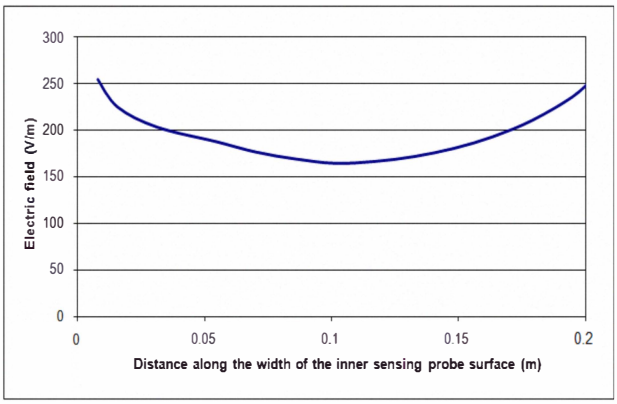

Fig. 5. The electric field distribution along the width of the inner sensing probe surface.

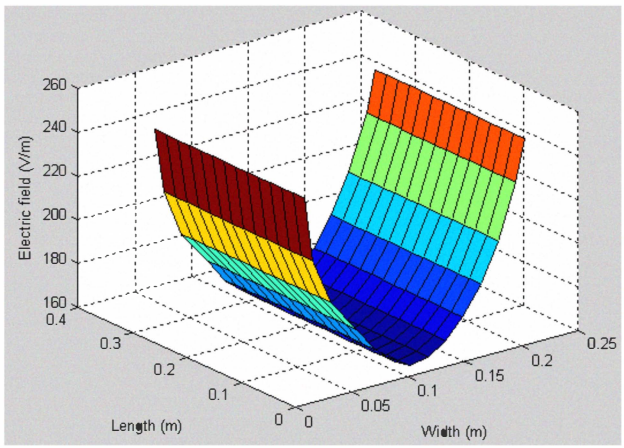

Fig. 6. The 3D representation of the electric field distribution on the entire sensing probe surface generated using Matlab.

B. *Experiment Results*

Several experiments have been carried out using random values of C_i such as 2.2nF, 3.3nF, 4.7nF, 6.8nF and 10nF. Furthermore, the height of the transducer is also varied between 1.5m, 2.0m and 2.5m, which was achieved using a crane attached to the HV insulator string. The whole transducer, with the exception of the sensing probe, is covered with an aluminium foil to act as a guard electrode to reduce any fringing effect and obtain more controlled distribution of the field on the transducer [6]. Figure 7(a) illustrates the output voltage obtained from each integrating capacitors at a fixed height of 2.5m above ground whereas Figure 7(b) shows the output voltage for 10nF integrating capacitor at various heights above ground.

In Figure 7(a), the output voltage decreases when Ci increases. There is a slight decrease in the output voltage value when the transducer is placed further away from the ground, as seen in Figure 7(b). From both of these figures, it can be deduced that Ci and height are the key elements in the system as they are the only controllable variables. These two factors can be controlled to obtain the desired output from the transducer.

Figure 8 shows an example of the measured voltage records from the proposed transducer using of 10nF and capacitive voltage divider. A small phase shift can be observed due to the fibre optic system. The results are obtained when the input voltage is set to 1kV and the transducer is placed 2.5m above ground.

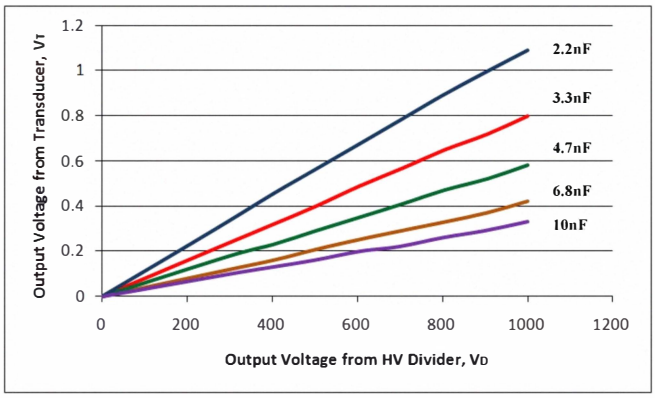

Fig. 7(a). Output Voltage produced by transducer for each integrating capacitors at fixed height of 2.5m above ground.

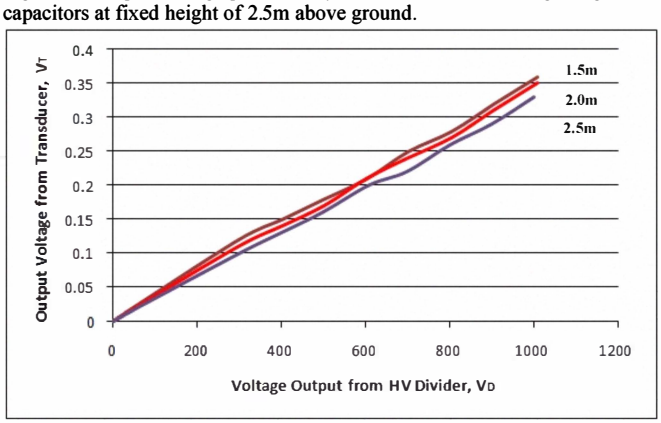

Fig. 7(b). Output Voltage produced by transducer for 10nF of integrating capacitors at varies height above ground.

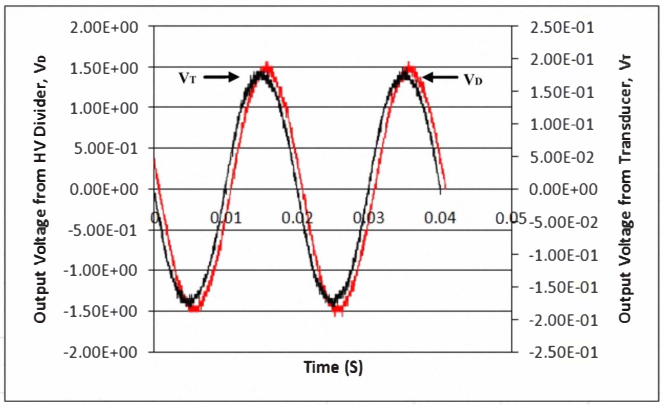

Fig. 8. Sinusoidal Output Voltage produced by transducer and HV Divider when connected with 10nF of integrating capacitors at height 2.5m.

VII. ANALYTICAL APPROACH

The electric charge (Q) induced upon the sensing probe surface is acquired using the electric field measurement, given by

$$Q = \iint_A E\varepsilon_0 dA\,. \tag{1}$$

where E is the electric field on the surface of the sensing probe, ε_0 is the permittivity of free space, and dA is the element area of the sensing probe surface.

Using the computed field values, presented in Figure 6, a total charge of 0.1nC is computed. From this, the capacitance, C_p obtained using the X-Y model can be calculated as

$$C = \frac{Q}{V} \tag{2}$$

where V is the voltage drop between the HV conductor and the sensing probe. The voltage drop is computed as 23.7V when the input voltage is set to 1kV, resulting in 4.2pF of C_p.

As indicated earlier, an equivalent permittivity is used to simulate the integrating capacitor C_i, a new permittivity ε_r is introduced by dividing the measured C_i values with C_p as shown below:

$$\varepsilon_r = \frac{C_i}{C_p} \tag{3}$$

Table 1 shows the simulation results when ε_r is inserted into the modelling simulations. In order to generate data as accurate as possible, actual measured value of capacitors are used instead of the manufactures value. The results show consistency between the simulations and the measured values of C_i, some small differences due to accuracy limits in the FE model are however seen.

TABLE 1
Comparison between measurement and simulation values of C_i

$C_{i\,(Manufacture)}$ (nF)	$C_{i(Measured)}$ (nF)	$C_{i\,Simulation}$ (nF)
2.2	2.07	2.07
3.3	3.25	3.12
4.7	4.12	4.11
6.8	6.06	5.94
10	8.65	8.63

VIII. CONCLUSION

A capacitance probe with an attached integrating capacitance is designed and constructed in this work to measure voltage on HV overhead line conductors. The simulation and numerical results of the electric field magnitudes on the sensing probe surface were used to calibrate the transducer. Laboratory experiments indicate satisfactorily results to date but external factor such as stray capacitance in the system should be taken into consideration in the analysis. Further refinement is in progress to enable its use under real conditions.

REFERENCES

[1] M.Muhr, S.Pack, and S.Jaufer, "Usage and Benefit of an Overhead Line Monitoring System," 2008 International Conference on High Voltage Engineering and Application, Chongqing, China, November 9-13, 2008.

[2] E.Kuffel, W.S.Zaengl and J.Kuffel, "High Voltage Engineering Fundamentals," Newness (2001), ISBN: 0-7506-3634-3, pp.49, 460.

[3] M.M.Werneck, and A.C.S.Abrantes, "Fiber-Optic-Based Current and Voltage Measuring System for High-Voltage Distribution Lines," IEEE Transactions on Power Delivery, Vol.19, No.3, July 2004.

[4] M.F.Hussin, A.Haddad and N.Harid, "Monitoring of High Voltage Distribution Line," 3rd UHVNet Colloquium on Technologies for Future High Voltage Infrastructure, University of Manchester, 19 & 20 January 2010.

[5] C.A.Spellman, A.Haddad, D.M.German and R.T.Waters, "Improved Three-Phase Voltage Measurement Using Capacitive Probe," Proceeding of the Universities Power Engineering Conference, Leicester, UK, Vol.1, pp.352-355, 1999.

[6] M.F.Hussin, A.Haddad and N.Harid, "A Voltage Transducer for High Voltage Applications," 2nd UHVnet Colloquium on High Voltage Measurement and Insulation Research, Glasgow Caledonian University, pp.41-44, 21st January 2009.

LIST OF FIGURES

LIST OF TABLES

LIST OF SYMBOLS AND ABBREVIATIONS

Symbols	Meaning	Page
CM	Condition monitoring	1-1
OHL	Overhead line	1-1
BEM	Boundary element method	1-2
FEM	Finite element method	1-2
HV	High voltage	1-2
PVC	Polyvinyl chloride	1-2
UG	Underground	2-7
XLPE	Cross-linked polyethylene	2-8
EMI	Electromagnetic interference	2-9
PT	Potential transformers	2-9
VT	Voltage transformers	2-9
DGA	Dissolved gas analysis	2-10
PD	Partial discharge	2-10
EOVT	Electro-optic voltage transducer	2-19
OMU	Optic metering unit	2-19
MOCT	Magneto-optic current transducer	2-19
NCCP	Non-contact capacitive voltage probe	2-19
SF6	Sulphur hexafluoride	2-19
C_i	Integrating capacitance	3-19
C_G	Capacitance from the transducer sensing probe to ground	3-19
C_T	Geometric capacitance	3-19
DSO	Digital storage oscilloscope	4-2
PCB	Printed circuit board	4-2
T_x	Optical fibre system transmitter	4-7
R_x	Optical fibre system receiver	4-7
USB	Universal serial bus	4-9
ε_0	Free space permittivity	4-20
ε_r	Equivalent permittivity	4-20
2D	Two-dimensional	5-2
3D	Three-dimensional	5-2
LED	Light emitting diode	5-2